# Constraints on shock physics, wind structure, and dynamics from high-resolution X-ray spectroscopy of massive stars

David Cohen
Swarthmore College

with Jon Sundqvist & Stan Owocki (U. Delaware), Maurice Leutenegger (GSFC),
Marc Gagné & Véronique Petit (West Chester University), Asif ud-Doula (Penn St.),
Alex Fullerton (STScI),
and
Emma Wollman (Swarthmore '09; Caltech), Erin Martell (Swarthmore '09; U. Chicago),
James MacArthur (Swarthmore '11; Sandia National Laboratory)
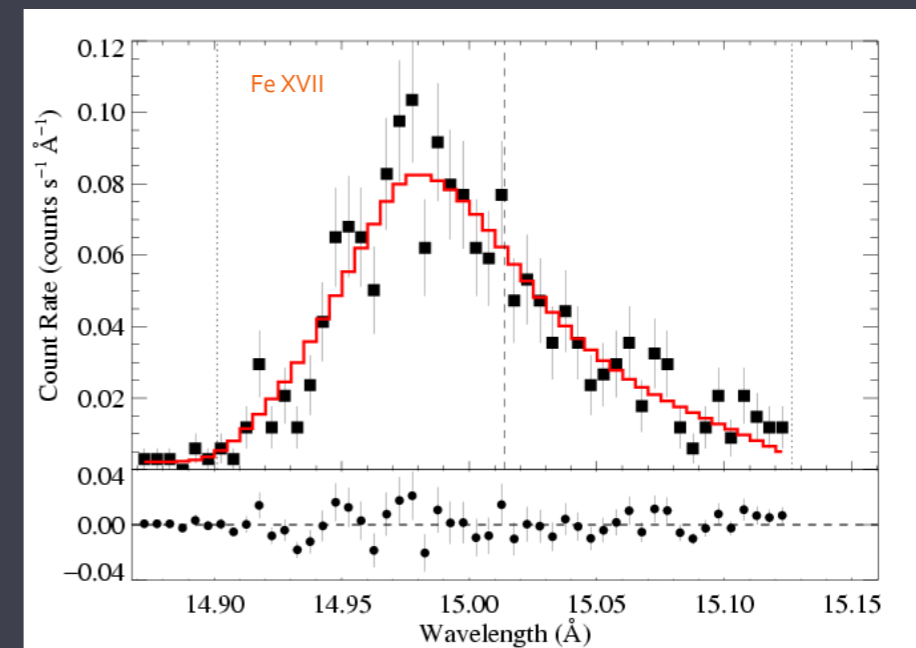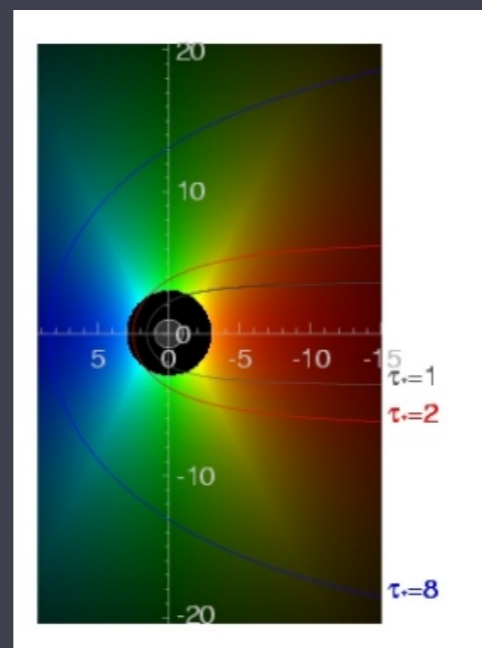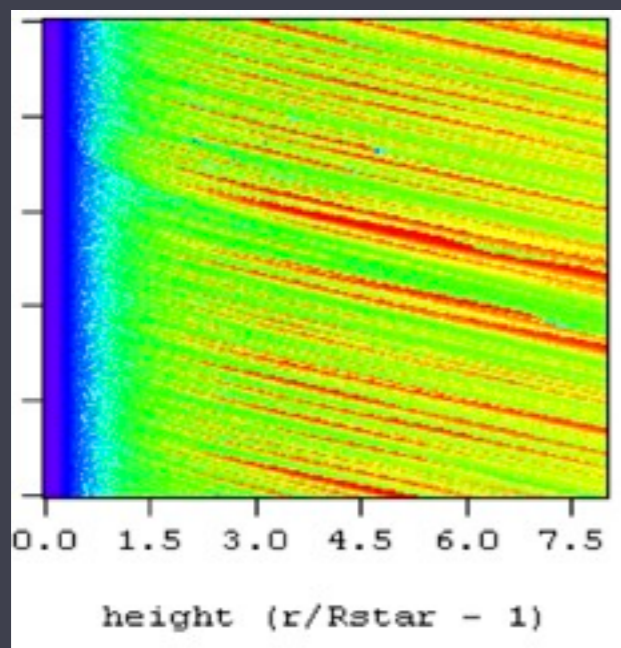
OB stars dominate their environments
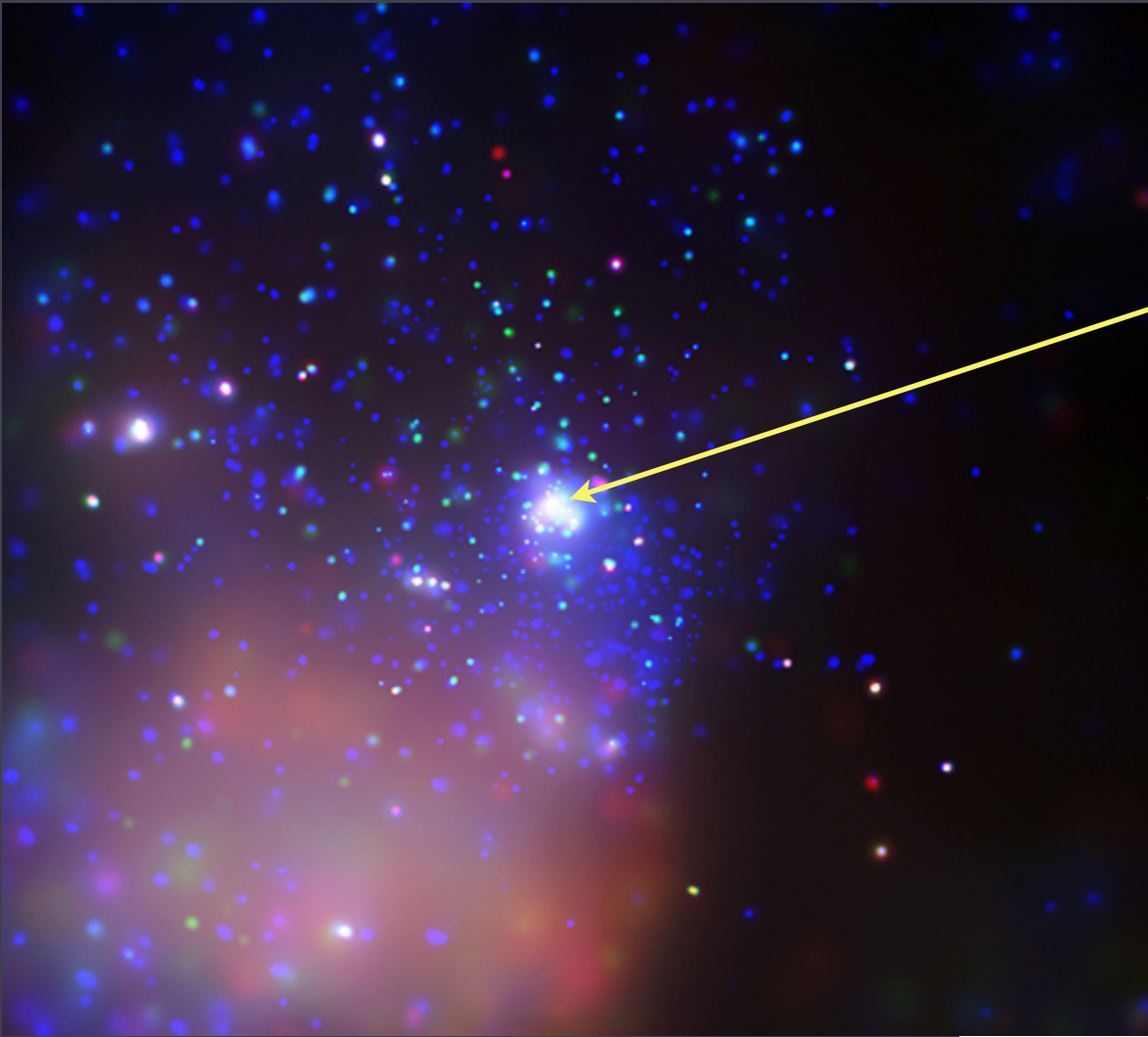## *winds play a large role*

ESO: Carina Nebula

keep in mind: O star winds can be strong ($\dot{M} \sim 10^{-6}$ to 10^{-5} M$_{sun}$/yr and $v_\infty \sim 2000$ to 3000 km/s); B star winds are much weaker
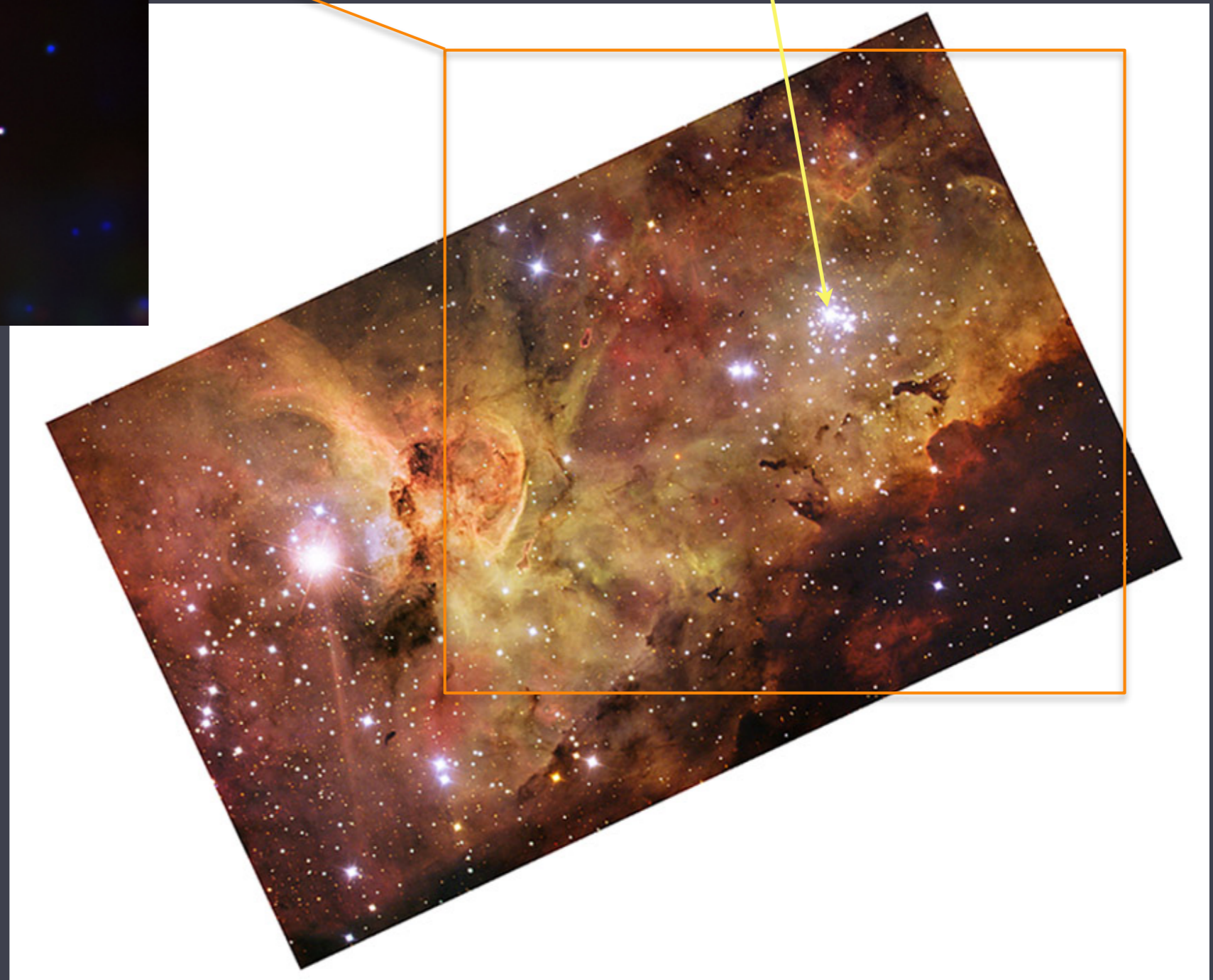

ESO: Carina Nebula
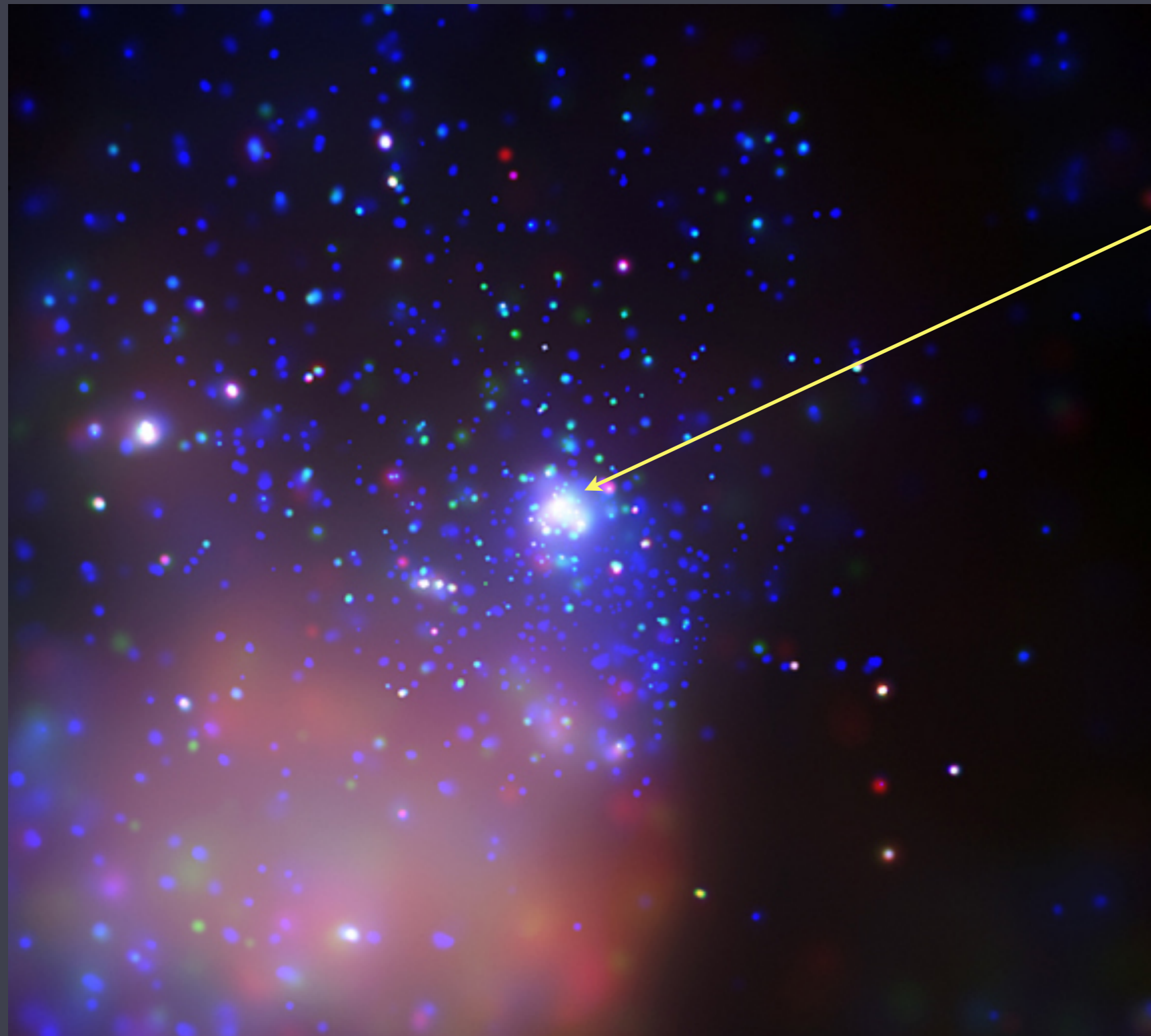
HD 93129A (O2 If*)

Tr 14: *Chandra:*
X-ray image, color-coded by
photon energy

Carina: ESO

O supergiants are quite X-ray luminous
(L_x up to 10^{33} erg/s)

HD 93129A
(O2If*)

Tr 14: *Chandra*   X-ray image, color-coded by photon energy

We will focus on *effectively single* stars

HD 93129A (O2If*)

Multiple massive stars in this system, but X-rays are dominated by embedded wind shocks from the earliest component.

Tr 14: *Chandra*

First:
focus on non-magnetic O stars

Later:
magnetic OB stars

Circumstellar Dynamics at High Resolution

High energy view of OB star wind structure and dynamics (including clumping)

via (mostly) X-ray spectroscopy

Circumstellar Dynamics at High Resolution

High energy view of OB star wind structure and **dynamics** (including **clumping**)

Doppler shift/broadening

multi-wavelength diagnostics: ρ vs. ρ^2

via (mostly) X-ray spectroscopy

Chandra gratings (R < 1000)

Questions

How is hot (> 10^6 K), X-ray emitting plasma produced?

What are its kinematics? Its distribution in the stellar wind?

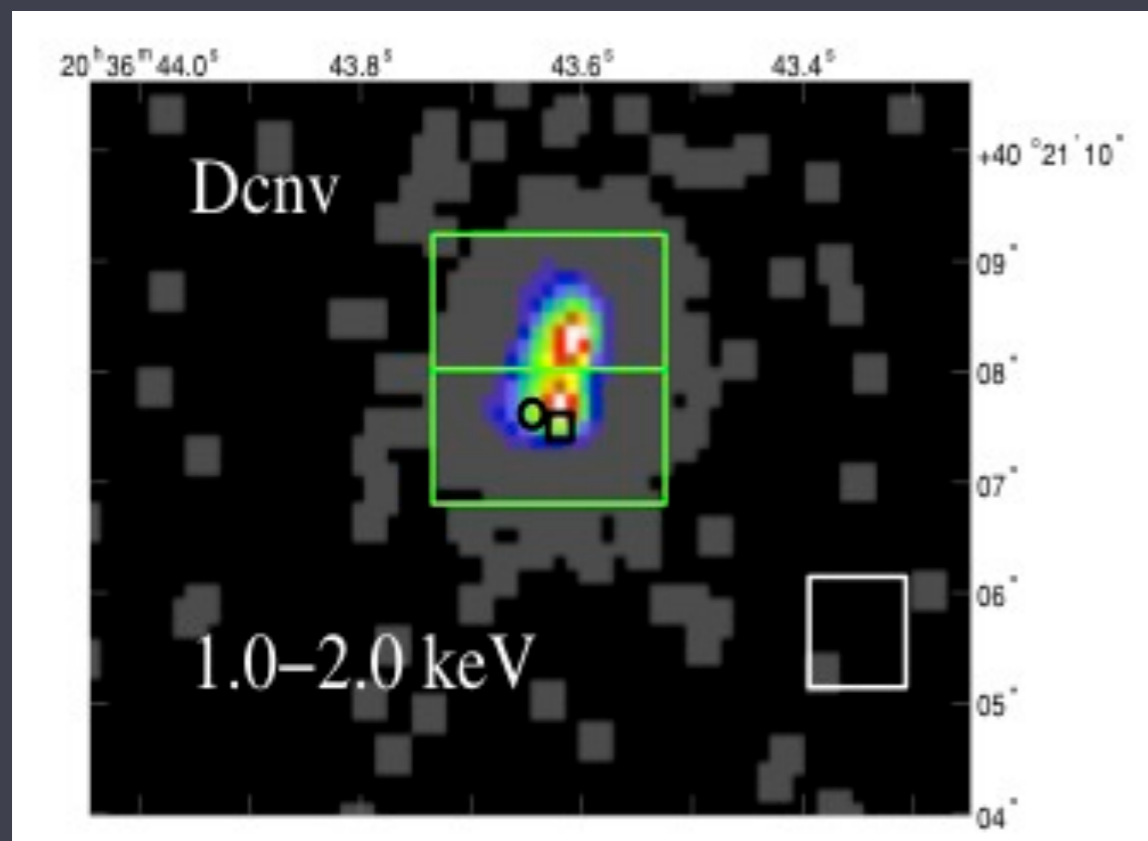What is the relationship among wind instabilities, X-rays, and wind structure/clumping?

Aside:

colliding wind binaries (CWBs) can be even stronger sources of X-rays

recent spatially resolved X-ray image of wind interaction region

WR 147: Zhekov et al. 2010

CWBs: beyond the scope of this talk

but interesting open questions:

- what determines level of X-ray emission (wind, binary properties)?
- role of thin-shell instabilities in shock-compressed wind interaction region

X-ray Spectral Formation

Thermal emission

Equilibrium

Optically thin

X-ray Spectral Formation

like the solar corona

low density

Thermal emission

Equilibrium

Optically thin

collisions up, spontaneous down; nearly all bound electrons in the ground state; "coronal approximation" ⇒ emission line dominated

X-ray Spectral Formation

like the solar corona

low density

Thermal emission

Equilibrium

Optically thin

steady-state; Maxwellian, $T_i = T_e$; ionization: collisional from ground state = recombination

X-ray Spectral Formation

like the solar corona

low density

Thermal emission

Equilibrium

Optically thin

some strong lines may show optical depth effects (2nd order effect on spectra); *But*, cold wind component can be optically thick to X-rays produced in the hot component

X-ray Spectral Formation

plasma with $T > 10^6$ K radiates X-rays ($h\nu > 100$ eV)

shocks heat plasma to $T \sim 10^6$ K
if $\Delta V_{shock} \sim 300$ km/s
and $T \sim (\Delta V_{shock})^2$

cool stars   vs.   hot stars

starfish, *in situ*, at the Monterey (California) Aquarium

Chandra grating (HETGS/MEG) spectra
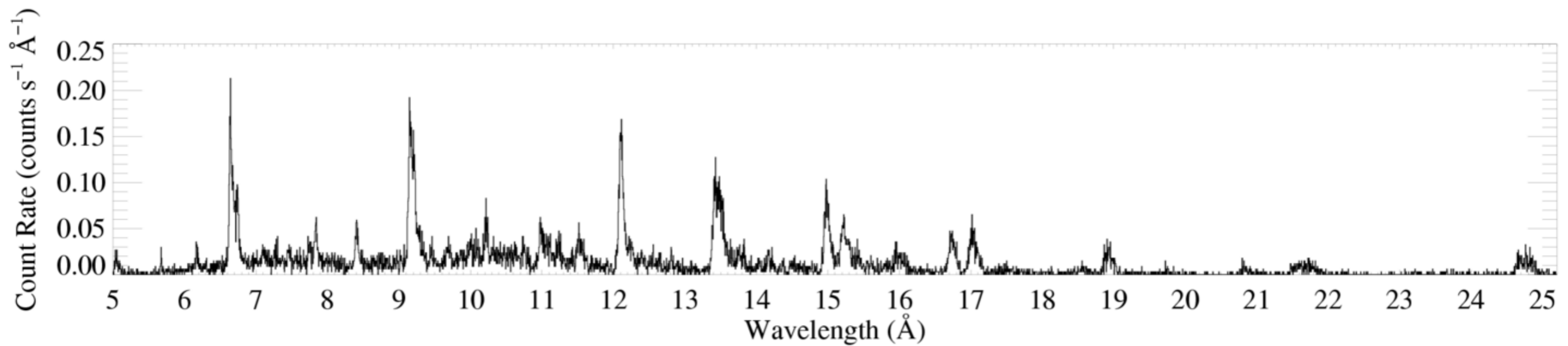
ζ Pup (O4 If)

5Å   15Å   25Å
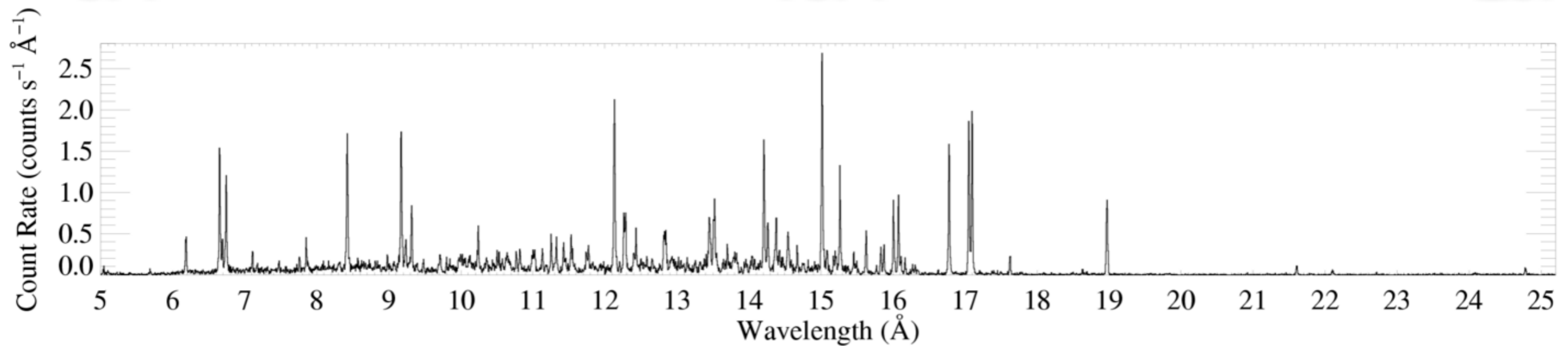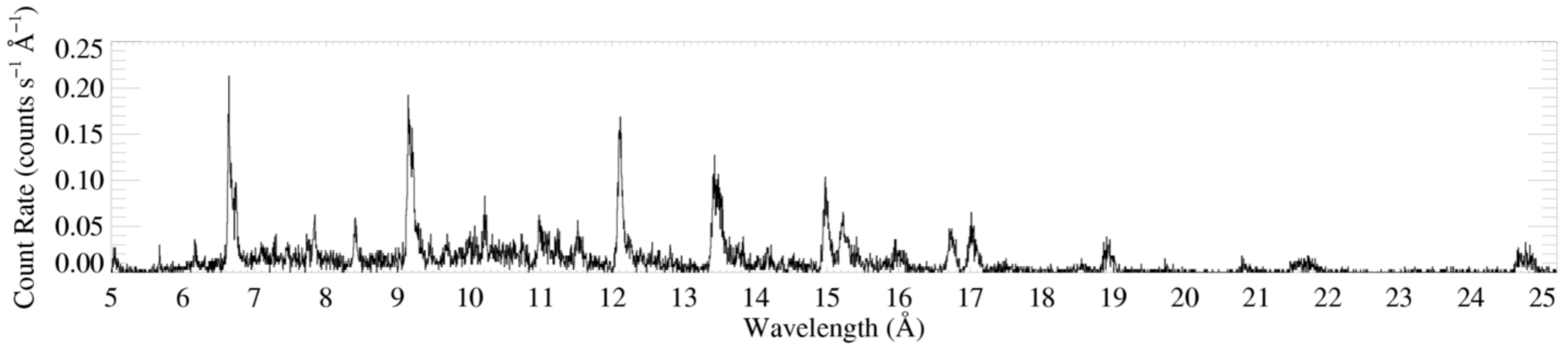
Capella (G5 III)
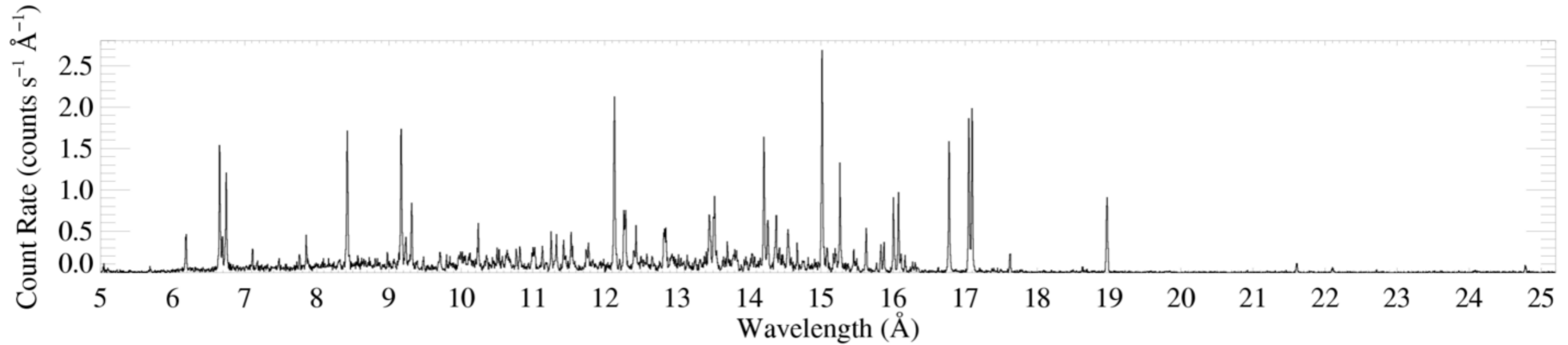
ζ Pup (O4 If)

Capella (G5 III)

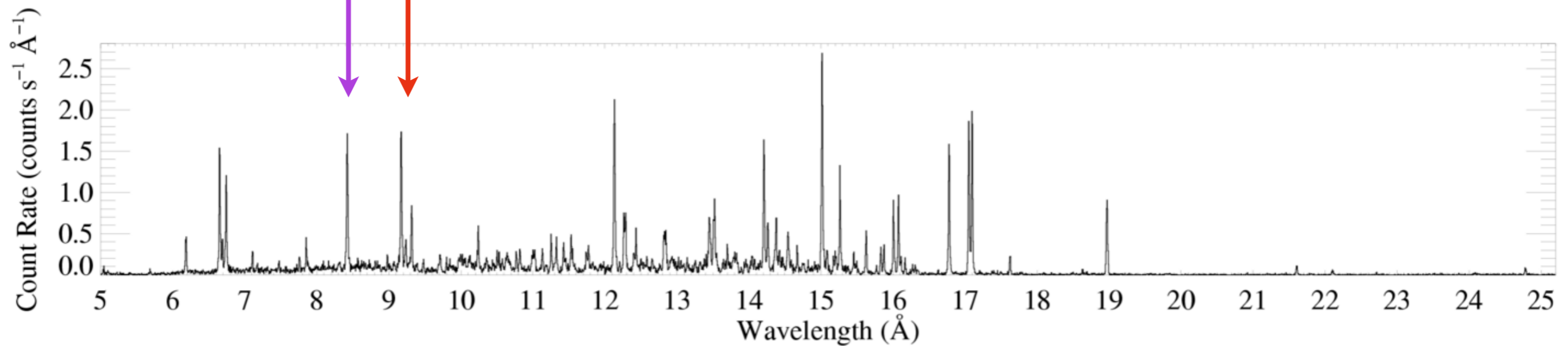*Chandra* grating (HETGS/MEG) spectra

ζ Pup (O4 If)

Mg XII   Mg XI   Ne X   Ne IX
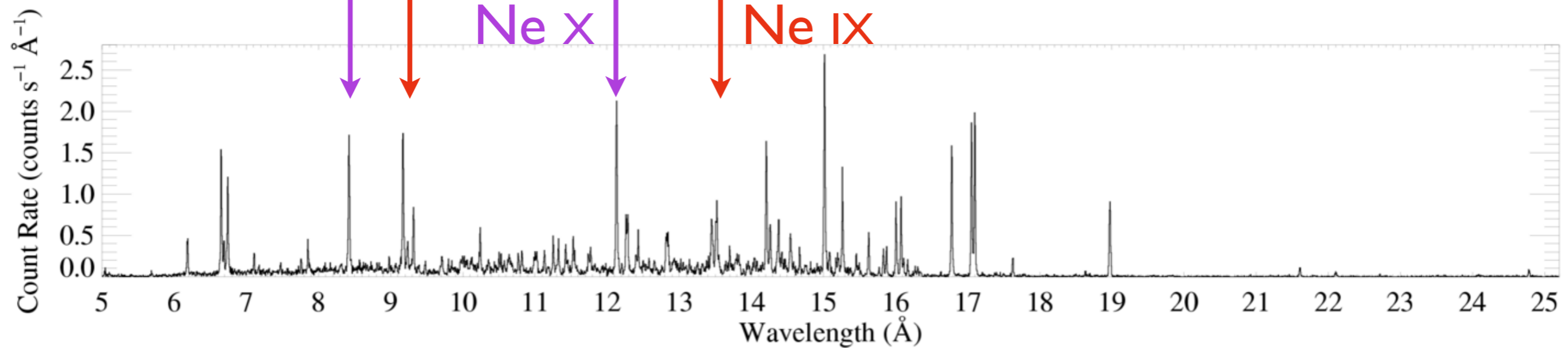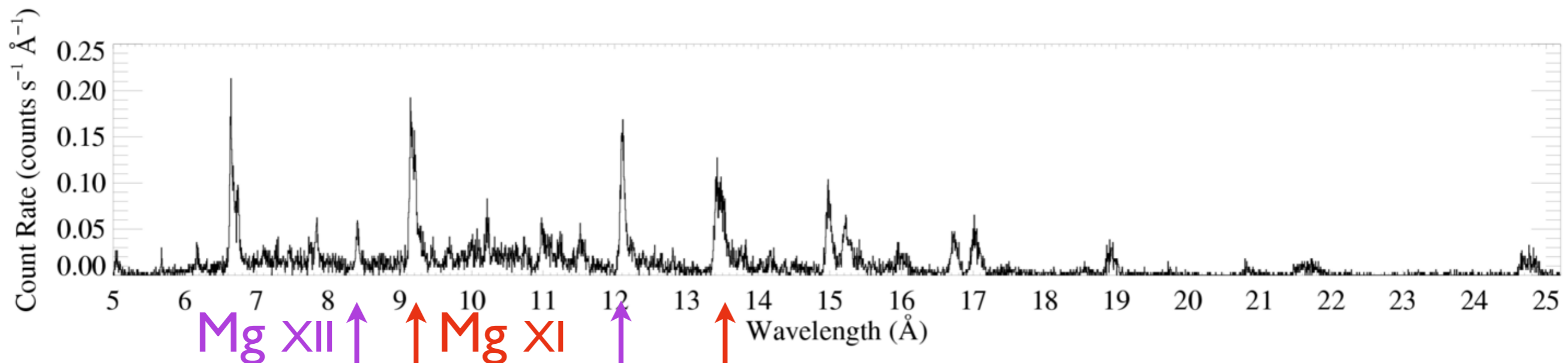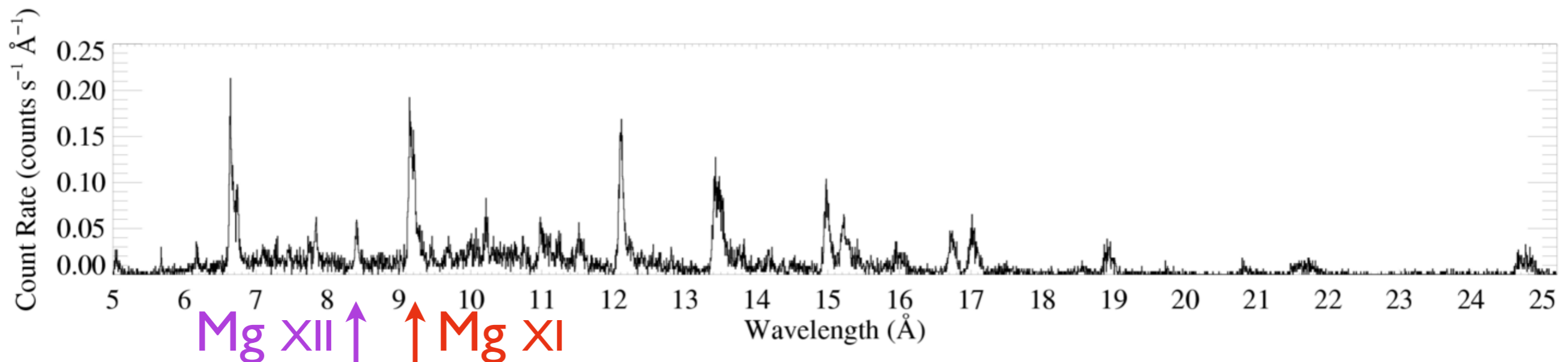
Capella (G5 III)

typical temperatures $T \sim$ few 10^6 K
(late-type stellar coronae tend to be hotter)   ζ Pup (O4 If)

Mg XII   Mg XI

Capella (G5 III)

Zoom in

ζ Pup (O4 If)

Ne X   Ne IX   Fe XVII

Capella (G5 III)

ζ Pup (O4 If)

Ne X   Ne IX   Fe XVII

~2000 km/s

Capella (G5 III)

ζ Pup (O4 If)

Ne X   Ne IX   Fe XVII

~2000 km/s

(unresolved)
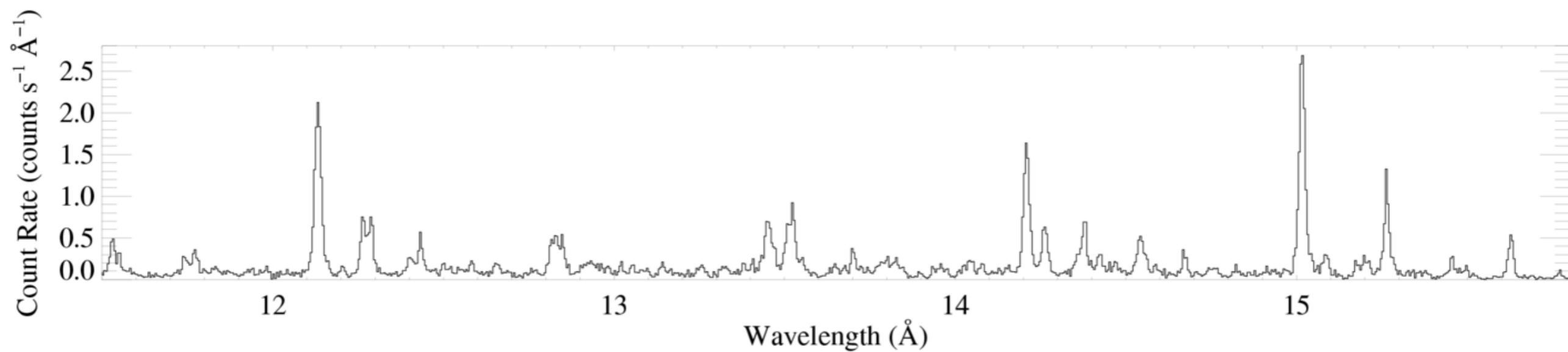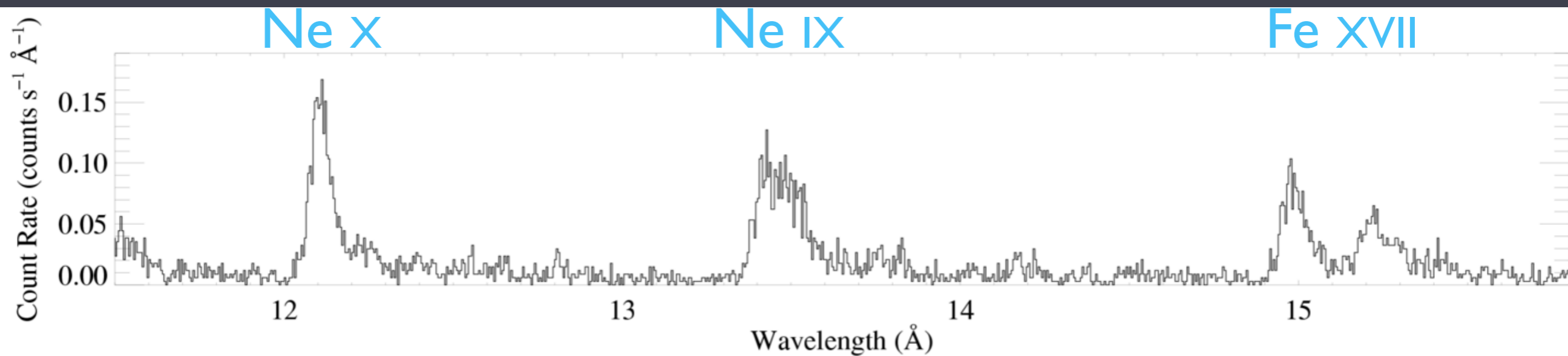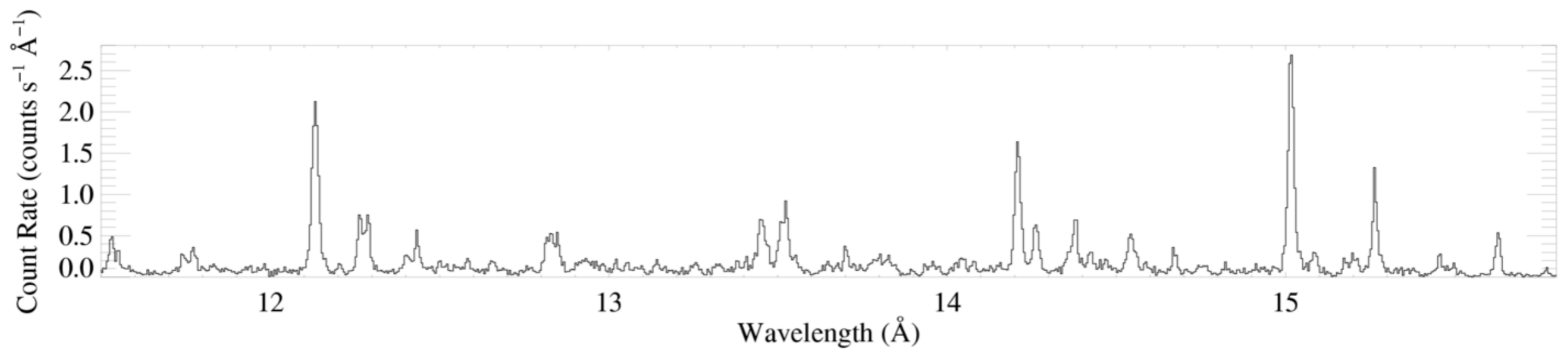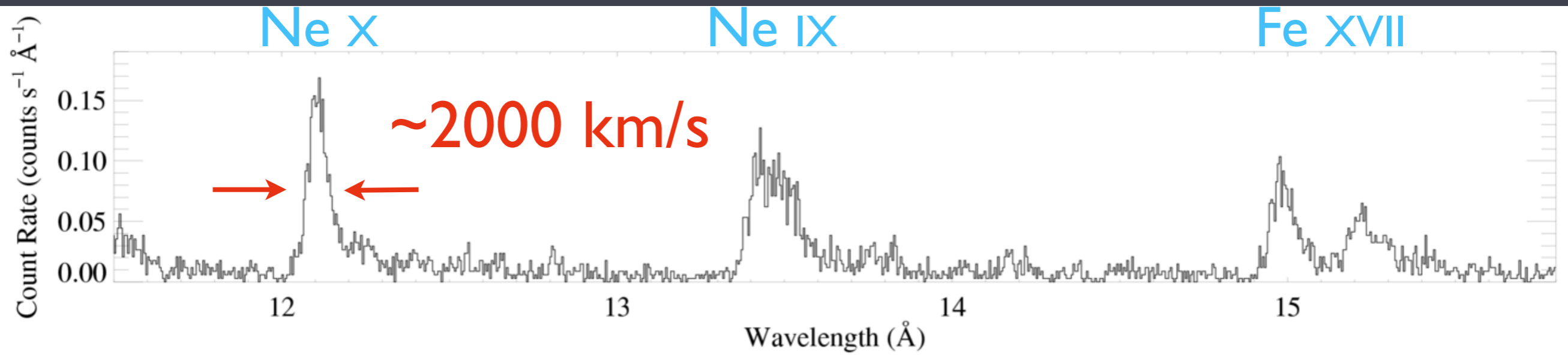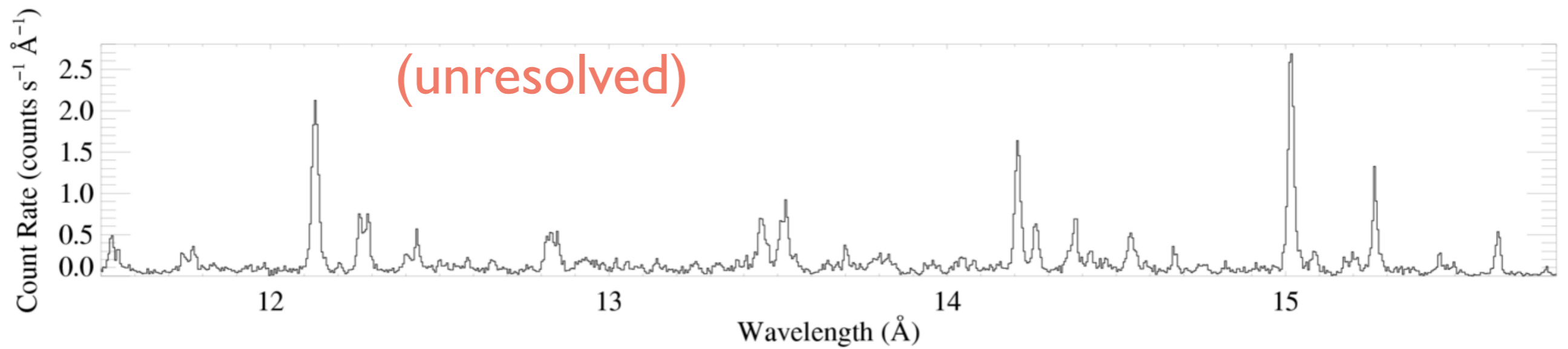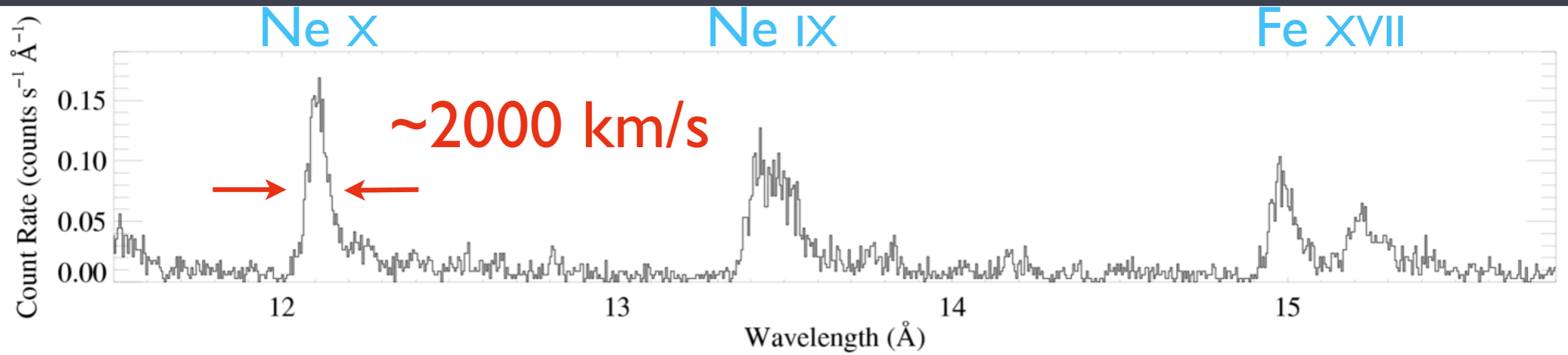
Capella (G5 III)

cool stars: narrow lines = magnetically confined coronal plasma

hot stars: broad lines = outflowing, shock-heated wind plasma

What produces the hot, X-ray emitting plasma in massive stars?

plasma with $T > 10^6$ K radiates X-rays (h$\nu > 100$ eV)

shocks heat plasma to $T \sim 10^6$ K
if $\Delta V_{shock} \sim 300$ km/s
and $T \sim (\Delta V_{shock})^2$

What produces the hot, X-ray emitting plasma in massive stars?
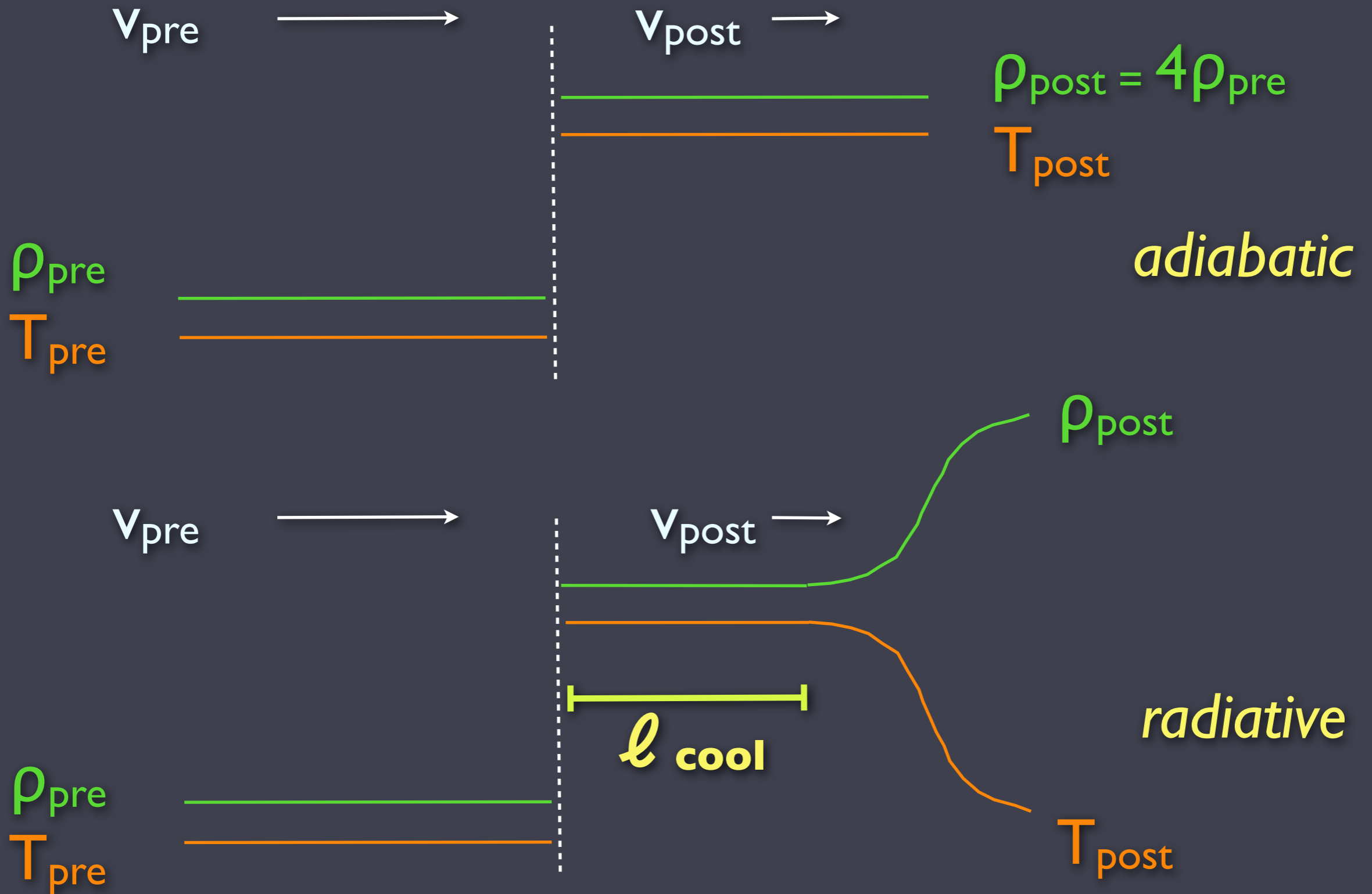
plasma with $T > 10^6$ K radiates X-rays (hν > 100 eV)

shocks heat plasma to $T \sim 10^6$ K
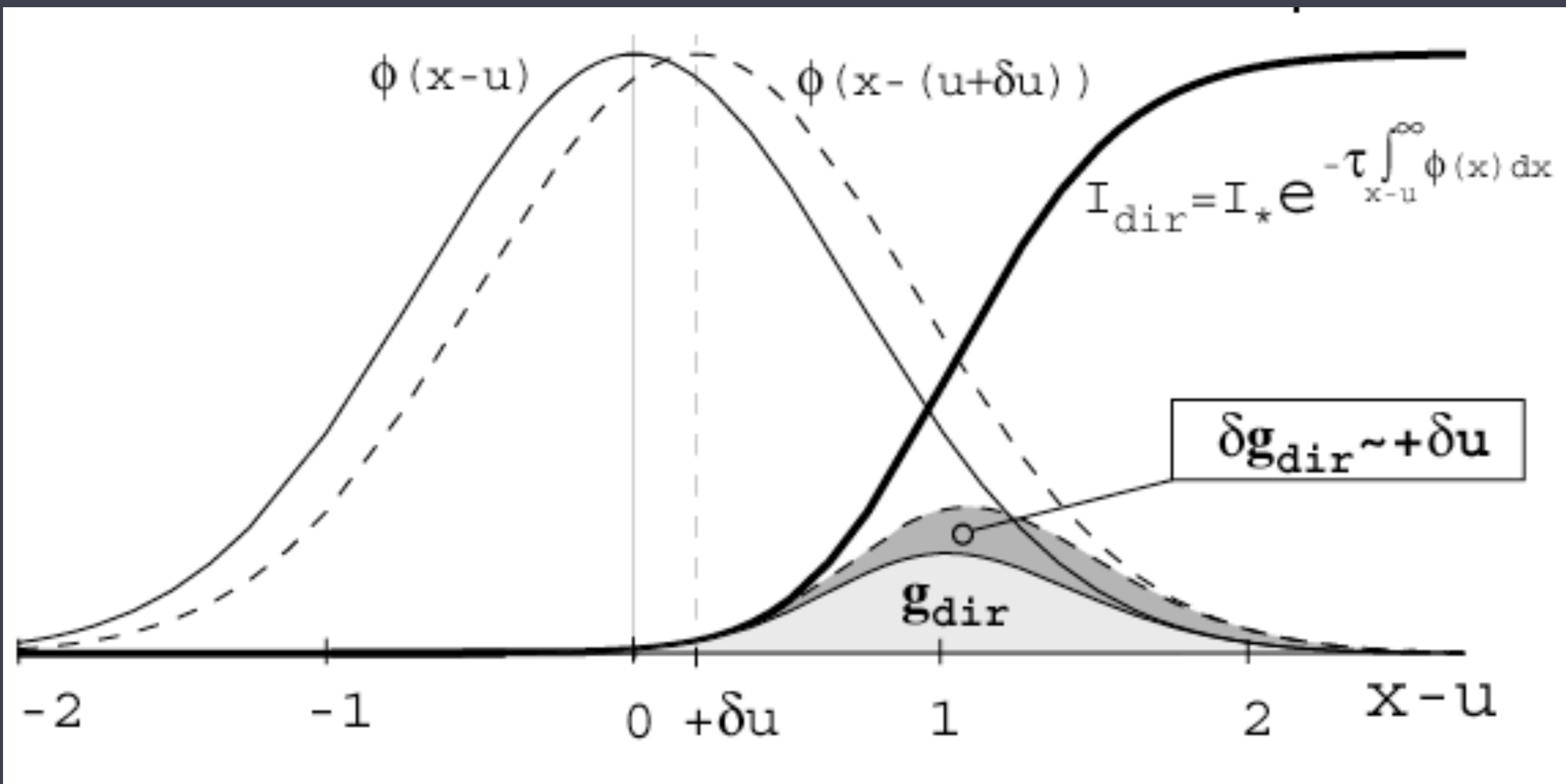if $\Delta V_{shock} \sim$ 300 km/s
and $T \sim (\Delta V_{shock})^2$

shocks are *radiative* in dense O star winds, but *adiabatic* in lower-density early B star winds

Theory

$$\phi(x-u) \qquad \phi(x-(u+\delta u))$$

$$I_{dir} = I_* e^{-\tau \int_{x-u}^{\infty} \phi(x)\,dx}$$

$$\delta g_{dir} \sim +\delta u$$

$$g_{dir}$$

$$-2 \qquad -1 \qquad 0 \ +\delta u \qquad 1 \qquad 2 \qquad x-u$$

positive velocity perturbation

line profile

photospheric radiation

$\phi(x-u)$

$\phi(x-(u+\delta u))$

$I_{dir} = I_* e^{-\tau \int_{x-u}^{\infty} \phi(x)\,dx}$

$\delta g_{dir} \sim +\delta u$

g_{dir}

$-2 \quad -1 \quad 0 \quad +\delta u \quad 1 \quad 2 \quad x-u$
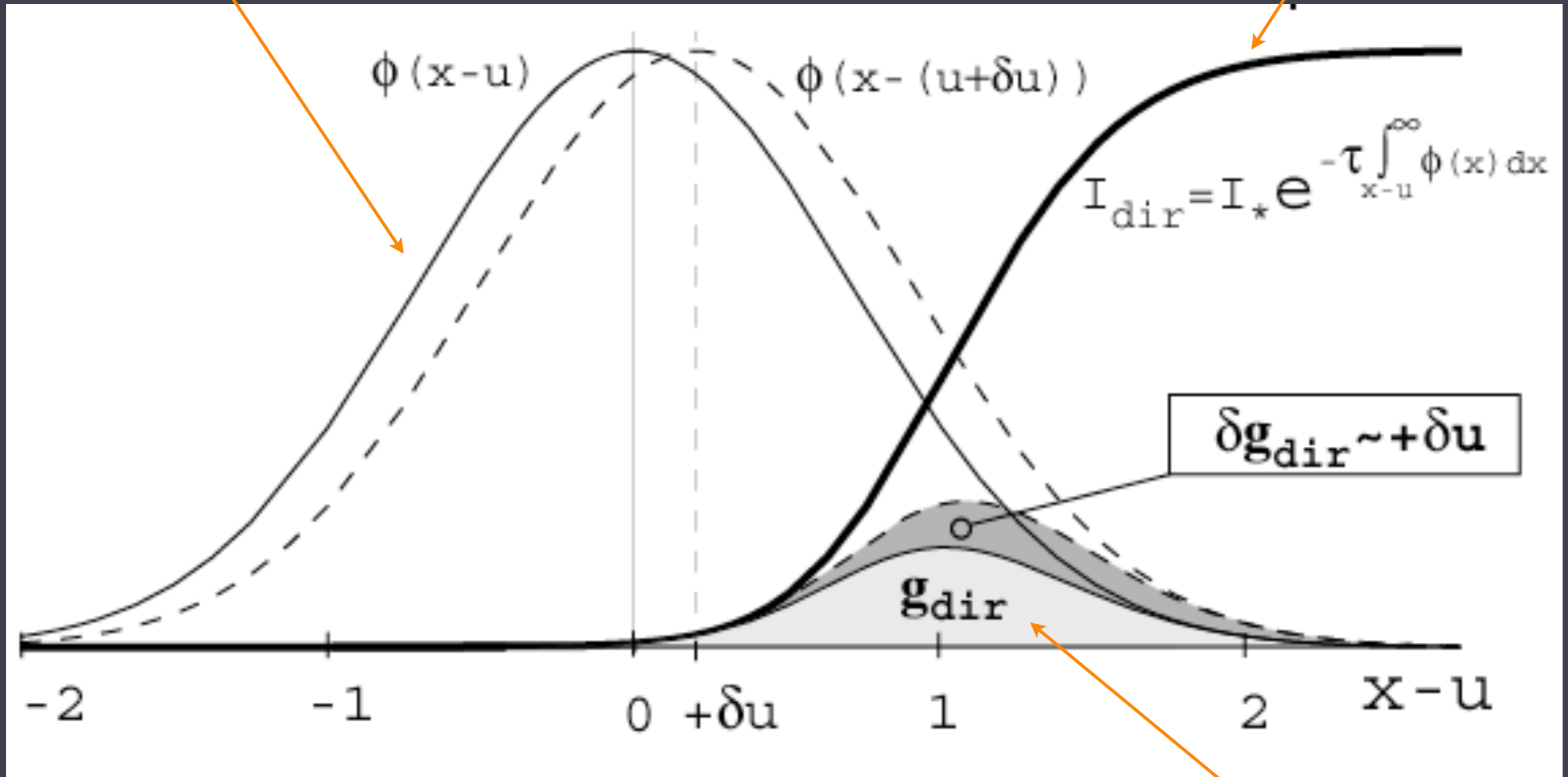
frequency

radiation force

positive velocity perturbation

line profile

photospheric radiation

$\phi(x-u)$

$\phi(x-(u+\delta u))$

$I_{dir} = I_* e^{-\tau \int_{x-u}^{\infty} \phi(x)\,dx}$

$\delta \mathbf{g}_{dir} \sim + \delta u$

$\mathbf{g}_{dir}$
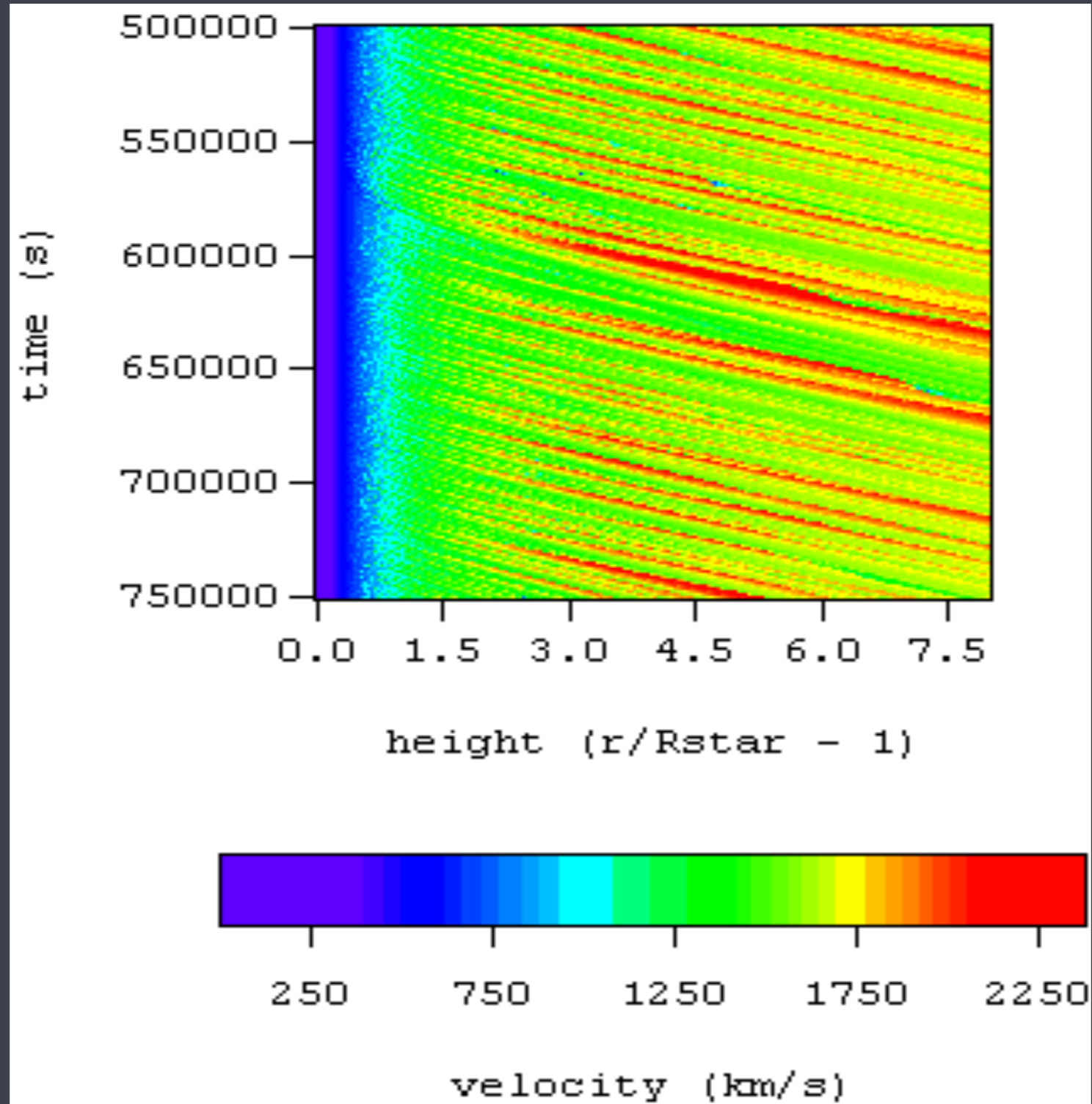
-2 $\quad -1 \quad$ 0 $+\delta u$ $\quad 1 \quad$ 2 $\quad x-u$
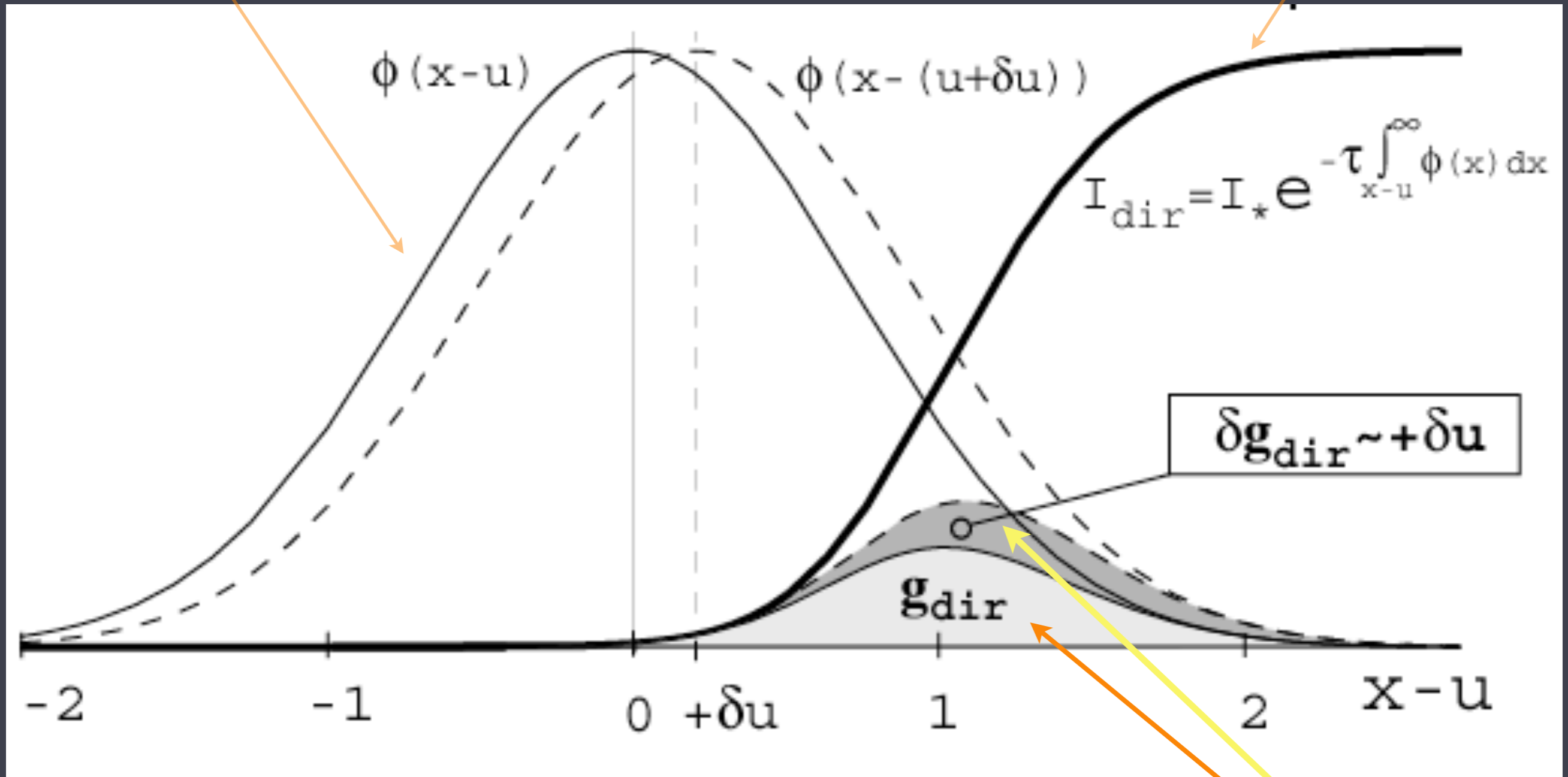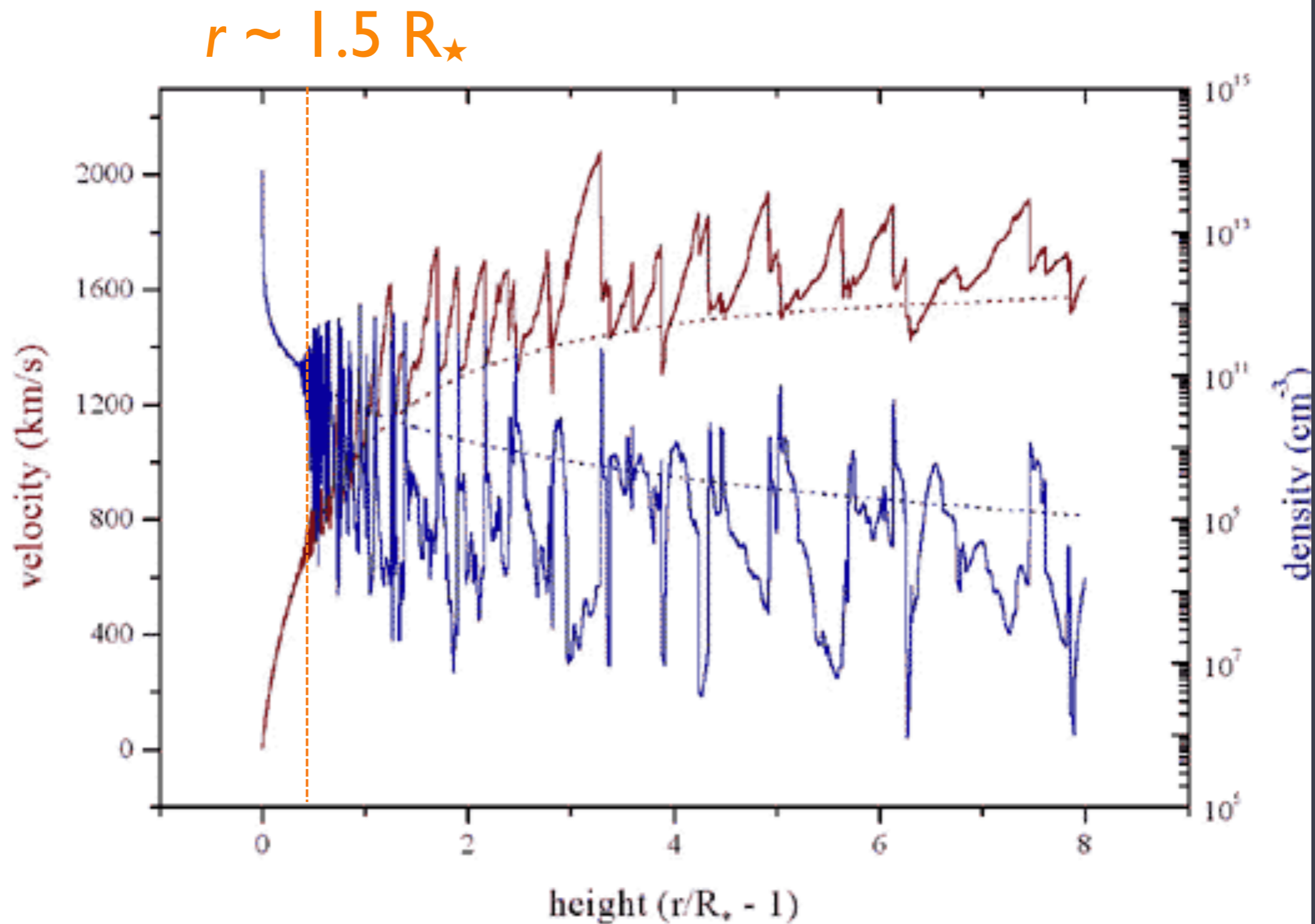
frequency

radiation force **increases**

Numerical simulations of the line-deshadowing instability (LDI)

Owocki, Cooper, Cohen 1999

shock jump velocities ~ few 100 km/s

r ~ 1.5 R★
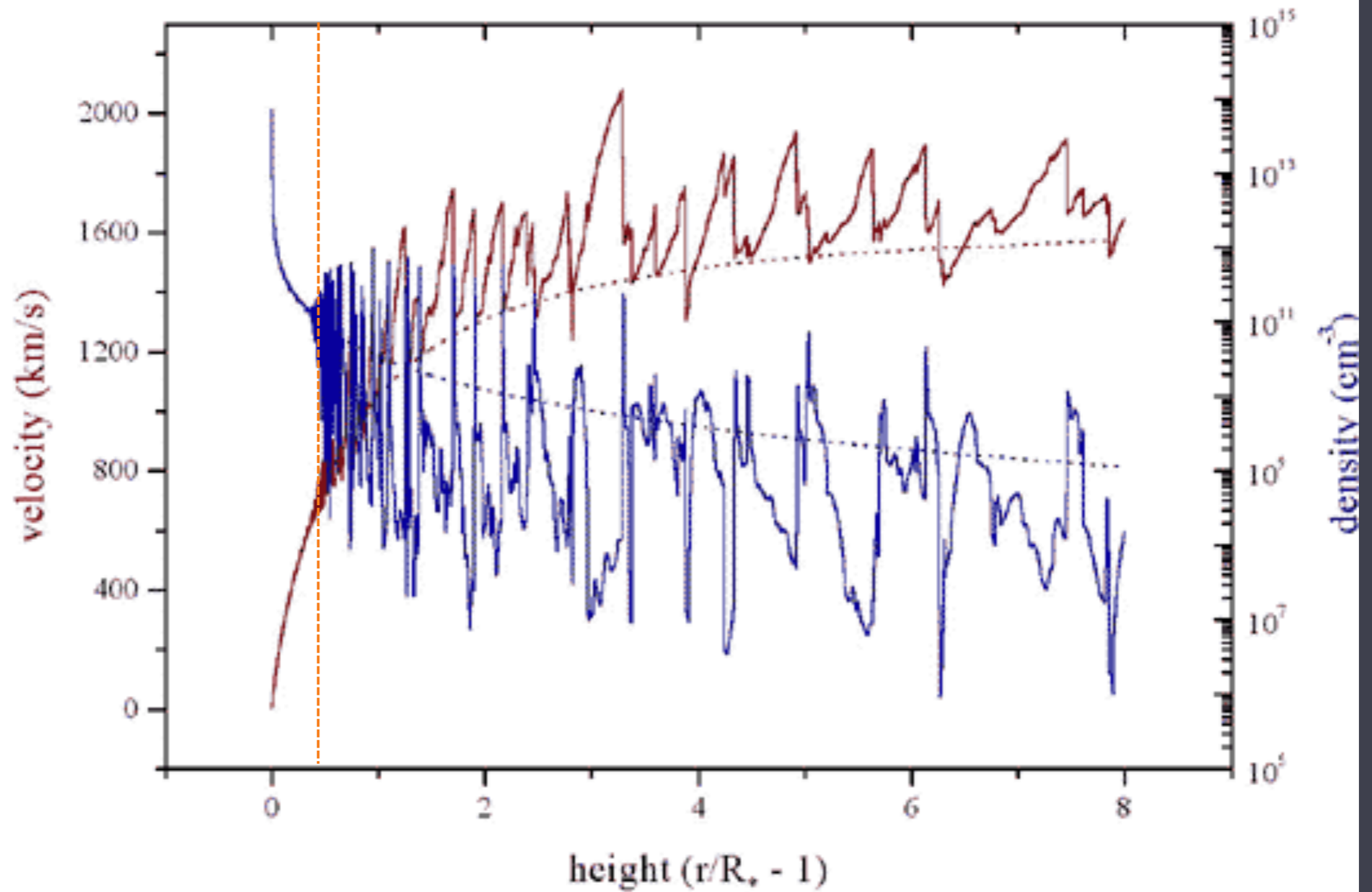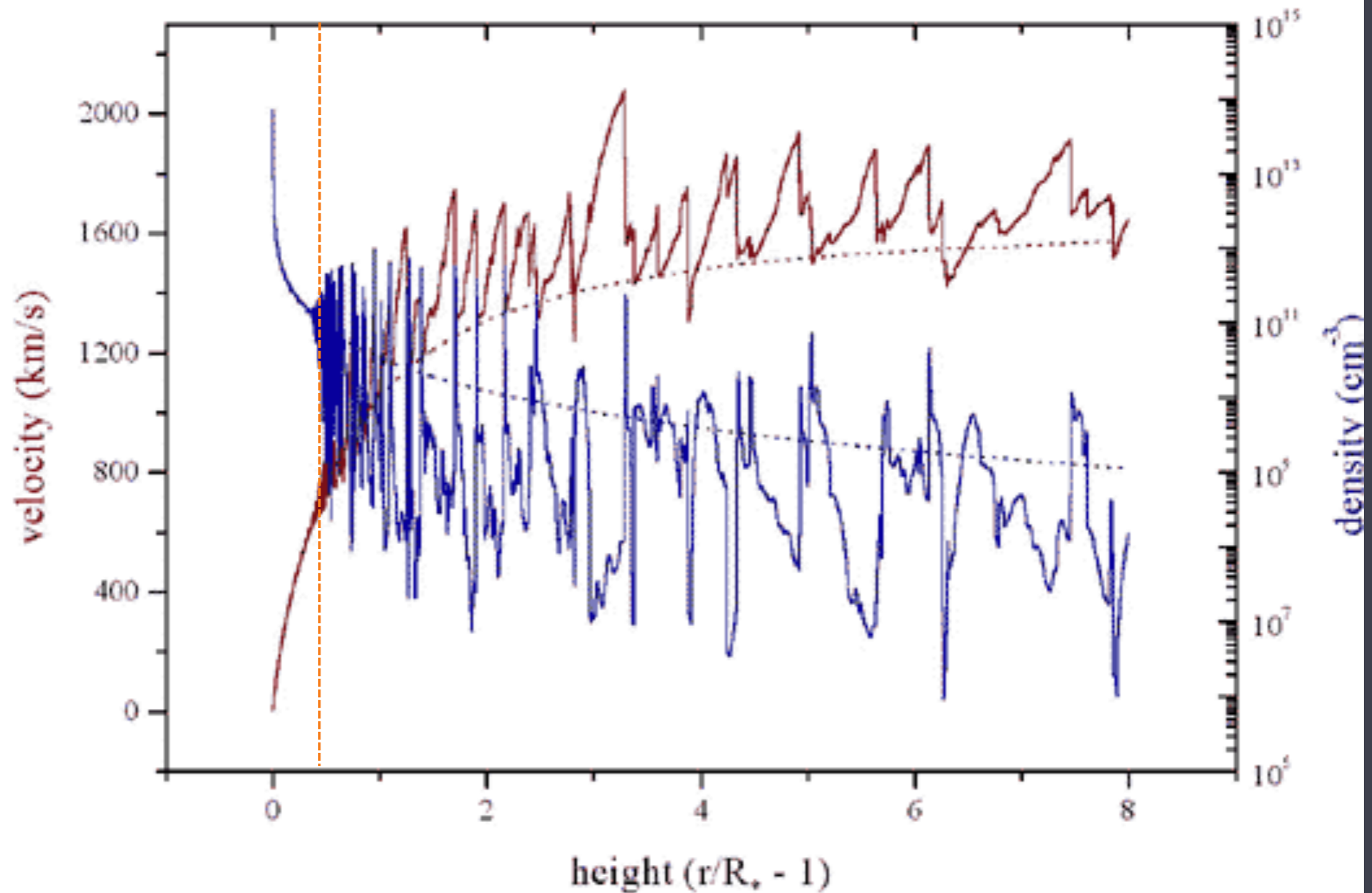
$V_{shock} \sim 300$ km/s : $T \sim 10^6$ K
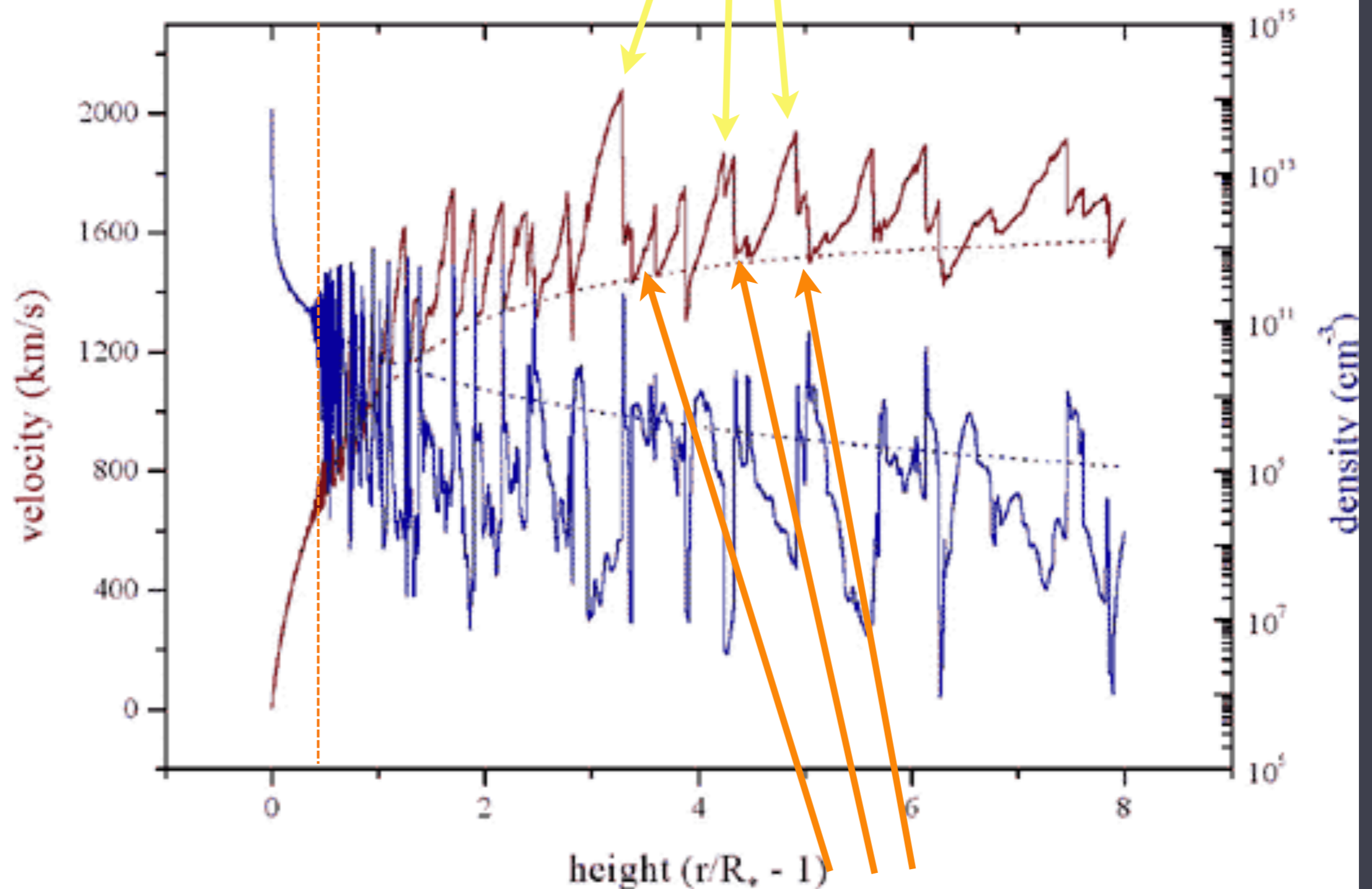
shocked wind plasma is decelerated back down to the local CAK wind velocity

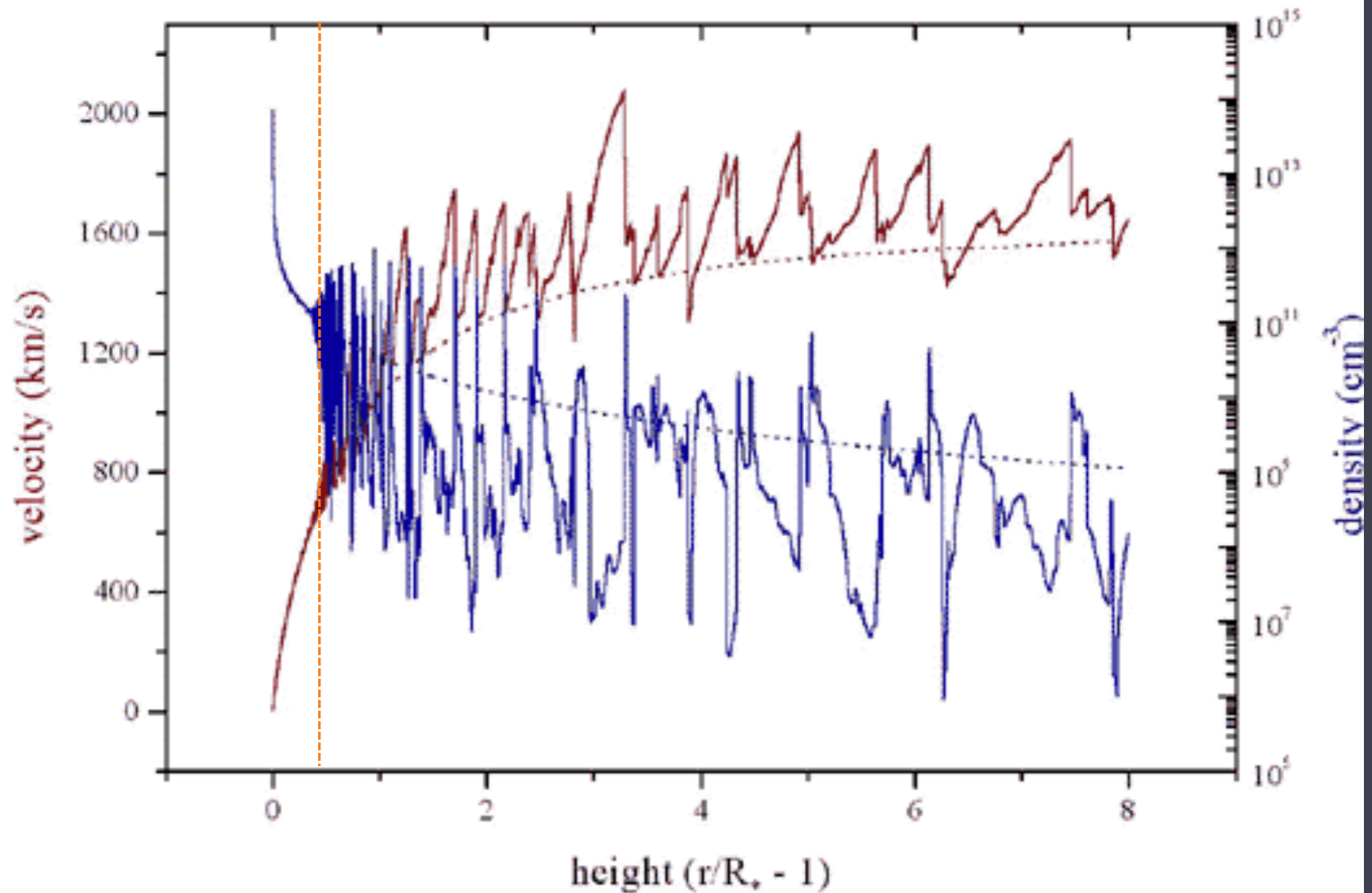# Shocked plasma is moving at *v* ~ 1000 km/s

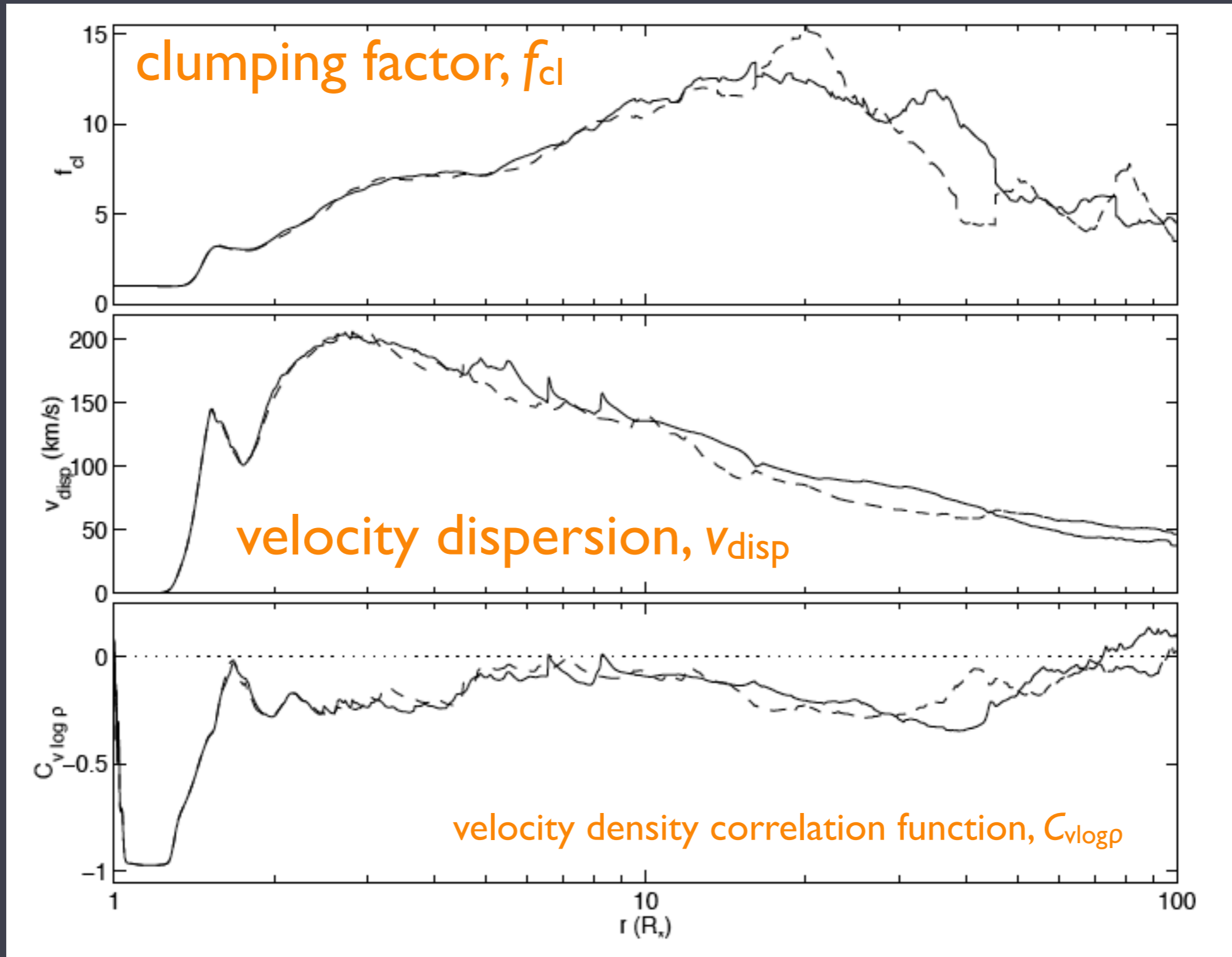# X-ray emission lines should be **Doppler broadened**

Less than 1% of the wind is emitting X-rays

>99% of the wind is cold and X-ray *absorbing*

Statistics (time-average quantities) from 1-D simulations

clumping factor, f_{cl}

velocity dispersion, v_{disp}

velocity density correlation function, $C_{vlog\rho}$

Runacres & Owocki 2002

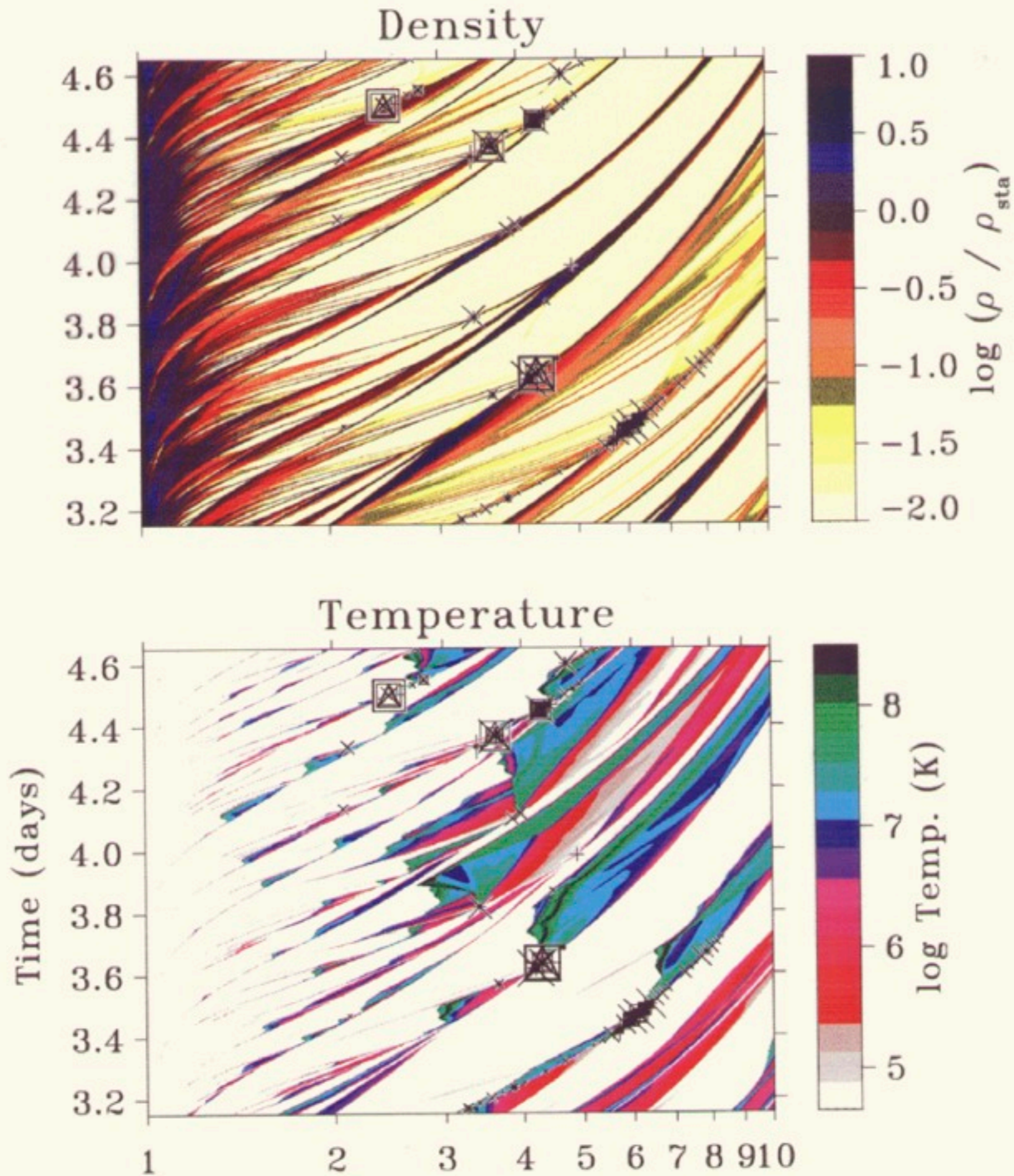The instability in these simulations is not seeded

the predicted X-ray flux is too low

sound waves or turbulence at the wind base seeds the instability and leads to clump-clump collisions

Feldmeier et al. 1997

Density

Temperature
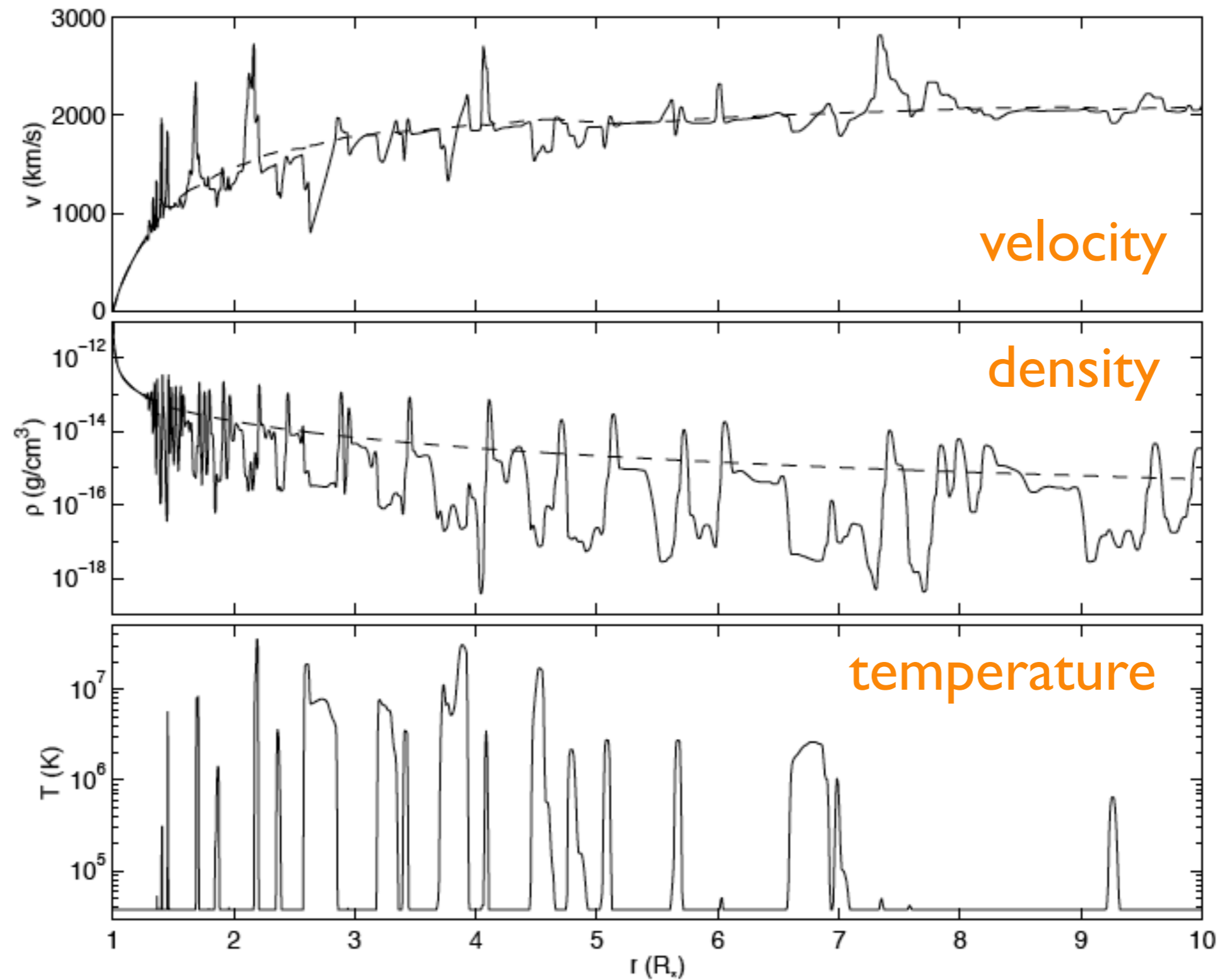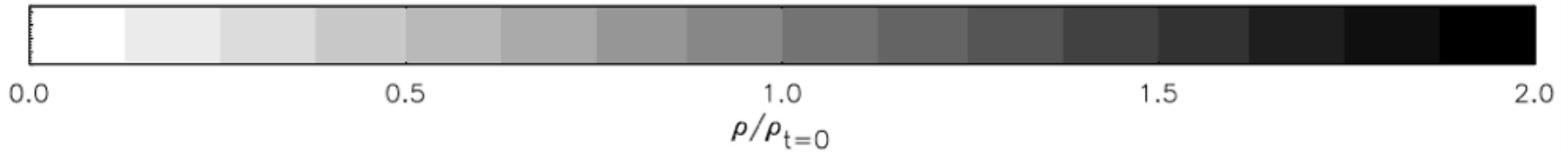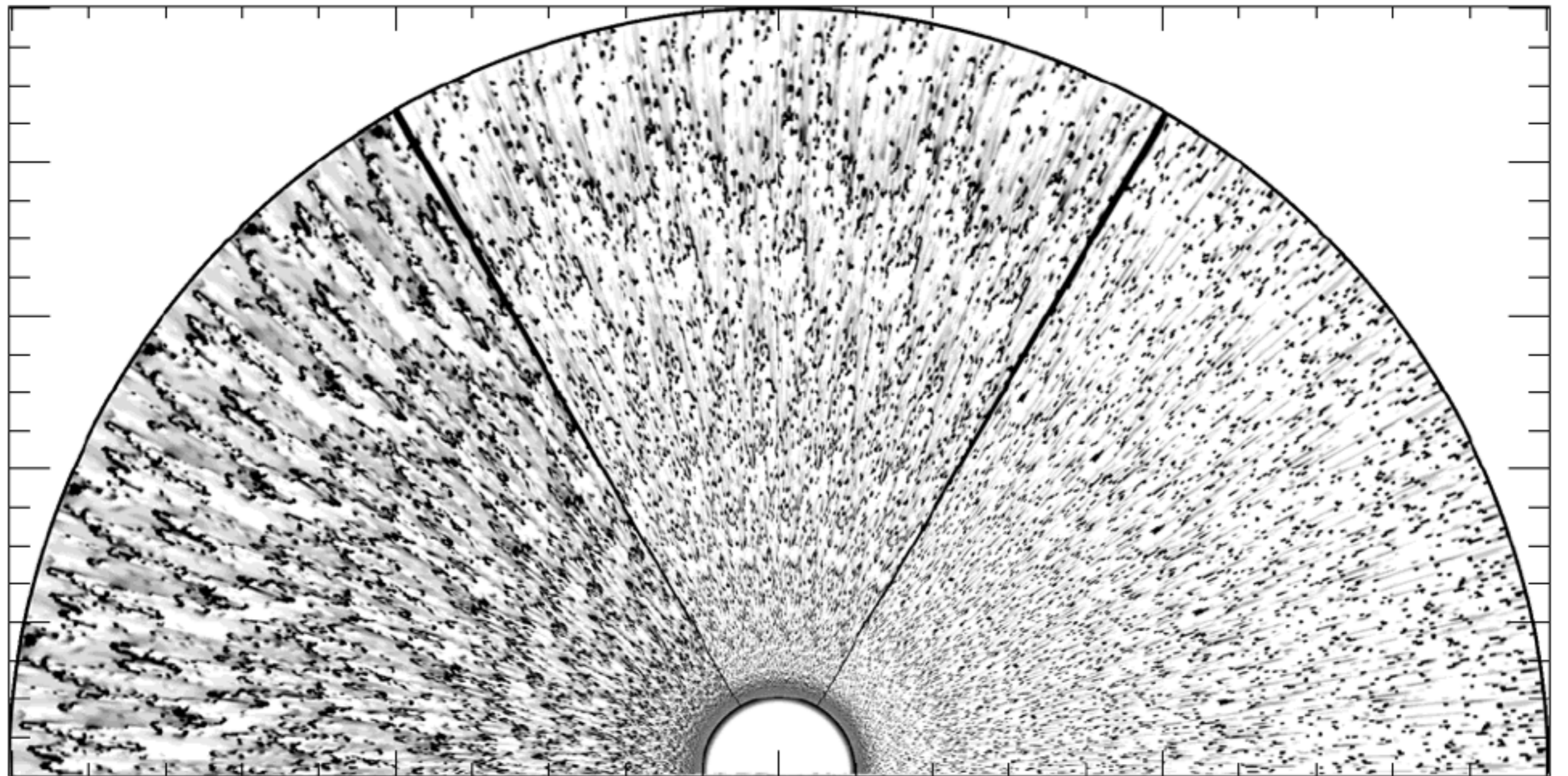
time

Time (days)

$\log (\rho / \rho_{sta})$

log Temp. (K)
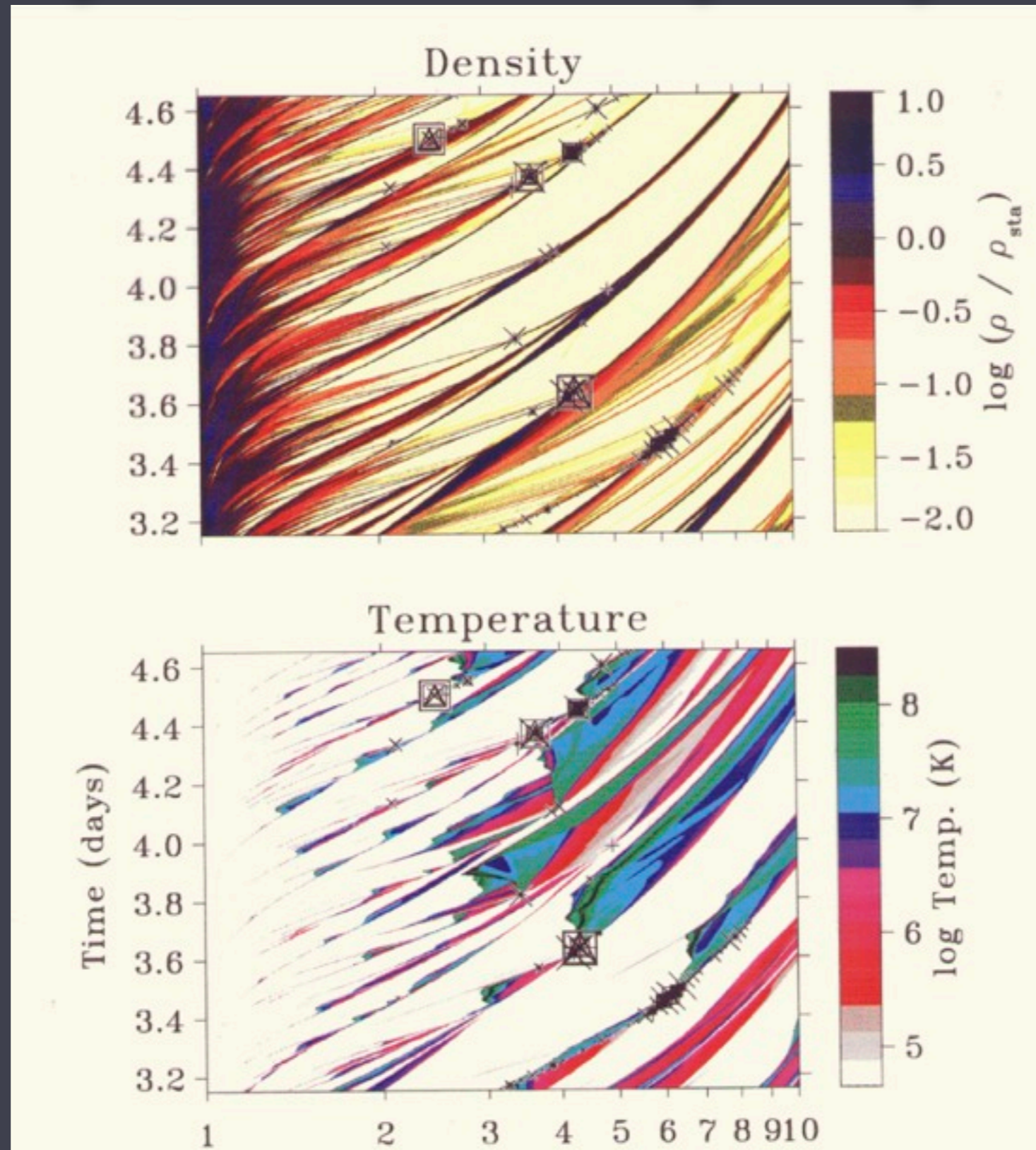
Fig. 8. Snapshot of the inner wind at 2.0 Msec after the start of the simulation, for the model with $\kappa_{max} = 10^{-2}\kappa_0$. The dashed line in the upper panels represents time-averaged values.

1-D is a severe limitation

lack of observed time variability suggests
numerous (>100) individual post-shock cooling
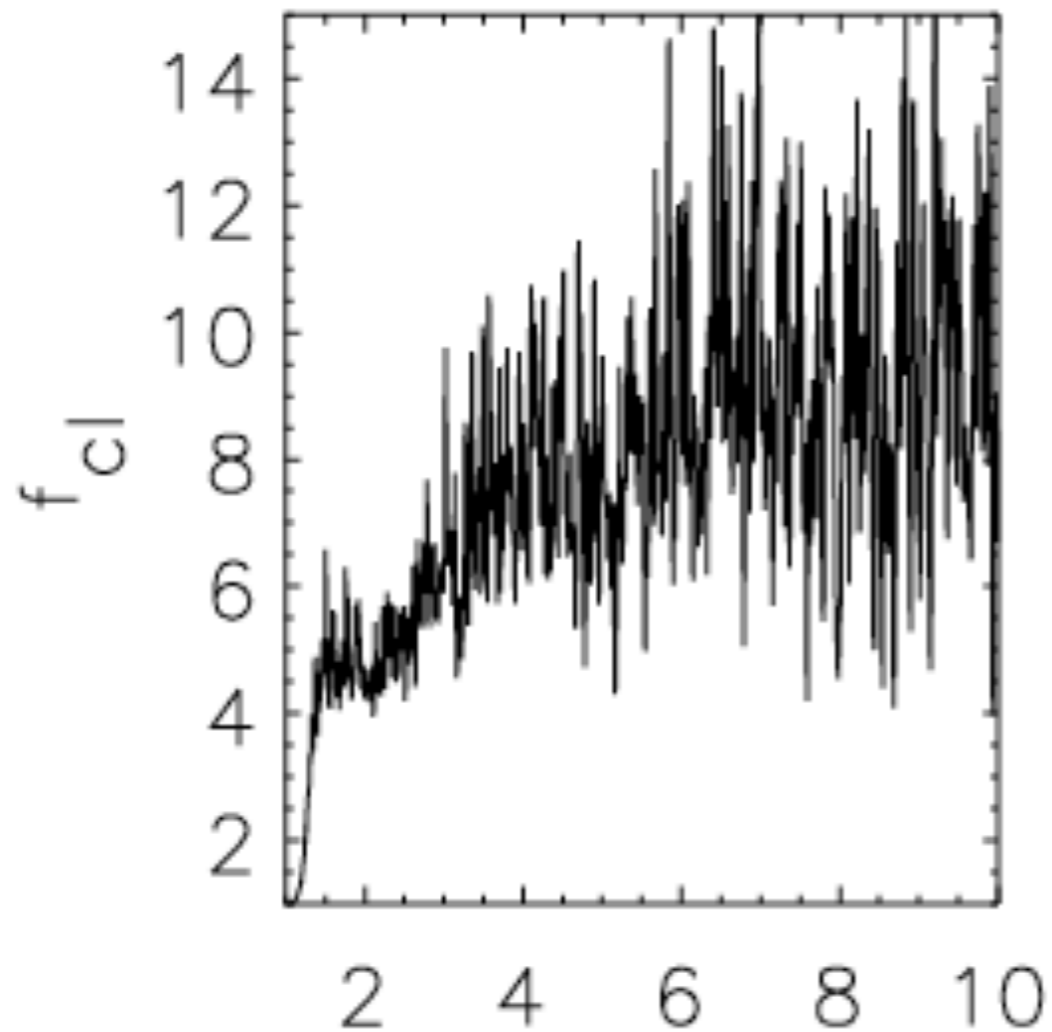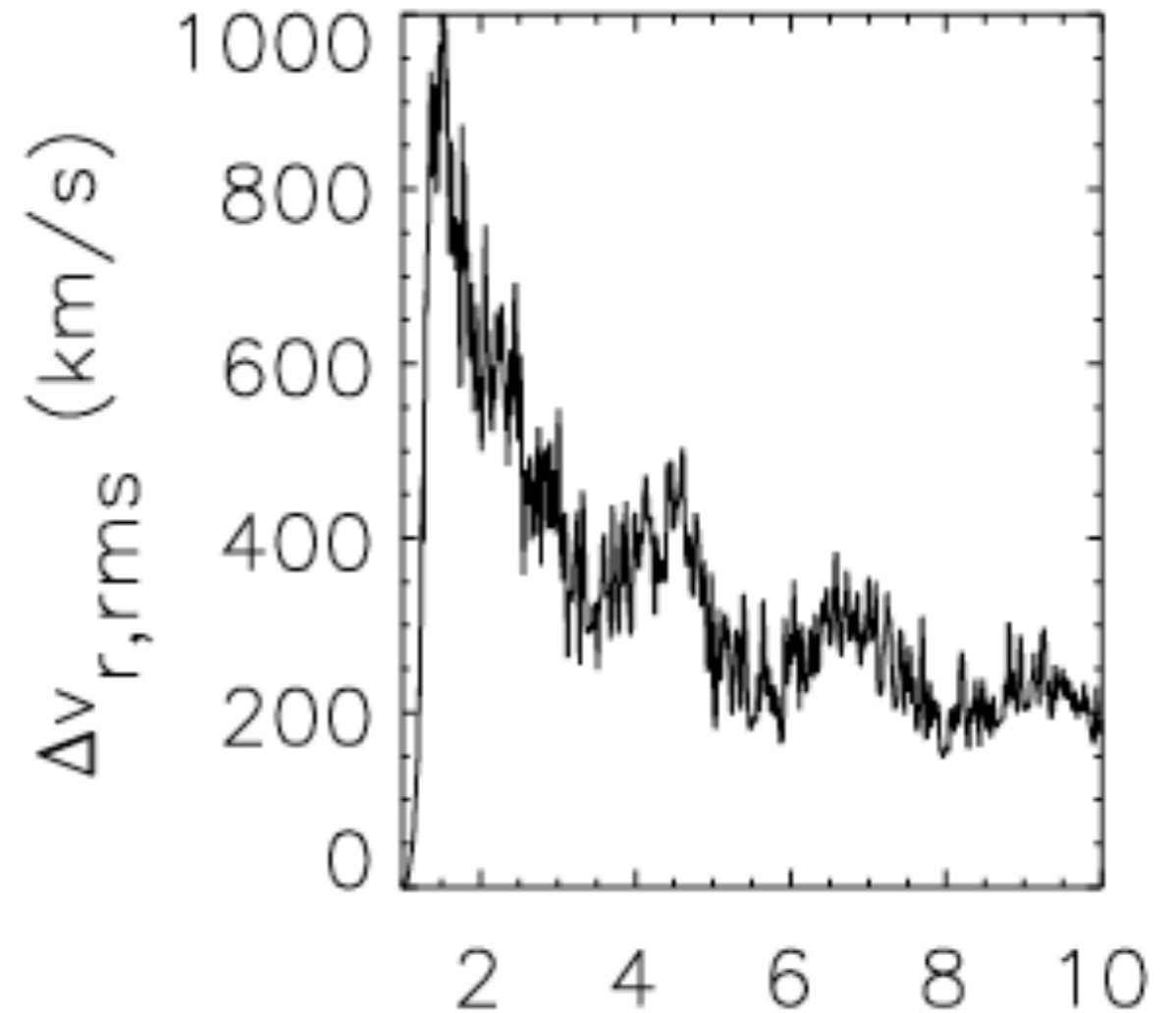volumes in the wind

2-D simulations

$\rho / \rho_{t=0}$

Dessart & Owocki 2003

Statistics (time-average quantities) from 2-D simulations

clumping factor, f_{cl} velocity dispersion, v_{rms}

height (R⋆)   height (R⋆)

Dessart & Owocki 2005

Summary of hydro simulation results

- line-deshadowing instability is robust

- seeding the instability with sound waves or turbulence at the base leads to clump-clump collisions & enhanced X-ray production

- small-scale clumping, with over-density of $f_{cl} \sim 10$

- shocks start producing hot plasma above $r \sim 1.5\ R_\star$ thus the X-ray emitting plasma is at high velocity

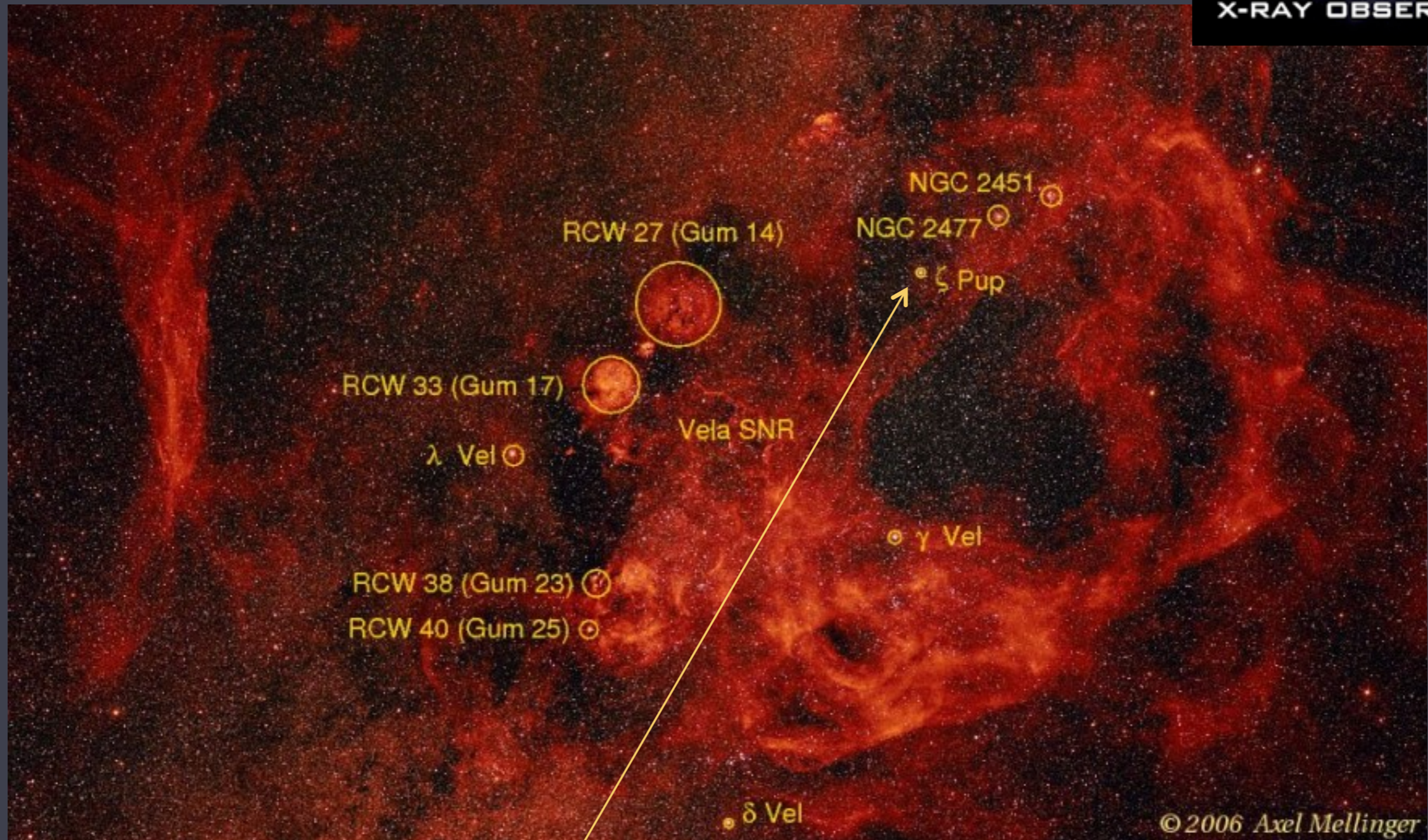2-D models developed in the 2000s, but no energy equation and lateral radiation transport is rudimentary

major result: structures/clumps are quite small

also, velocity dispersion is higher than in 1-D models

Let's look at some data - X-ray spectra - in light of this context

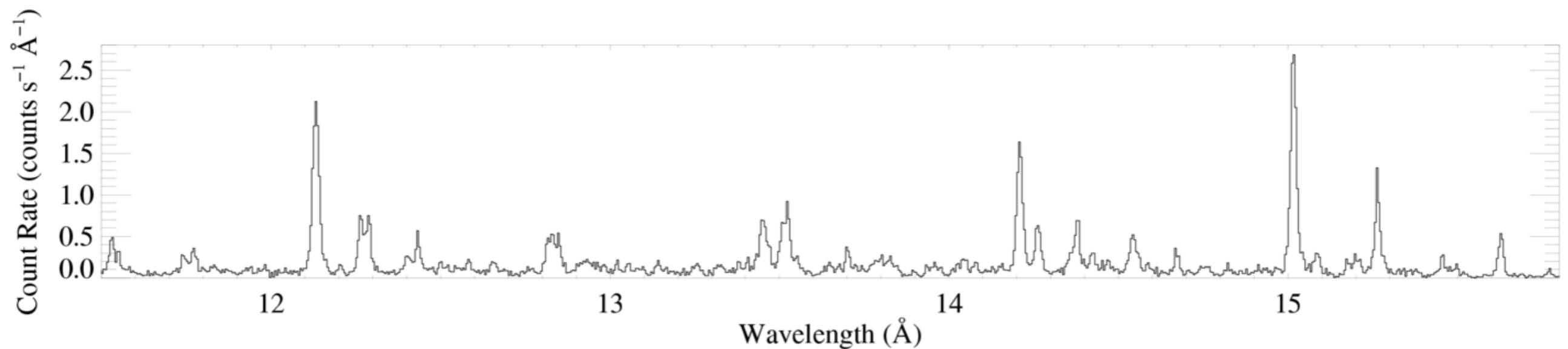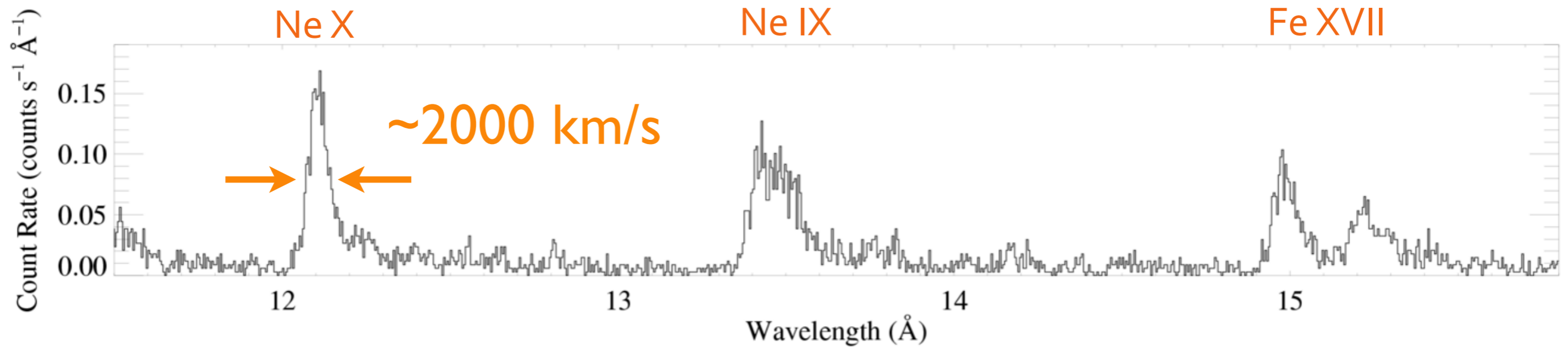*Chandra* grating spectroscopy (R < 1000)

ζ Pup (O4 If)

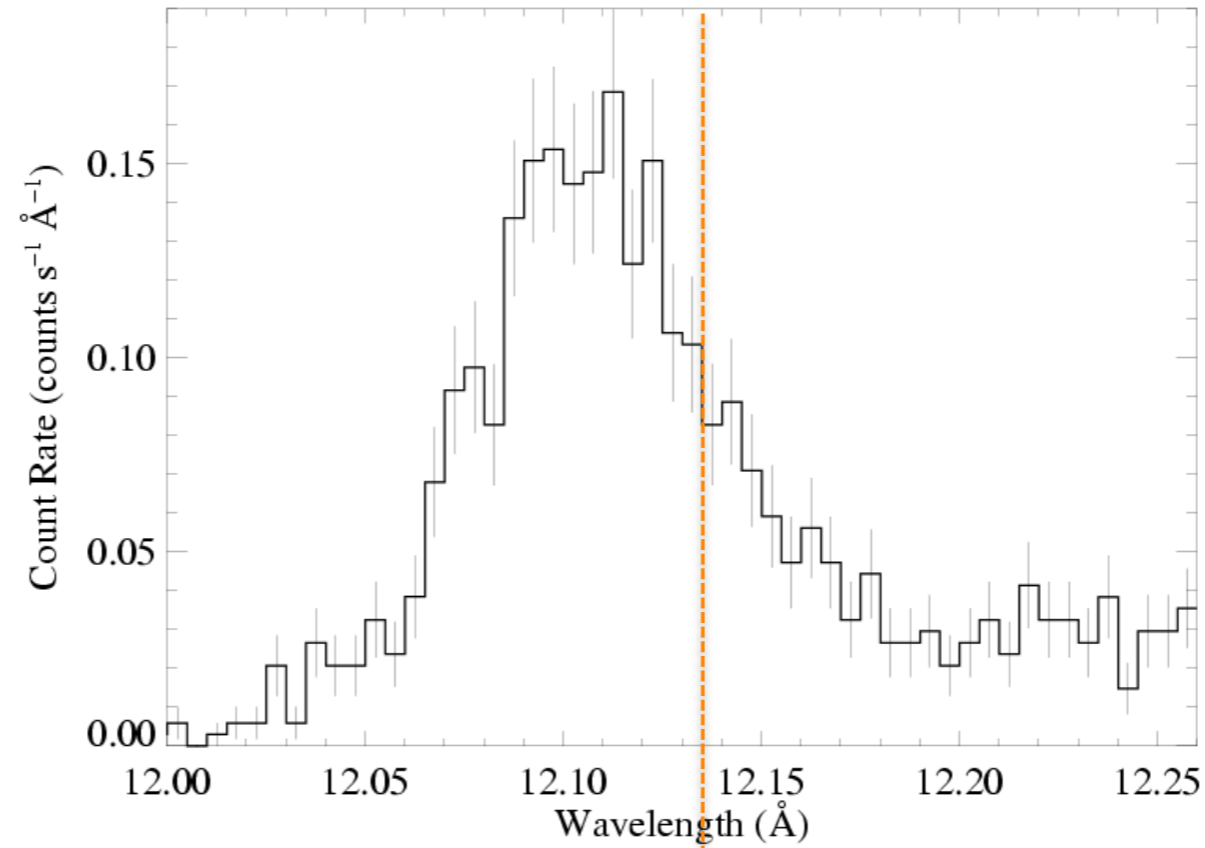# O supergiant X-ray emission lines are **broad**

Chandra grating spectrum
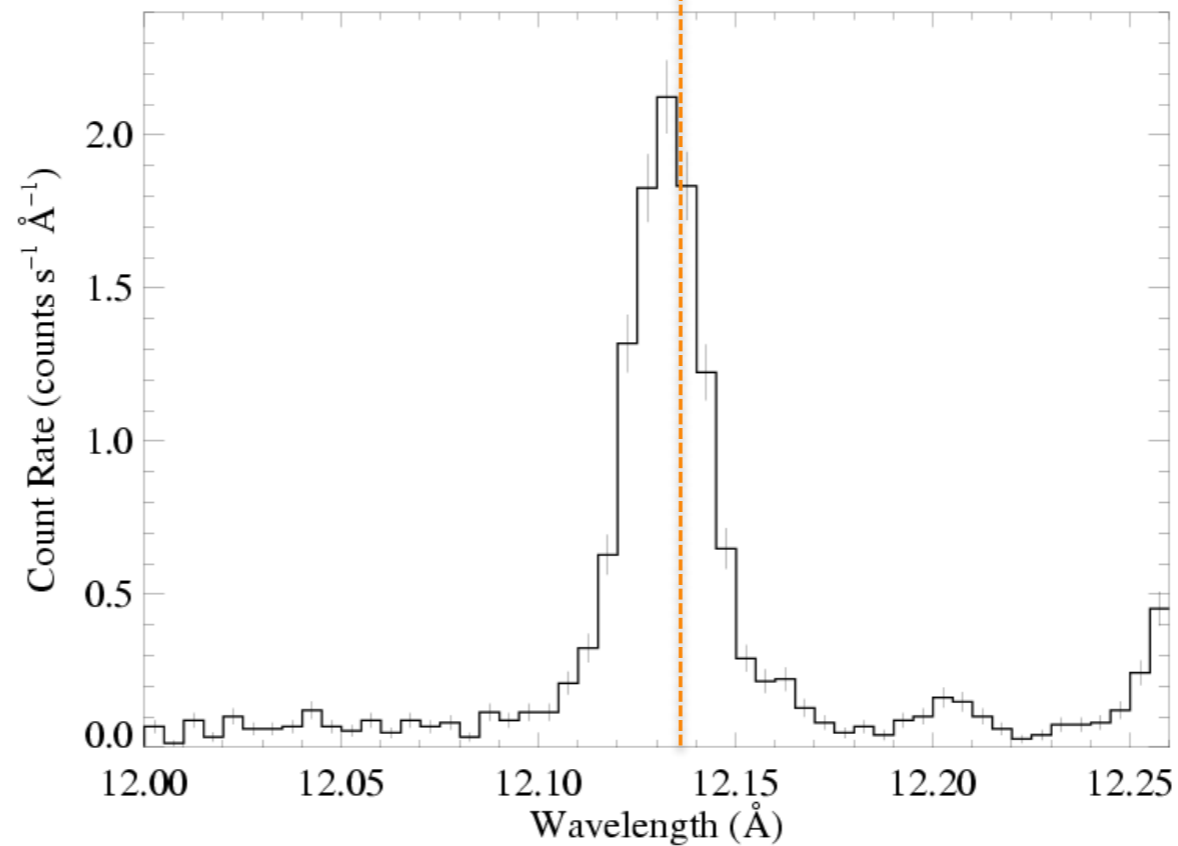
ζ Pup (O4If)

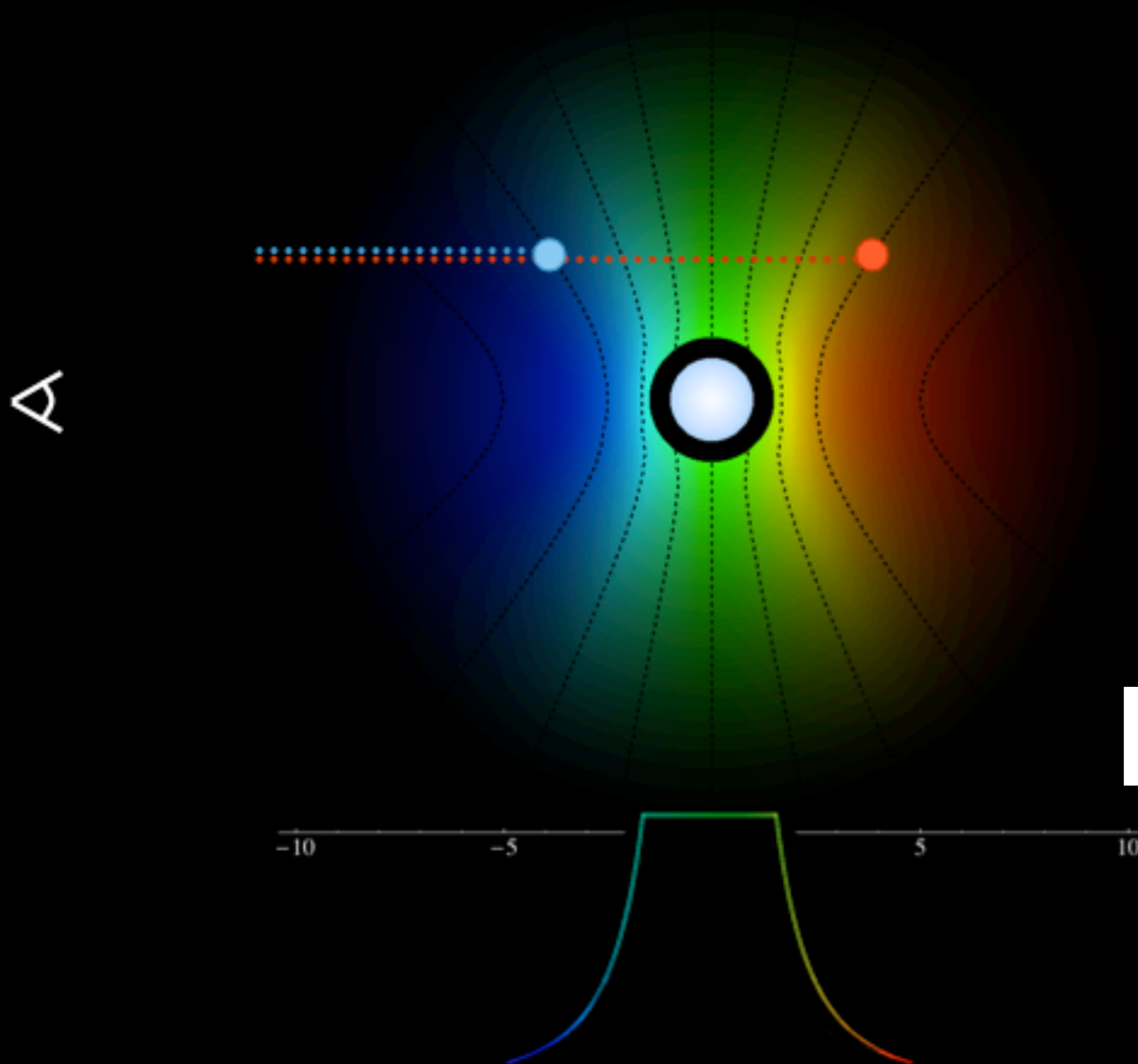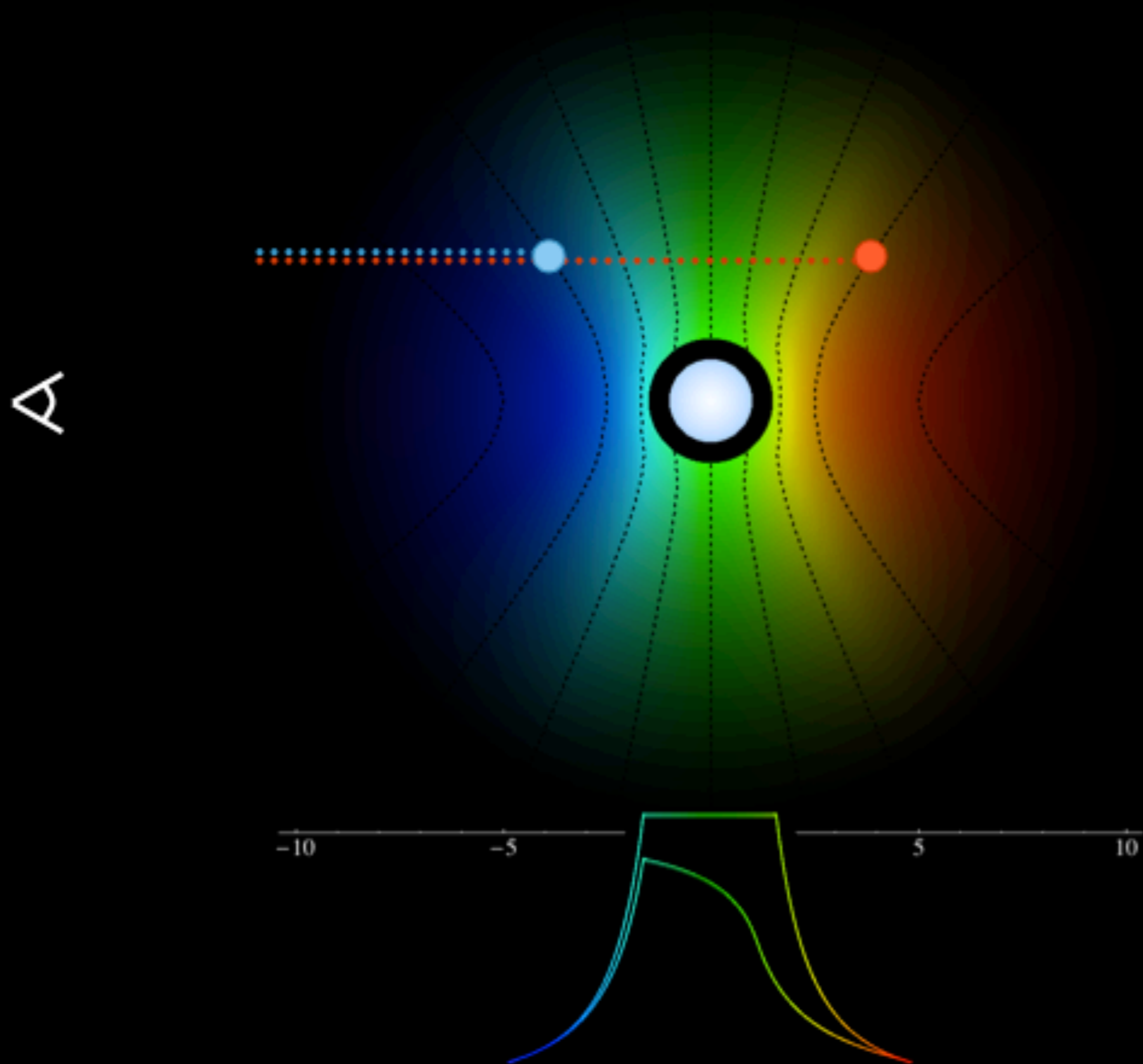Capella: G star for comparison (narrow lines)

lines are asymmetric

ζ Pup (O4If)

Capella (G5 III)

Line Asymmetry
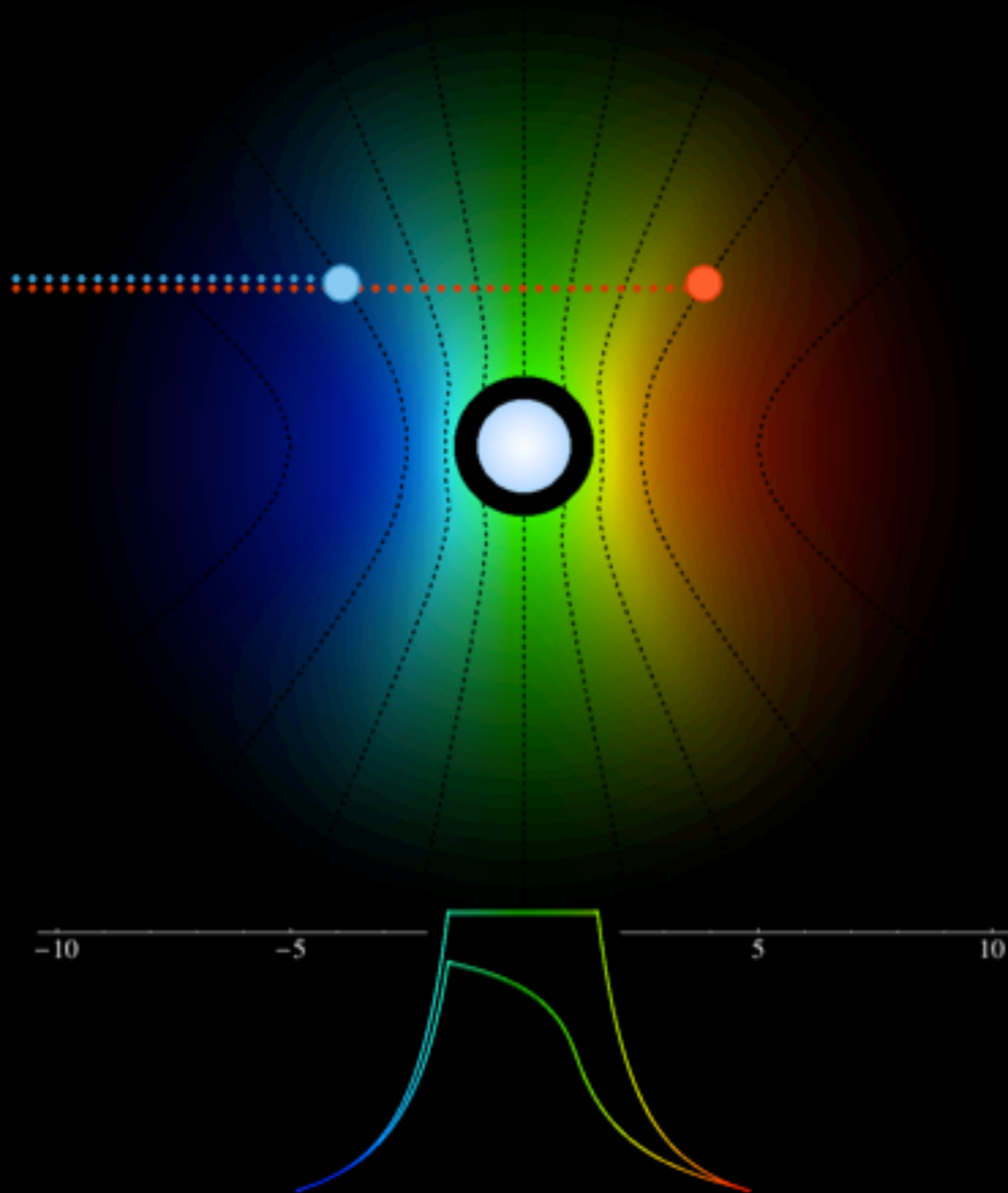
$$v = v_\infty (1 - r/R_\star)^\beta$$

Line Asymmetry

Line Asymmetry

$$\tau = \tau_* \int_z^\infty \frac{R_* dz'}{r'^2 (1 - R_*/r')^\beta}$$

Line profile shapes

$\tau_* = 1, 2, 8$

$R_o = 1.5$

$R_o = 3$
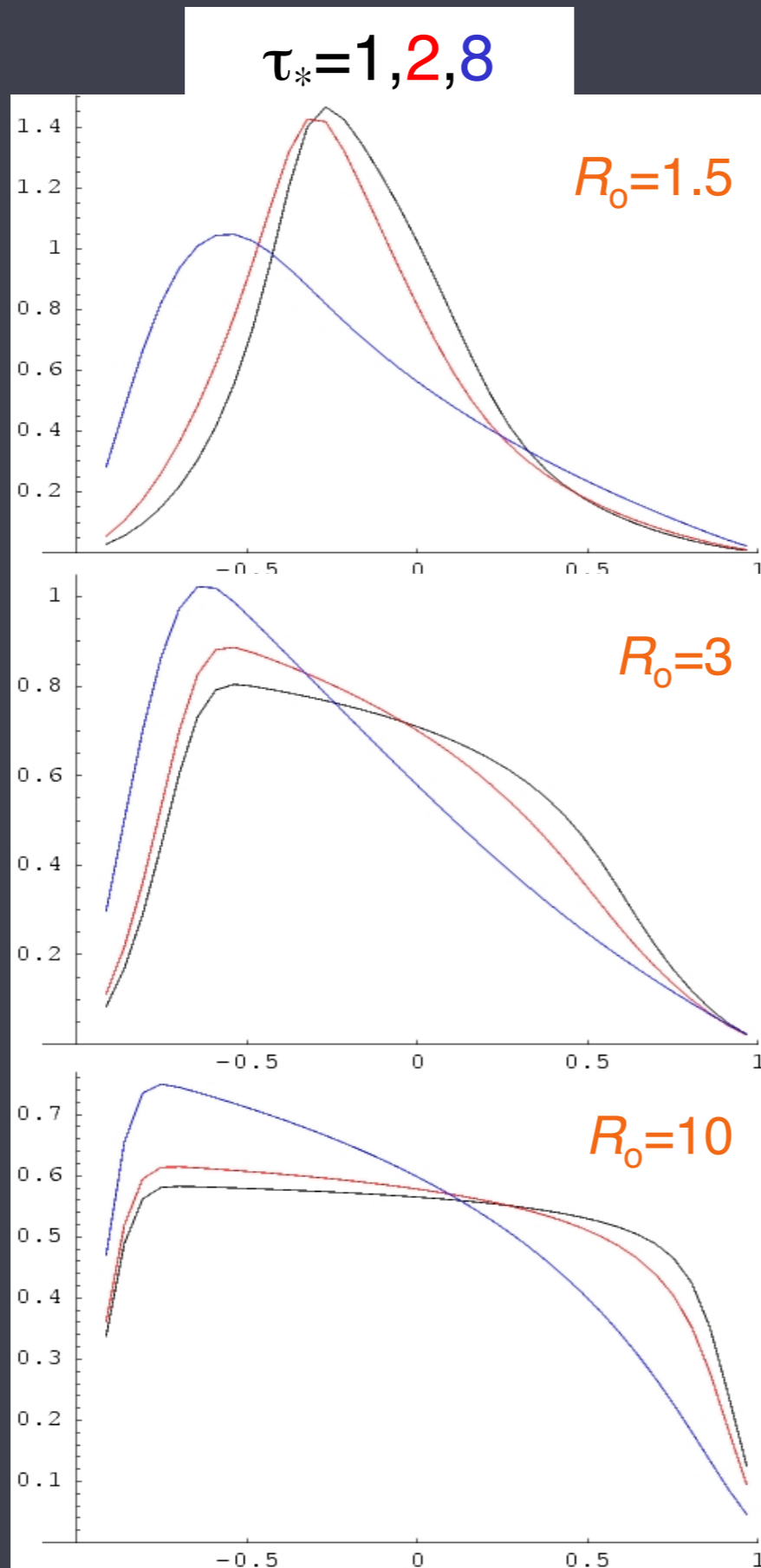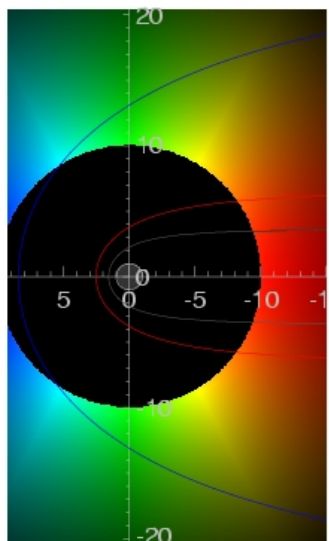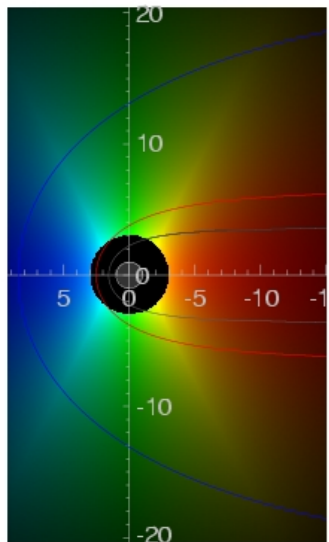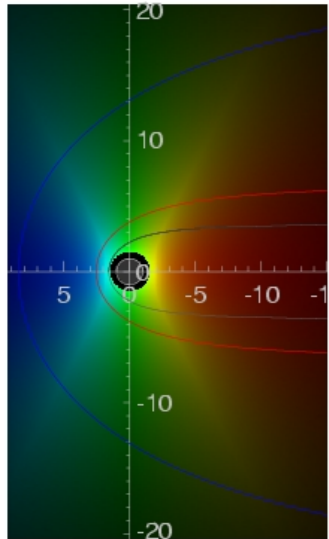
$R_o = 10$

key parameters: R_o & $\tau_\star$

$$v = v_\infty (1 - r/R_\star)^\beta$$
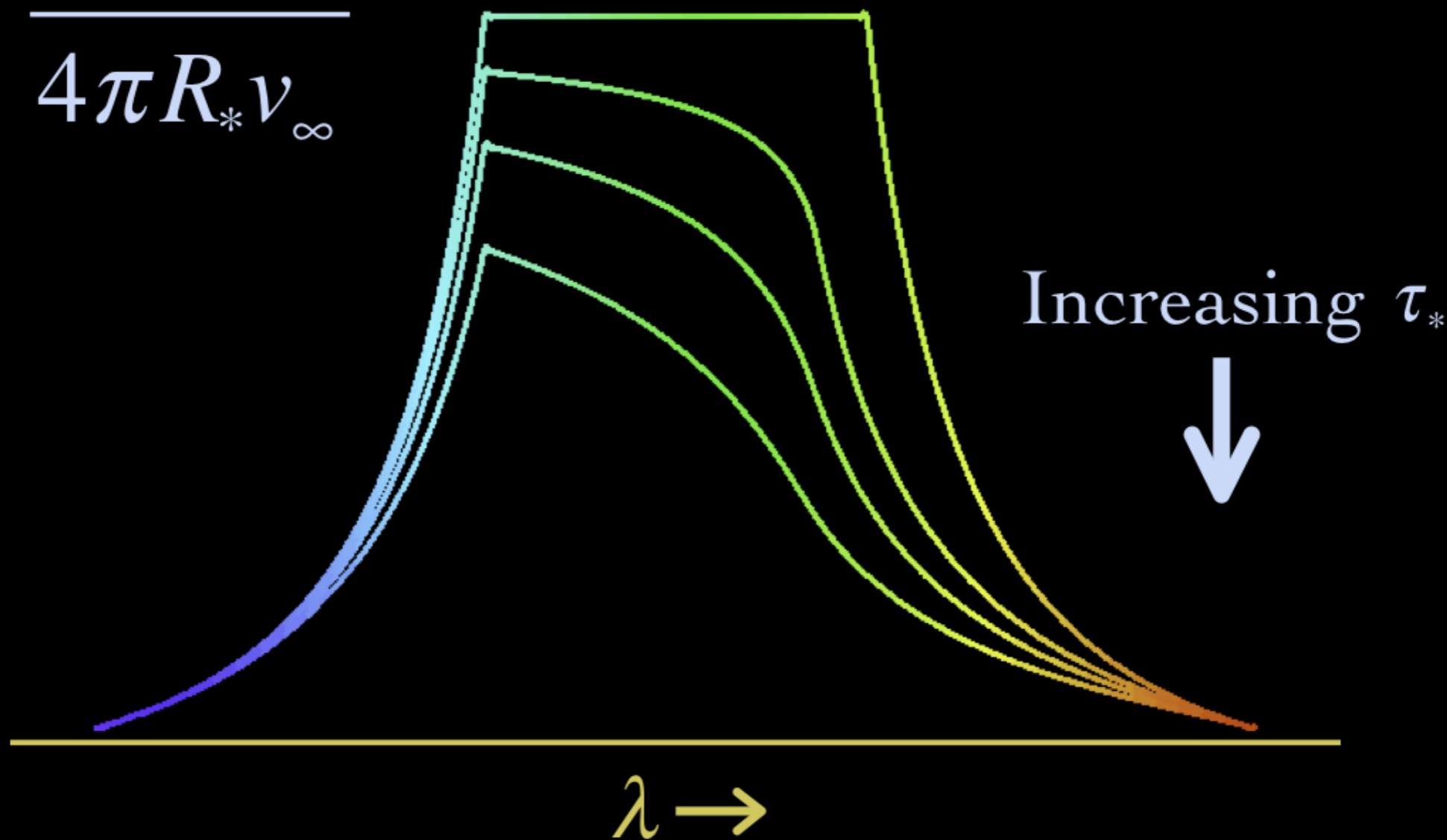
$j \sim \rho^2$ for $r/R_* > R_o$,

$= 0$ otherwise

$$\tau = \tau_* \int_z^\infty \frac{R_* dz'}{r'^2 (1 - R_*/r')^\beta}$$

$$\tau_* \equiv \frac{\kappa \dot{M}}{4\pi R_* v_\infty}$$
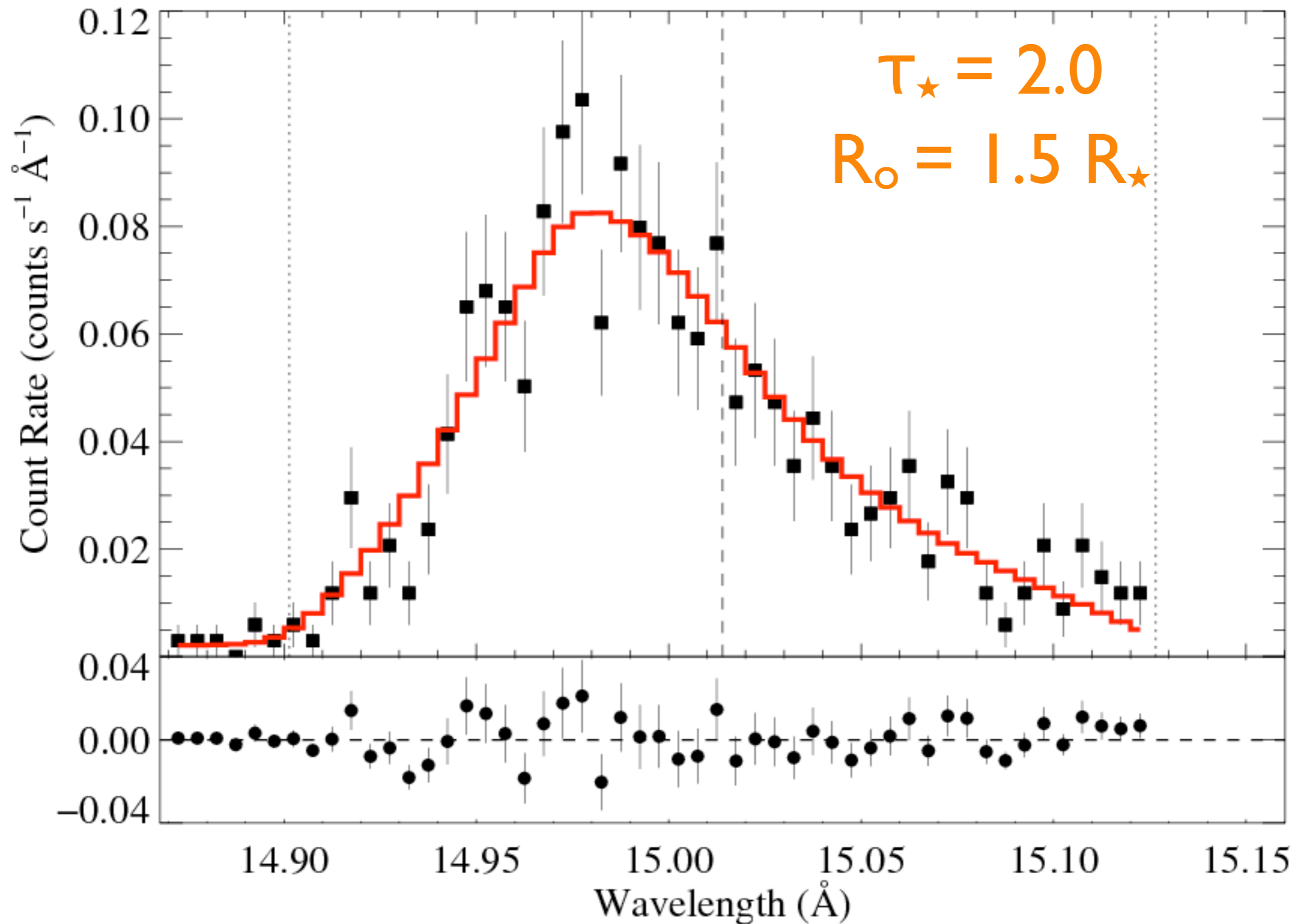
Hot plasma kinematics and location

R_o controls the line width via v(r)

$R_o = 1.5\ R_\star$
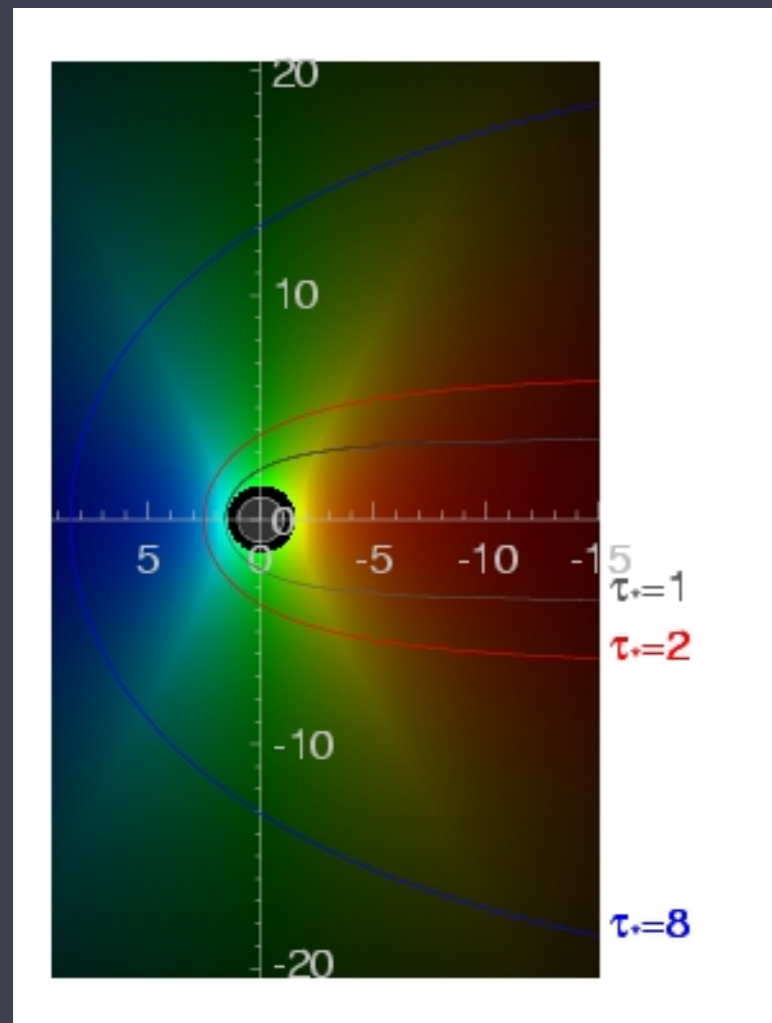
$R_o = 3\ R_\star$
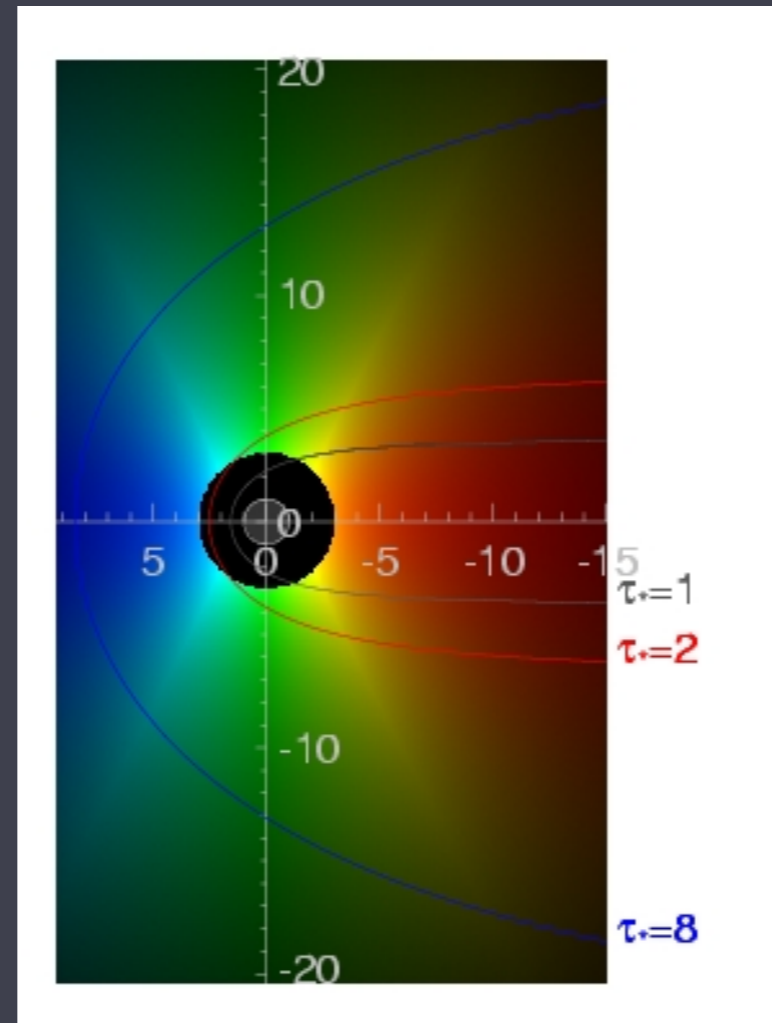
$R_o = 10\ R_\star$
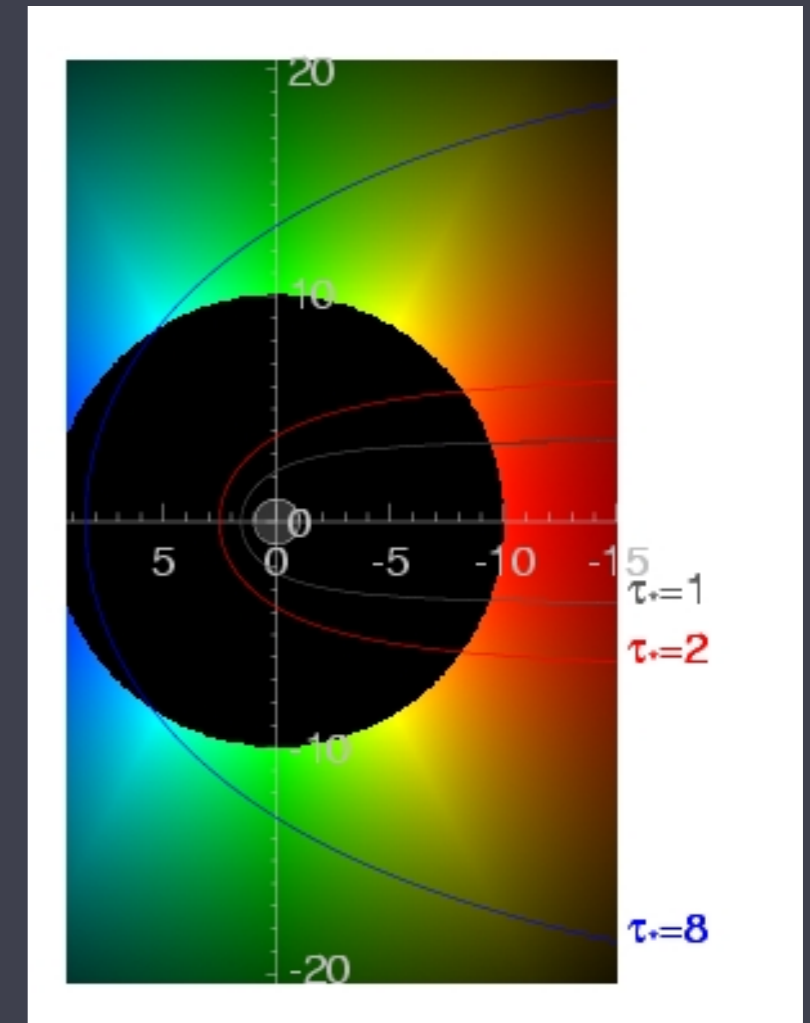
Distribution of R_o values for ζ Pup

consistent with a global value of $R_o = 1.5 R_\star$
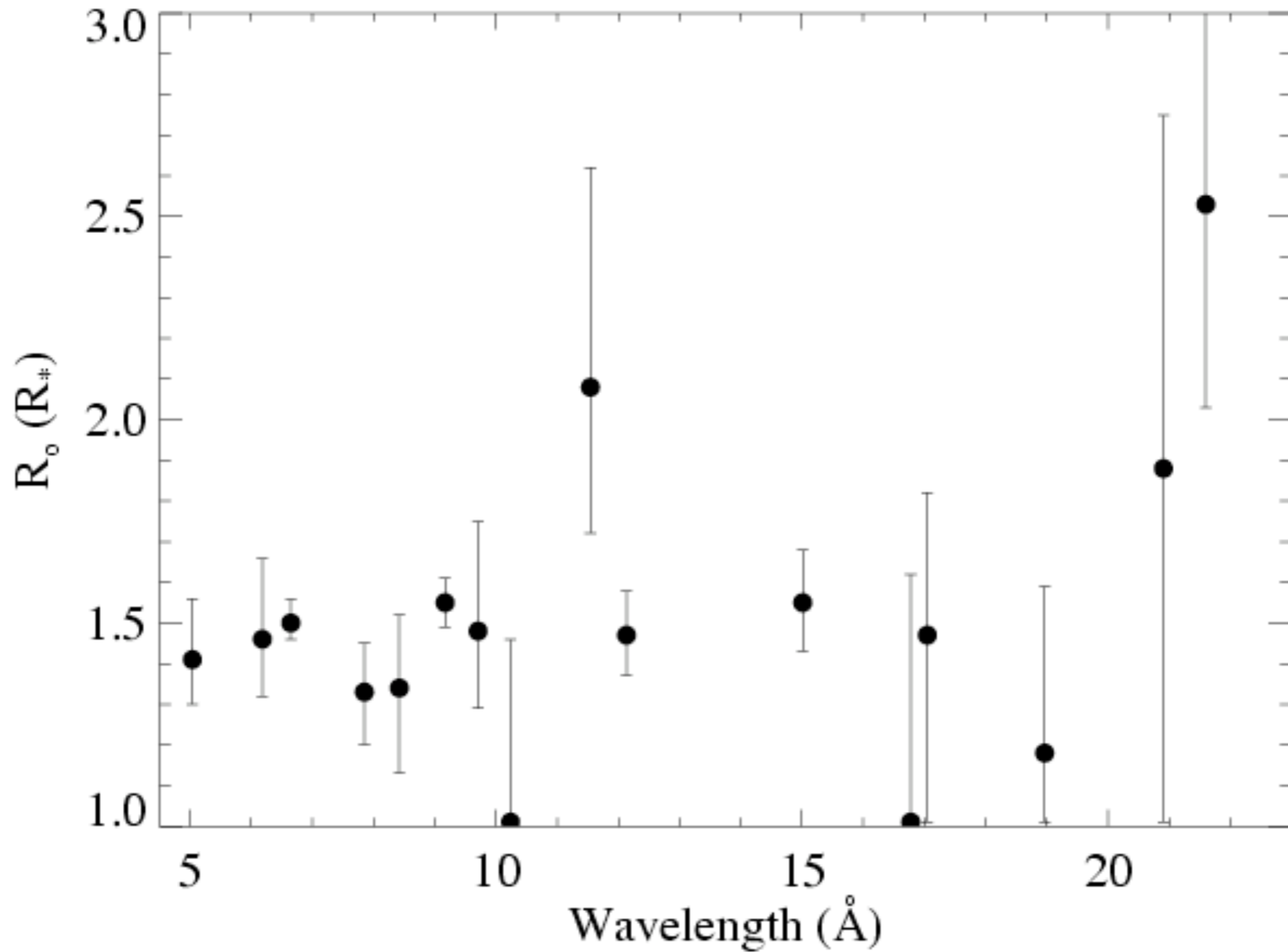
v_∞ can be constrained by the line fitting too

v_∞ = 2250 km/s from UV

68% confidence limit on mean from five lines
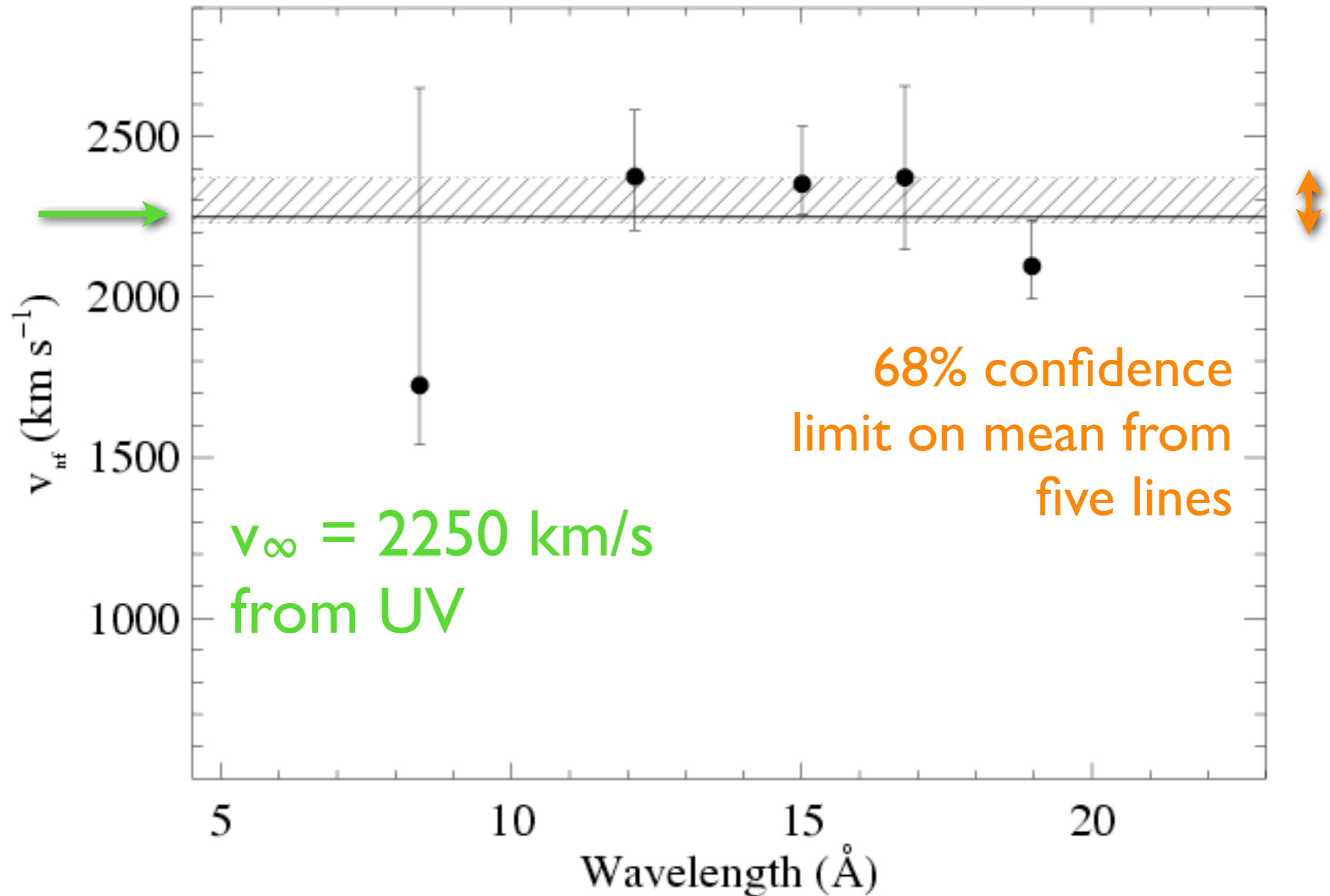
X-ray plasma and mean wind have same kinematics

$v_\infty = 2250$ km/s from UV

68% confidence limit on mean from five lines
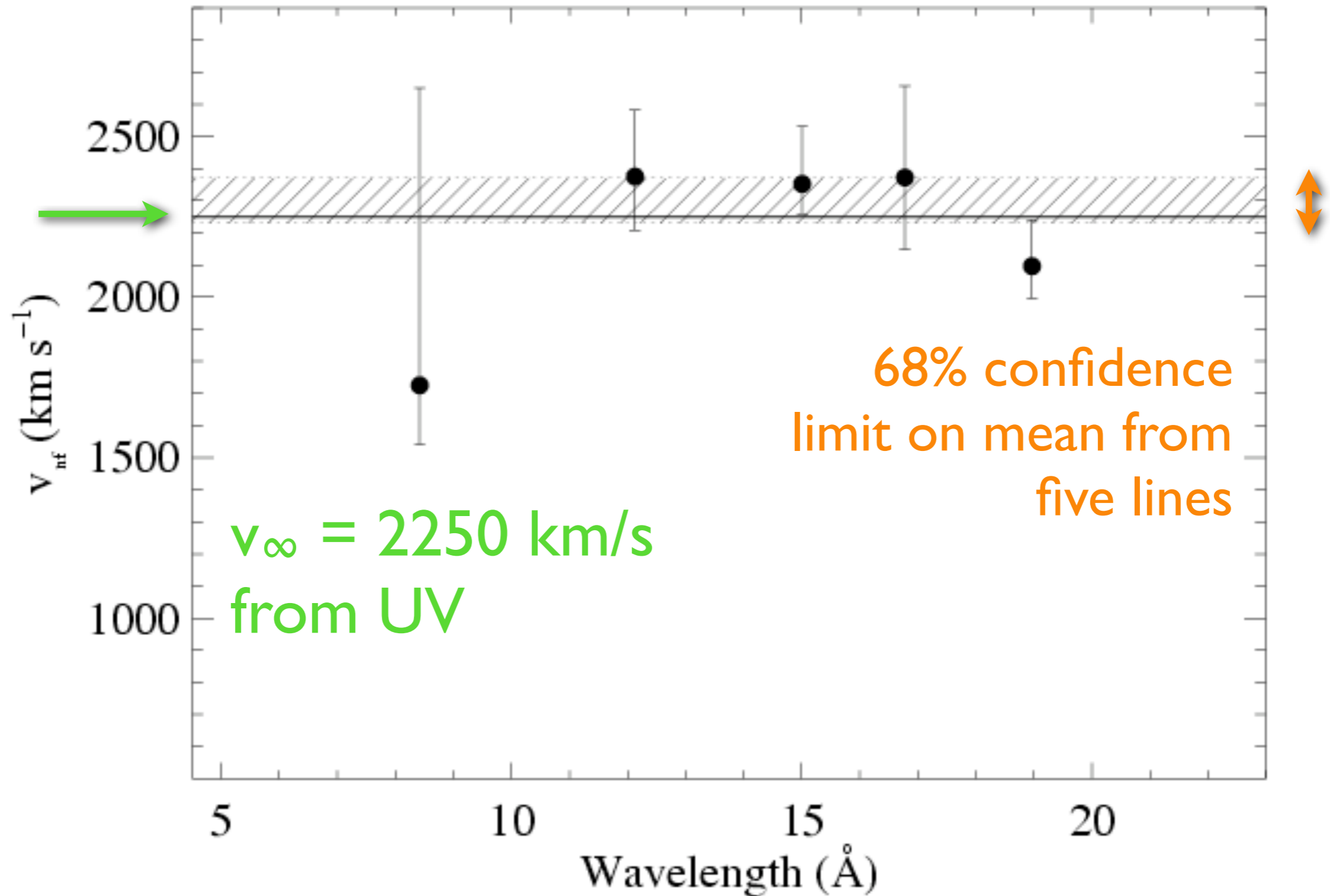
The profiles also tell us about the level of wind absorption

Wind Profile Model

$$\tau_* = \frac{\kappa \dot{M}}{4\pi R_* v_\infty}$$

Increasing τ_*

$\lambda \rightarrow$

ζ Pup: *Chandra* MEG

Fe XVII

$\tau_\star = 2.0$

$R_o = 1.5\ R_\star$
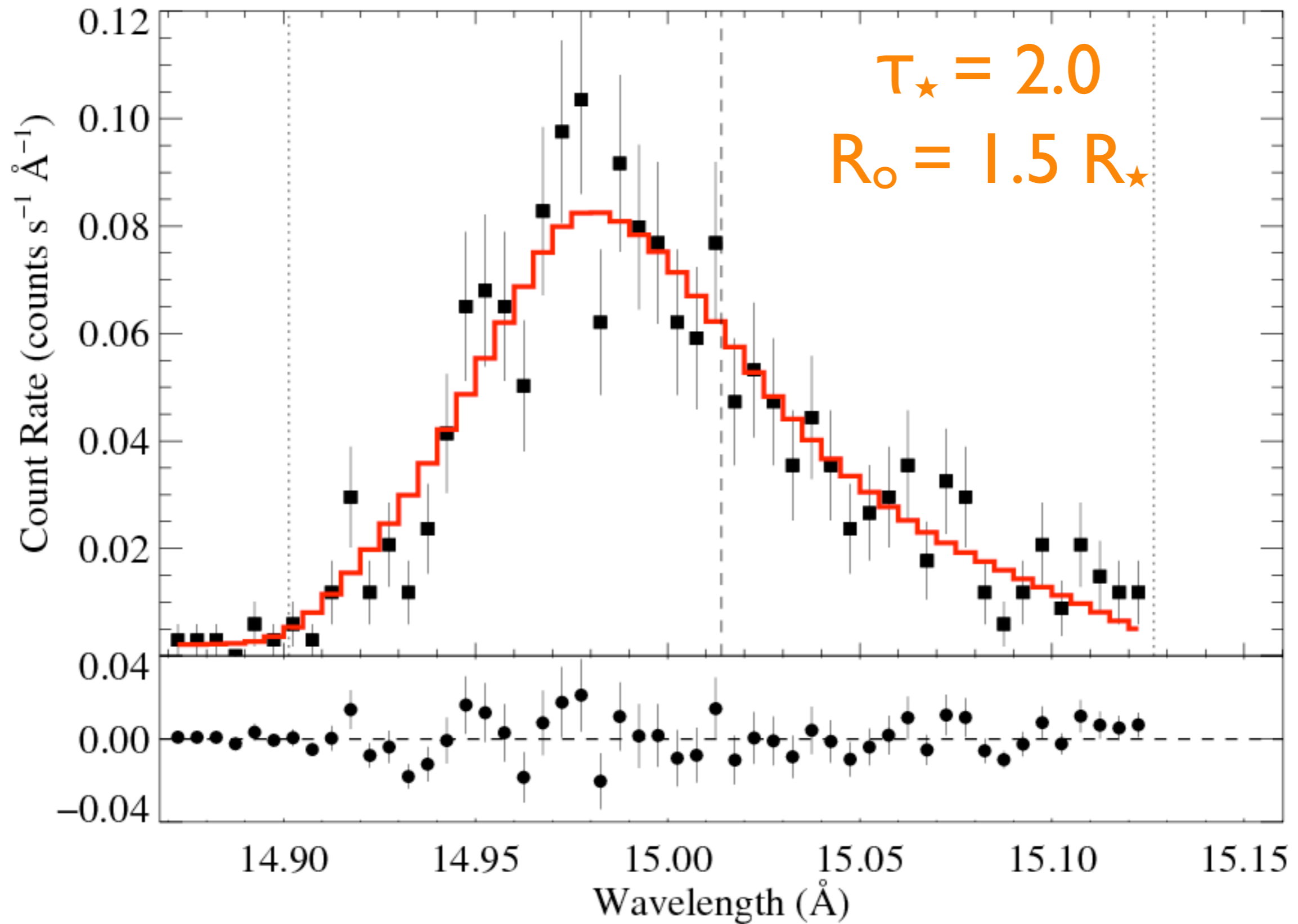
Quantifying the wind optical depth

opacity of the cold wind component (due to bound-free transitions in C, N, O, Ne, Fe)

wind mass-loss rate

$$\dot{M} = 4\pi r^2 v \rho$$

$$\tau_* \equiv \frac{\kappa \dot{M}}{4\pi R_* v_\infty}$$

stellar radius

wind terminal velocity

CNO processed

$$\tau_* \equiv \frac{\kappa \dot{M}}{4\pi R_* v_\infty}$$

Solar

Si V

Mg IV

Ne IV

Fe L

O IV

note: emission comes from hot wind component, while absorption arises in cool wind component
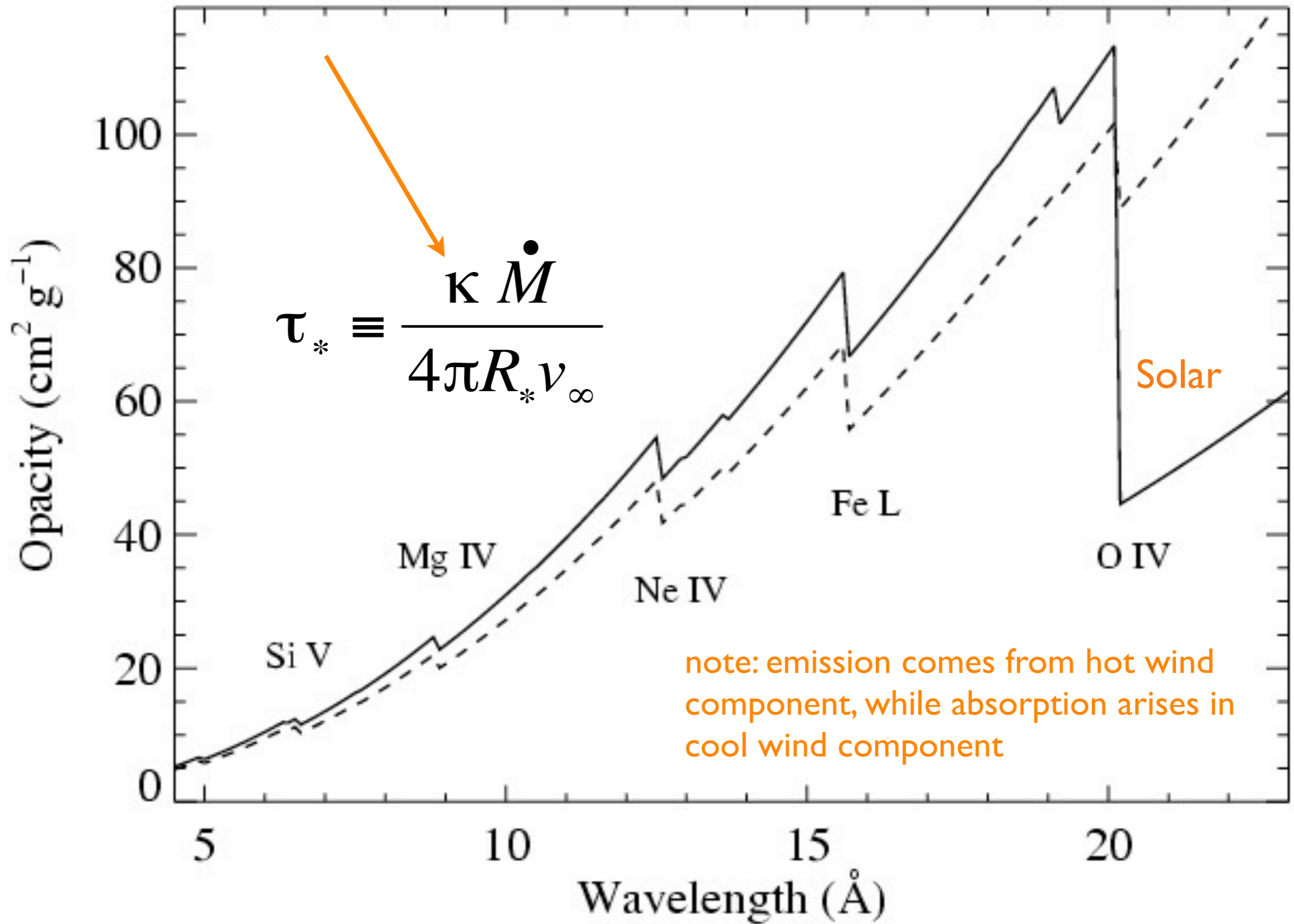
ζ Pup *Chandra*: three emission lines

Mg Lyα: 8.42 Å   Ne Lyα: 12.13 Å   O Lyα: 18.97 Å
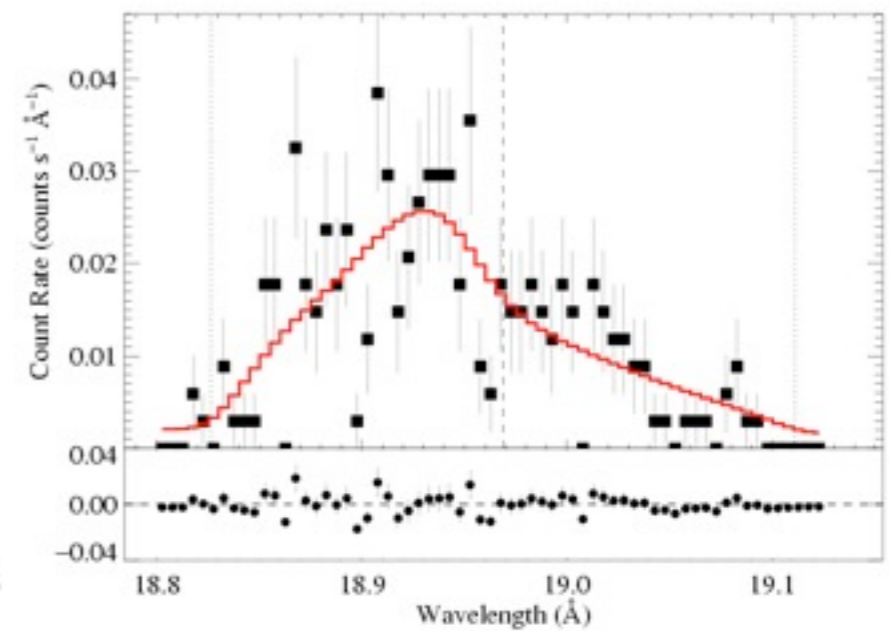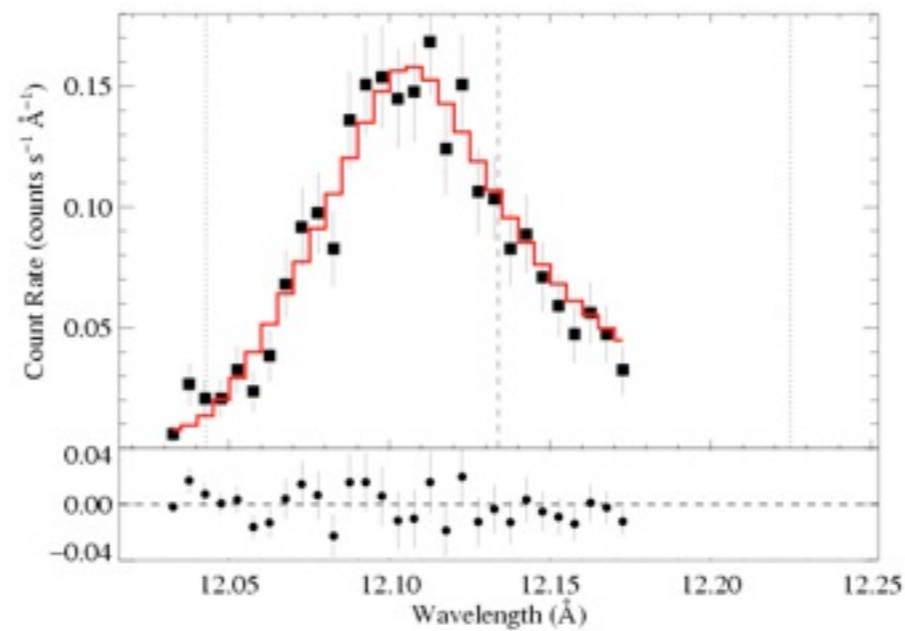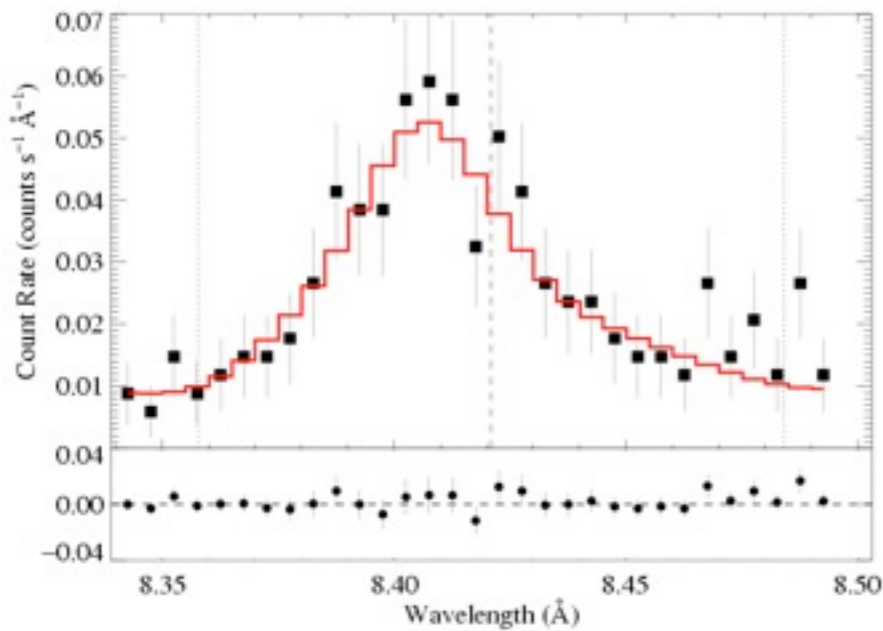
τ* ~ 1   τ* ~ 2   τ* ~ 3

Recall:

$$\tau_* \equiv \frac{\kappa \, \dot{M}}{4\pi R_* v_\infty}$$

Results from the 3 line fits shown previously
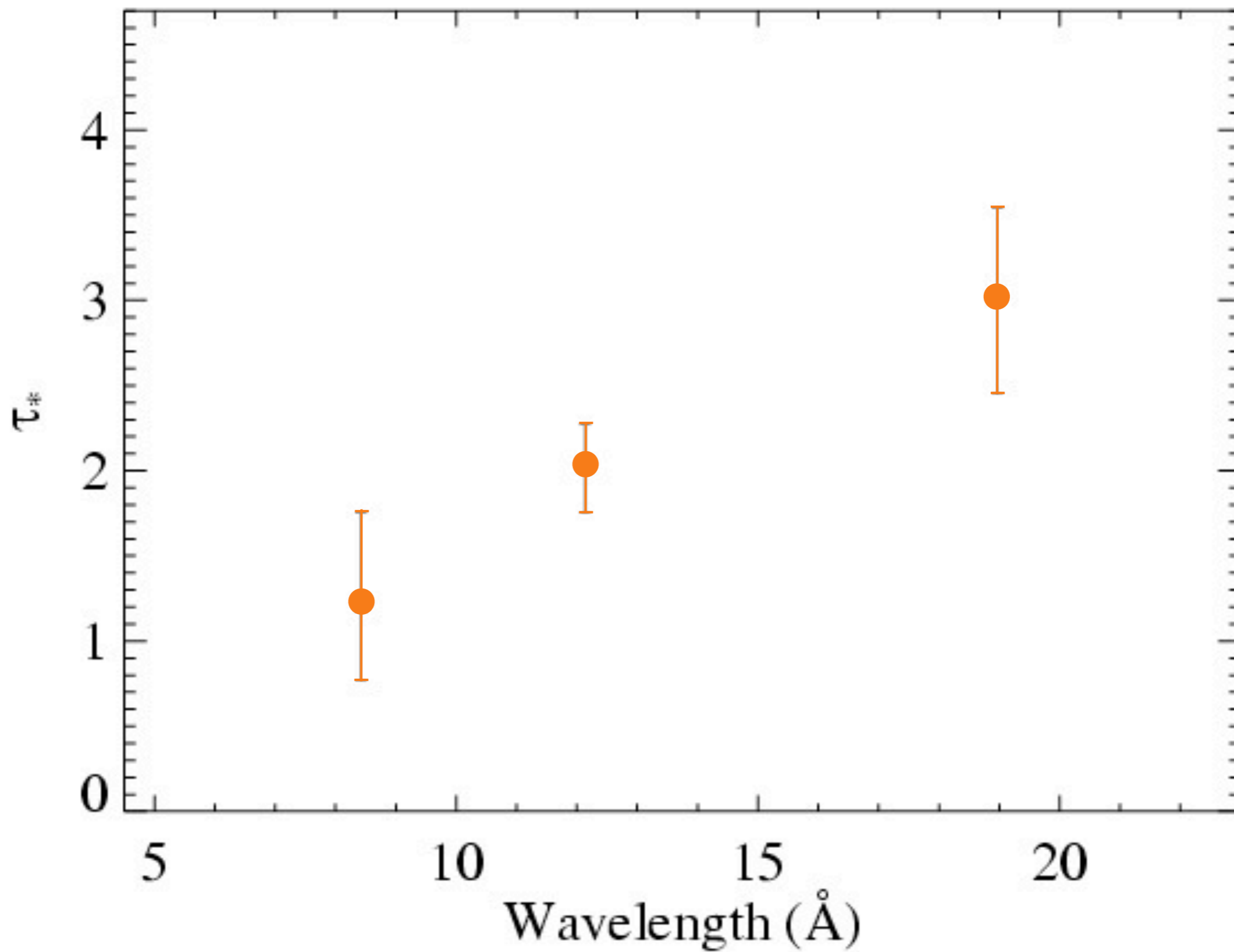
Fits to 16 lines in the *Chandra* spectrum of ζ Pup
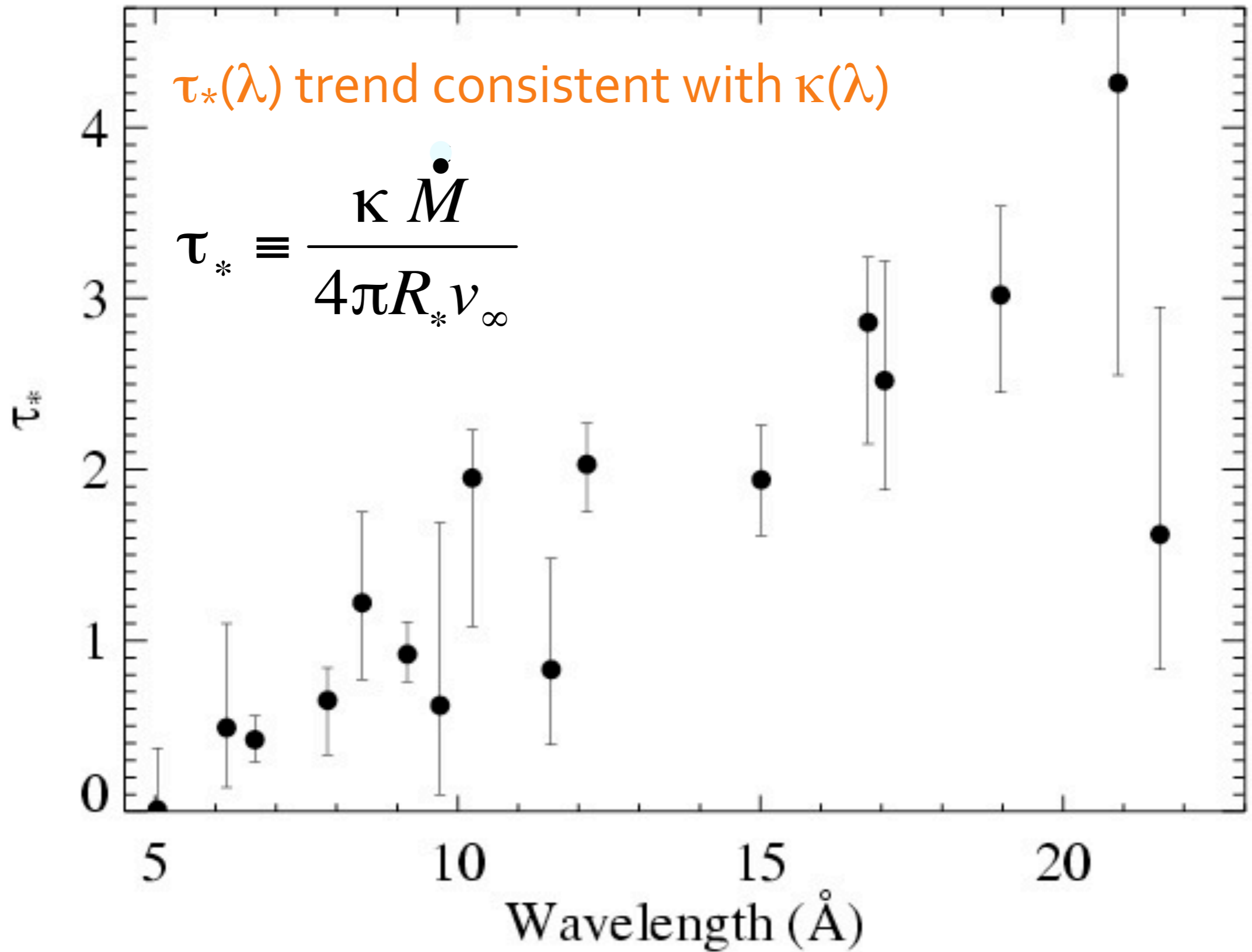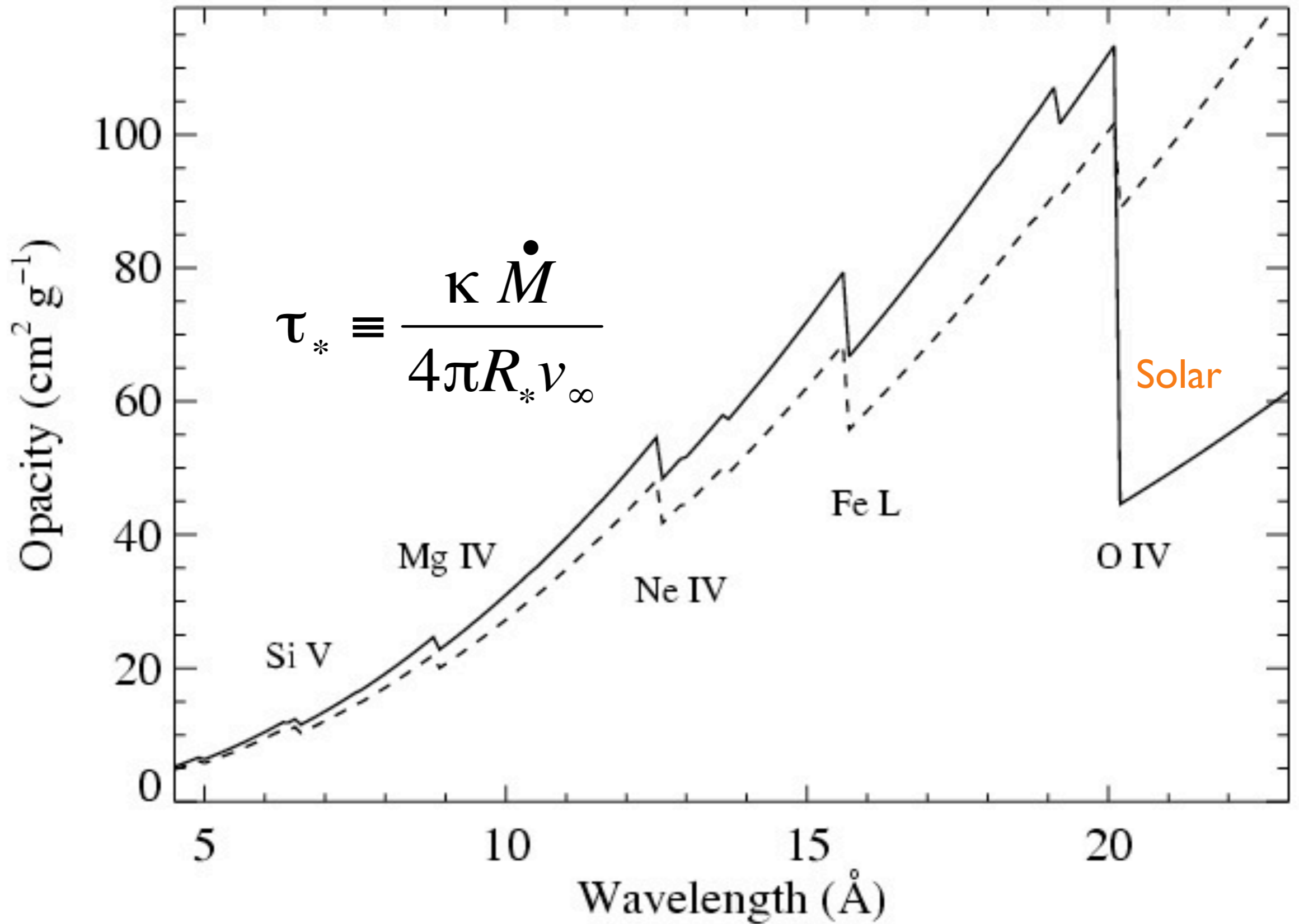
τ$_*$(λ) trend consistent with κ(λ)

$$\tau_* \equiv \frac{\kappa \dot{M}}{4\pi R_* v_\infty}$$

$$\tau_* \equiv \frac{\kappa \, \dot{M}}{4\pi R_* v_\infty}$$

CNO processed

Solar

Fe L

Mg IV

Ne IV

Si V

O IV

$$\tau_* \equiv \frac{\kappa \, \dot{M}}{4\pi R_* v_\infty}$$

$\dot{M}$ becomes the free parameter of the fit to the $\tau_*(\lambda)$ trend

$\tau_*(\lambda)$ trend consistent with $\kappa(\lambda)$

$$\tau_* \equiv \frac{\kappa \, \dot{M}}{4\pi R_* v_\infty}$$

$\dot{M}$ becomes the free parameter of the fit to the $\tau_*(\lambda)$ trend

Traditional mass-loss rate:
8.3 X 10⁻⁶ M_sun/yr
From H_α ignoring clumping

Our best fit:
3.5 X 10⁻⁶ M_sun/yr
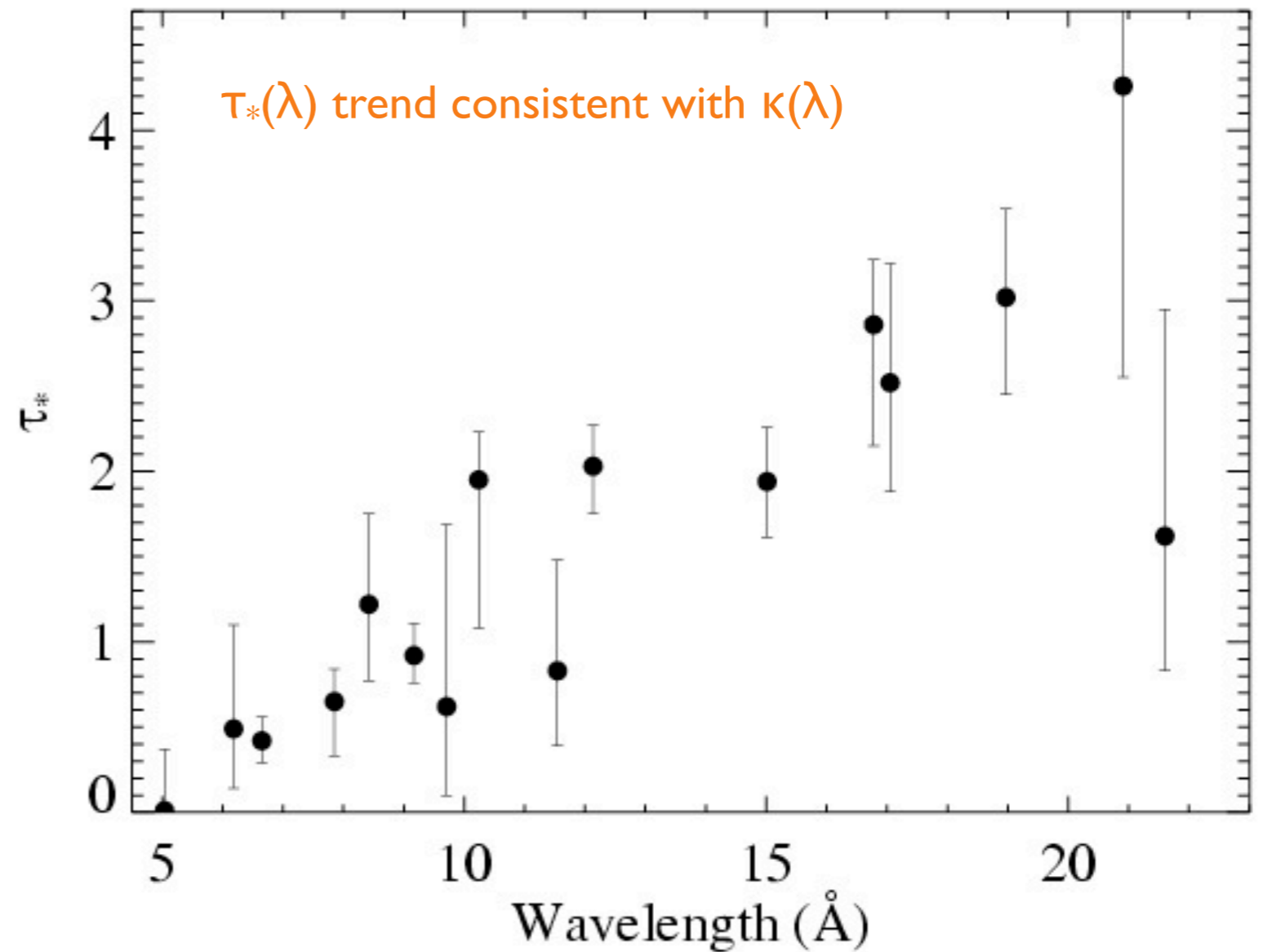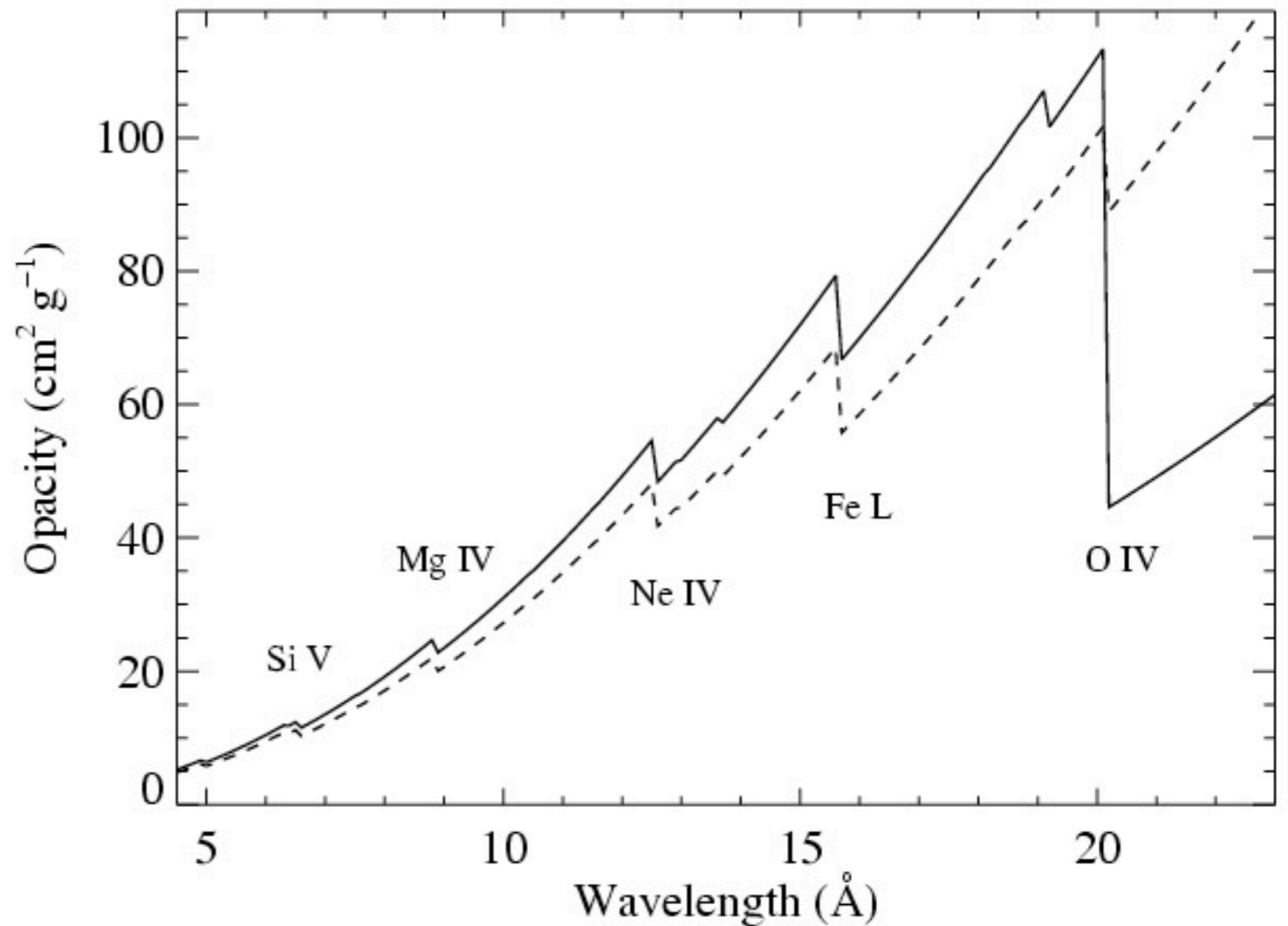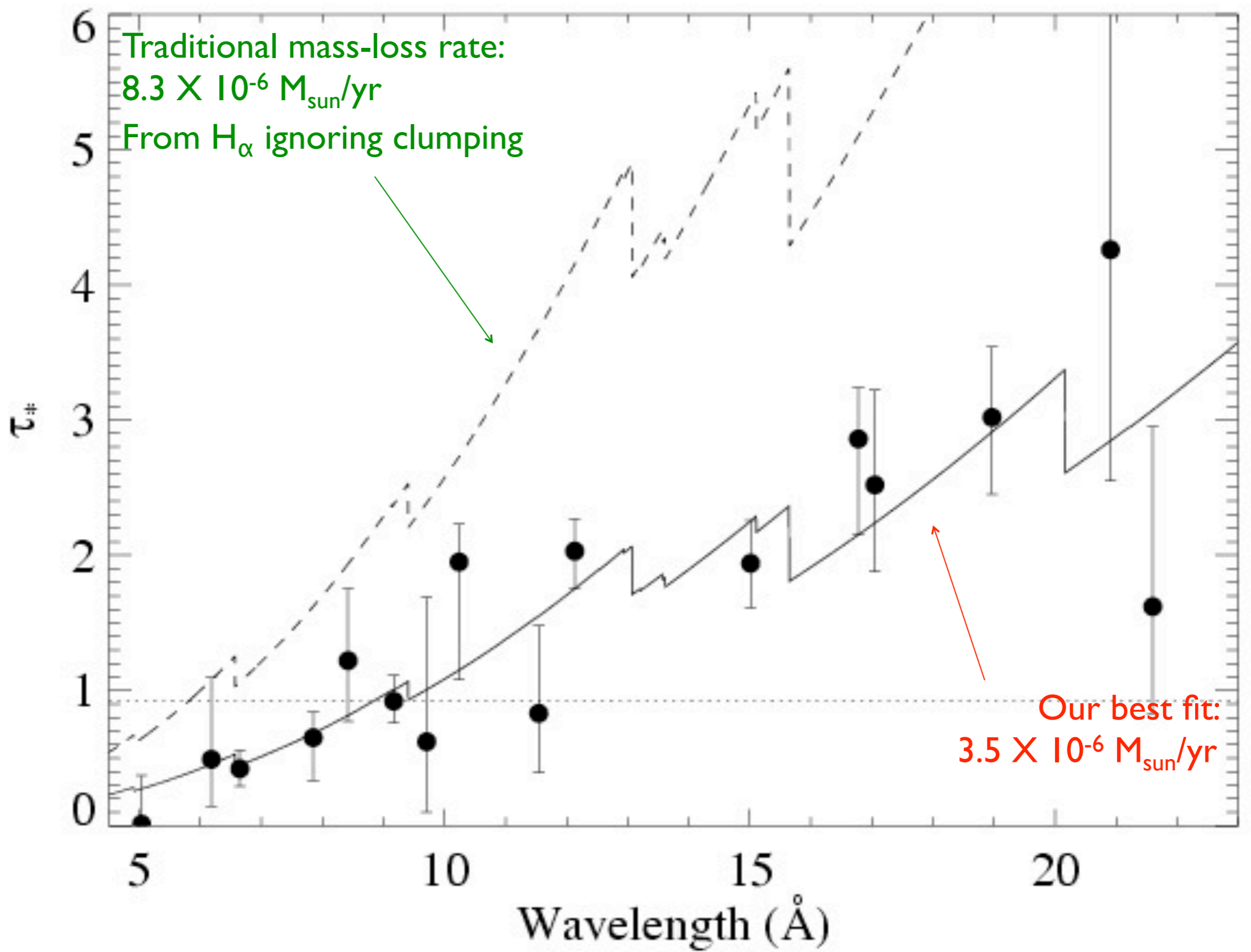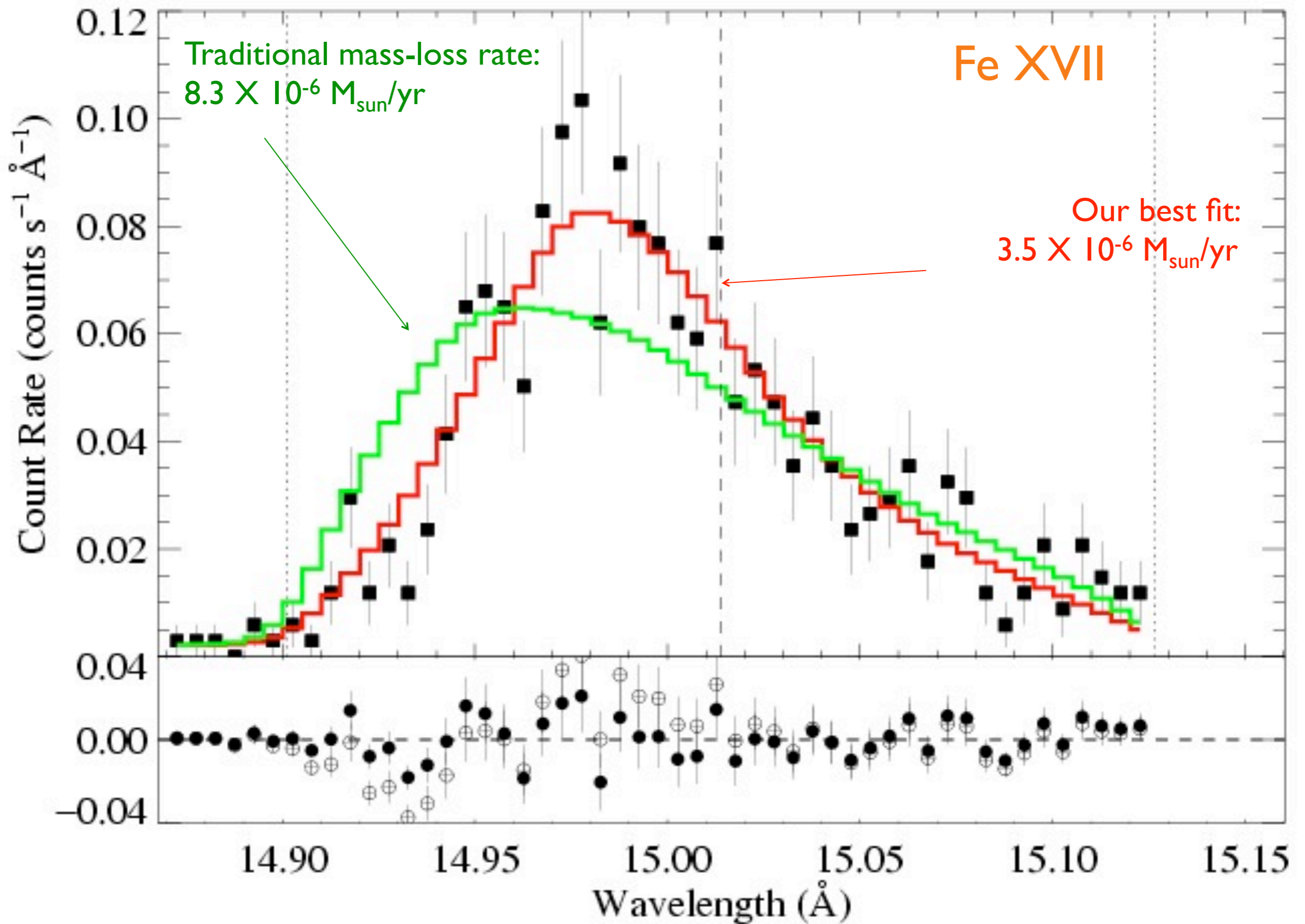
X-ray line profile based mass-loss rate: implications for clumping

basic definition: $f_{cl} \equiv \langle\rho^2\rangle/\langle\rho\rangle^2$

from density-squared
diagnostics like Hα, IR
& radio free-free

from (column) density
diagnostic like $\tau_\star$ from
X-ray profiles

Bright OB stars in the Galaxy

III. Constraints on the radial stratification of the clumping factor in hot star winds from a combined H$_\alpha$, IR and radio analysis[*]

J. Puls[1], N. Markova[2], S. Scuderi[3], C. Stanghellini[4], O. G. Taranova[5], A. W. Burnley[6] and I. D. Howarth[6]

[1] Universitäts-Sternwarte München, Scheinerstr. 1, D-81679 München, Germany, e-mail: uh101aw@usm.uni-muenchen.de
[2] Institute of Astronomy, Bulgarian National Astronomical Observatory, P.O. Box 136, 4700 Smoljan, Bulgaria,
   e-mail: nmarkova@astro.bas.bg
[3] INAF - Osservatorio Astrofisico di Catania, Via S. Sofia 78, I-95123 Catania, Italy, e-mail: scuderi@oact.inaf.it
[4] INAF - Istituto di Radioastronomia, Via P. Gobetti 101, I-40129 Bologna, Italy, e-mail: c.stanghellini@ira.inaf.it
[5] Sternberg Astronomical Institute, Universitetski pr. 13, Moscow, 119992, Russia, e-mail: taranova@sai.msu.ru
[6] Department of Physics and Astronomy, University College London, Gower Street, London WC1E 6BT, UK,
   e-mail: awxb@star.ucl.ac.uk, idh@star.ucl.ac.uk

Abstract. Recent results strongly challenge the canonical picture of massive star winds: various evidence indicates that currently accepted mass-loss rates, $\dot{M}$, may need to be revised downwards, by factors extending to one magnitude or even more. This is because the most commonly used mass-loss diagnostics are affected by "clumping" (small-scale density inhomogeneities), influencing our interpretation of observed spectra and fluxes.

Such downward revisions would have dramatic consequences for the evolution of, and feedback from, massive stars, and thus robust determinations of the clumping properties and mass-loss rates are urgently needed. We present a first attempt concerning this objective, by means of constraining the radial stratification of the so-called clumping factor.

To this end, we have analyzed a sample of 19 Galactic O-type supergiants/giants, by combining our own and archival data for H$_\alpha$, IR, mm and radio fluxes, and using approximate methods, calibrated to more sophisticated models. Clumping has been included into our analysis in the "conventional" way, by assuming the inter-clump matter to be void. Because (almost) all our diagnostics depends on the square of density, we cannot derive absolute clumping factors, but only factors normalized to a certain minimum.

This minimum was usually found to be located in the outermost, radio-emitting region, i.e., the radio mass-loss rates are the lowest ones, compared to $\dot{M}$ derived from H$_\alpha$ and the IR. The radio rates agree well with those predicted by theory, but are only upper limits, due to unknown clumping in the outer wind. H$_\alpha$ turned out to be a useful tool to derive the clumping properties inside $r < 3 \ldots 5 R_\star$. Our most important result concerns a (physical) difference between denser and thinner winds: for denser winds, the innermost region is more strongly clumped than the outermost one (with a normalized clumping factor of 4.1 ± 1.4), whereas thinner winds have similar clumping properties in the inner and outer regions.

Our findings are compared with theoretical predictions, and the implications are discussed in detail, by assuming different scenarios regarding the still unknown clumping properties of the outer wind.

trade-off/degeneracy between clumping factor and mass-loss rate

$$\dot{M}_{cl} \equiv \dot{M}_{smooth} / f_{cl}^{0.5}$$

Puls et al. (2006) : relative clumping (vs. radius), but free scale factor

ζ Pup mass-loss rate < 4.2 x 10^{-6} M_{sun}/yr

X-ray mass-loss rate breaks degeneracy and sets the scale factor

ζ Pup: radially varying clumping

for $\dot{M} = 3.5 \times 10^{-6}$ M$_{sun}$/yr

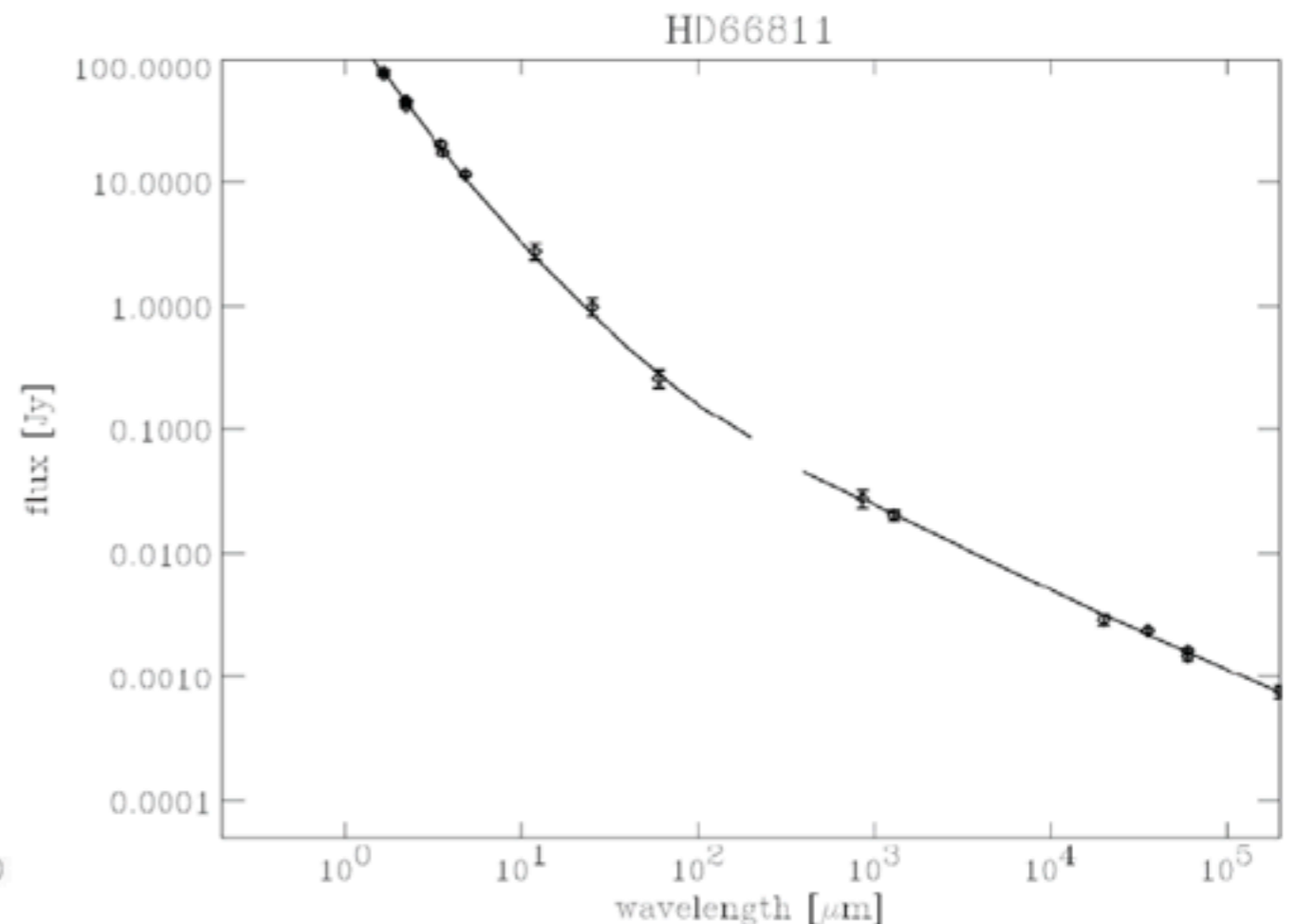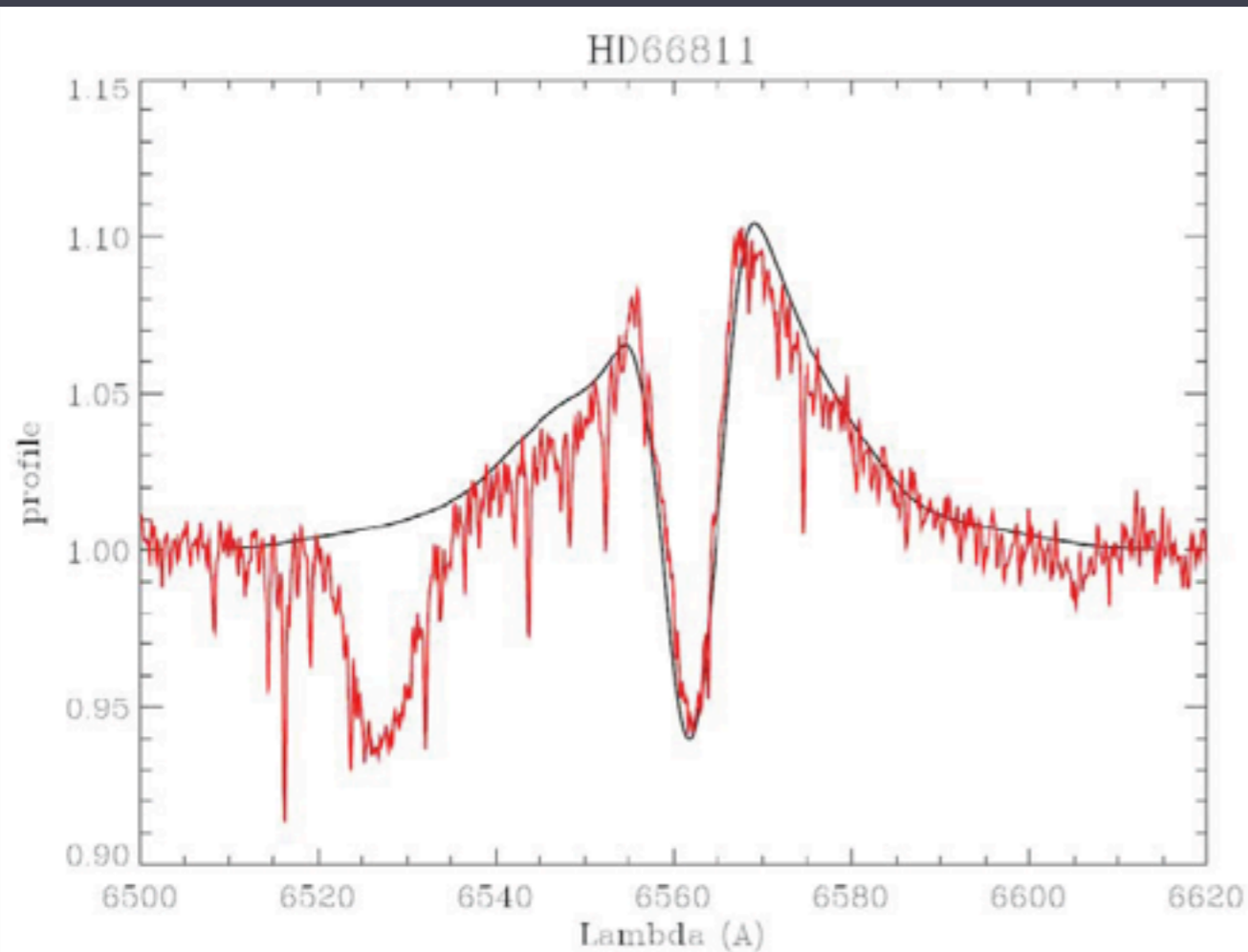$f_{cl} \equiv \langle\rho^2\rangle/\langle\rho\rangle^2$

$\dot{M}_{cl} \equiv \dot{M}_{smooth} / f_{cl}^{0.5}$

$f_{cl} = 1.3$ @ $r < 1.12$ R$_*$ Hα
$f_{cl} = 6.0$ @ $1.12 < r < 1.5$ R$_*$ Hα
$f_{cl} = 3.7$ @ $1.5 < r < 2$ R$_*$ Hα
$f_{cl} = 2.6$ @ $2 < r < 15$ R$_*$ IR
$f_{cl} = 1.3$ @ $r > 15$ R$_*$ radio

Hα   IR   radio

base of the wind ($r < 1.5\, R_\star$)

is clumped
...but...

$f_{cl} = 1.3$ @ $r < 1.12\, R_*$ Hα
$f_{cl} = 6.0$ @ $1.12 < r < 1.5\, R_*$ Hα
$f_{cl} = 3.7$ @ $1.5 < r < 2\, R_*$ Hα
$f_{cl} = 2.6$ @ $2 < r < 15\, R_*$ IR
$f_{cl} = 1.3$ @ $r > 15\, R_*$ radio

recall: X-ray $R_o = 1.5\, R_\star$
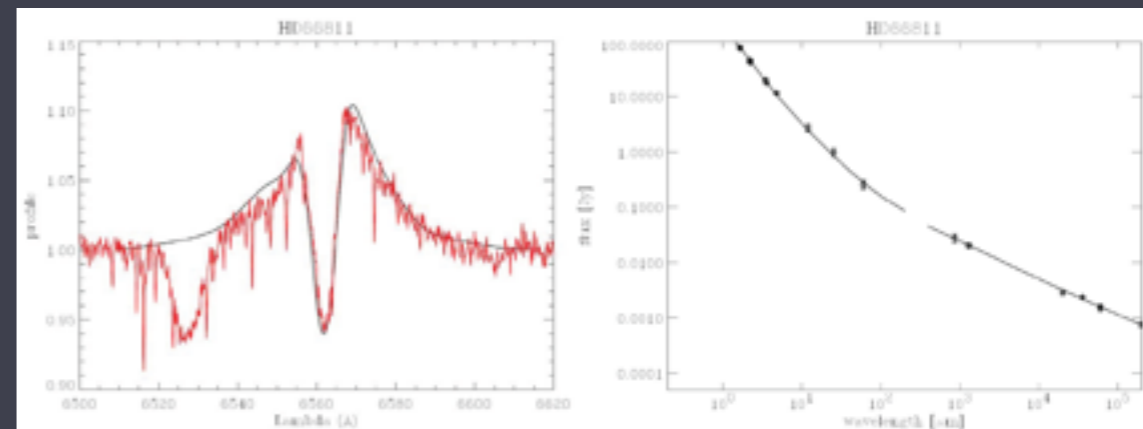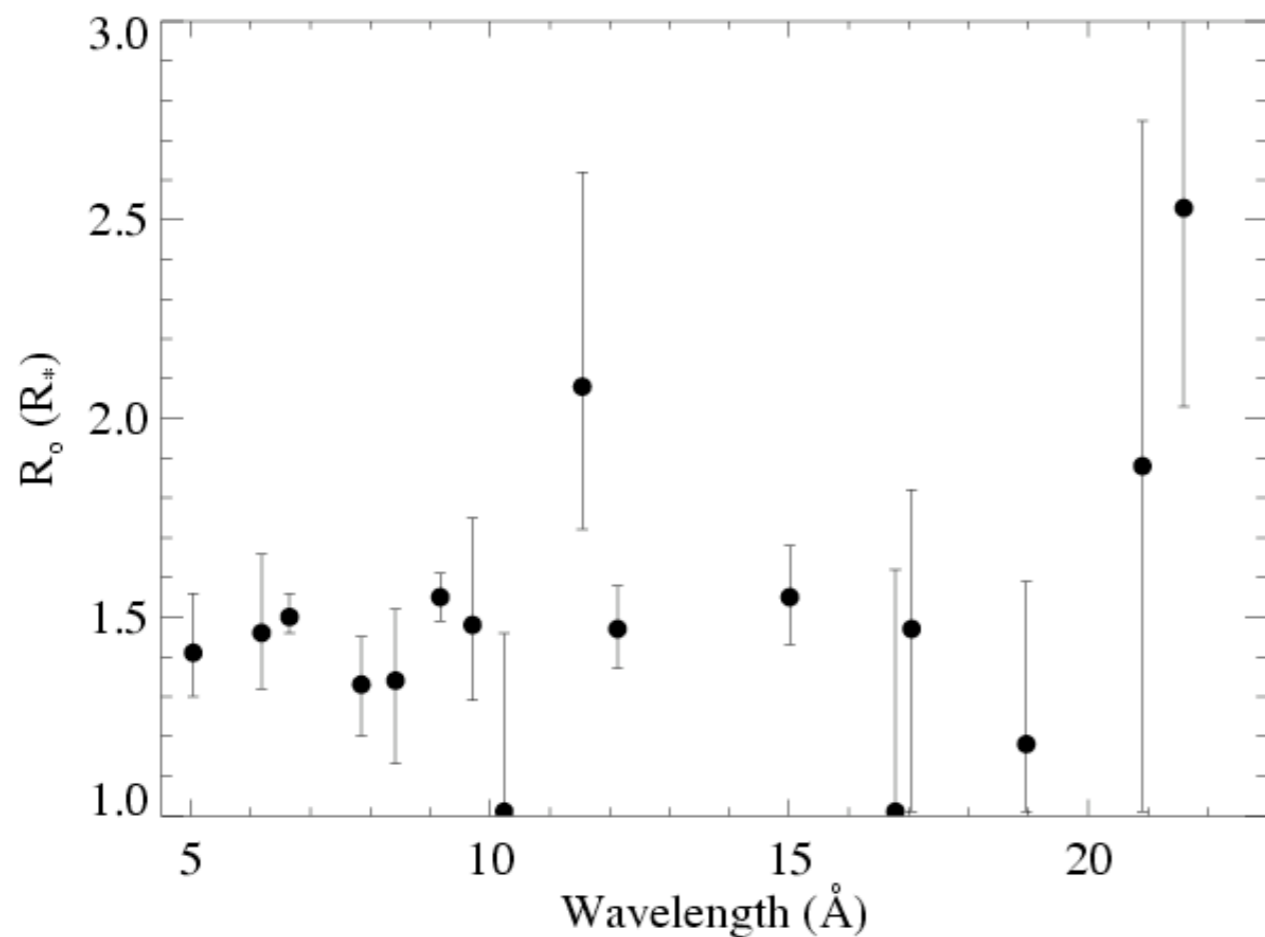
Porosity?

recall (J. Sundqvist): optically **thick** clumps

isotropic porosity
(spherical clumps)
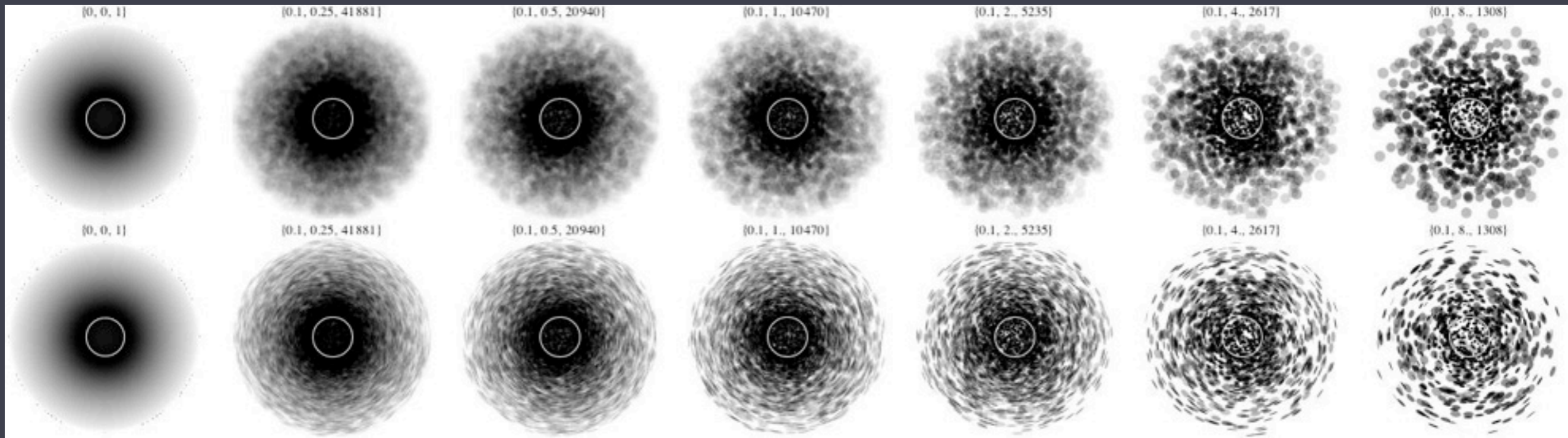
$h_\infty = 0$ $h_\infty = 0.25$ $h_\infty = 0.5$ $h_\infty = 1$ $h_\infty = 2$ $h_\infty = 4$ $h_\infty = 8$

anisotropic porosity
(flattened clumps)

Anisotropic porosity (flattened clumps)

lateral escape is enhanced

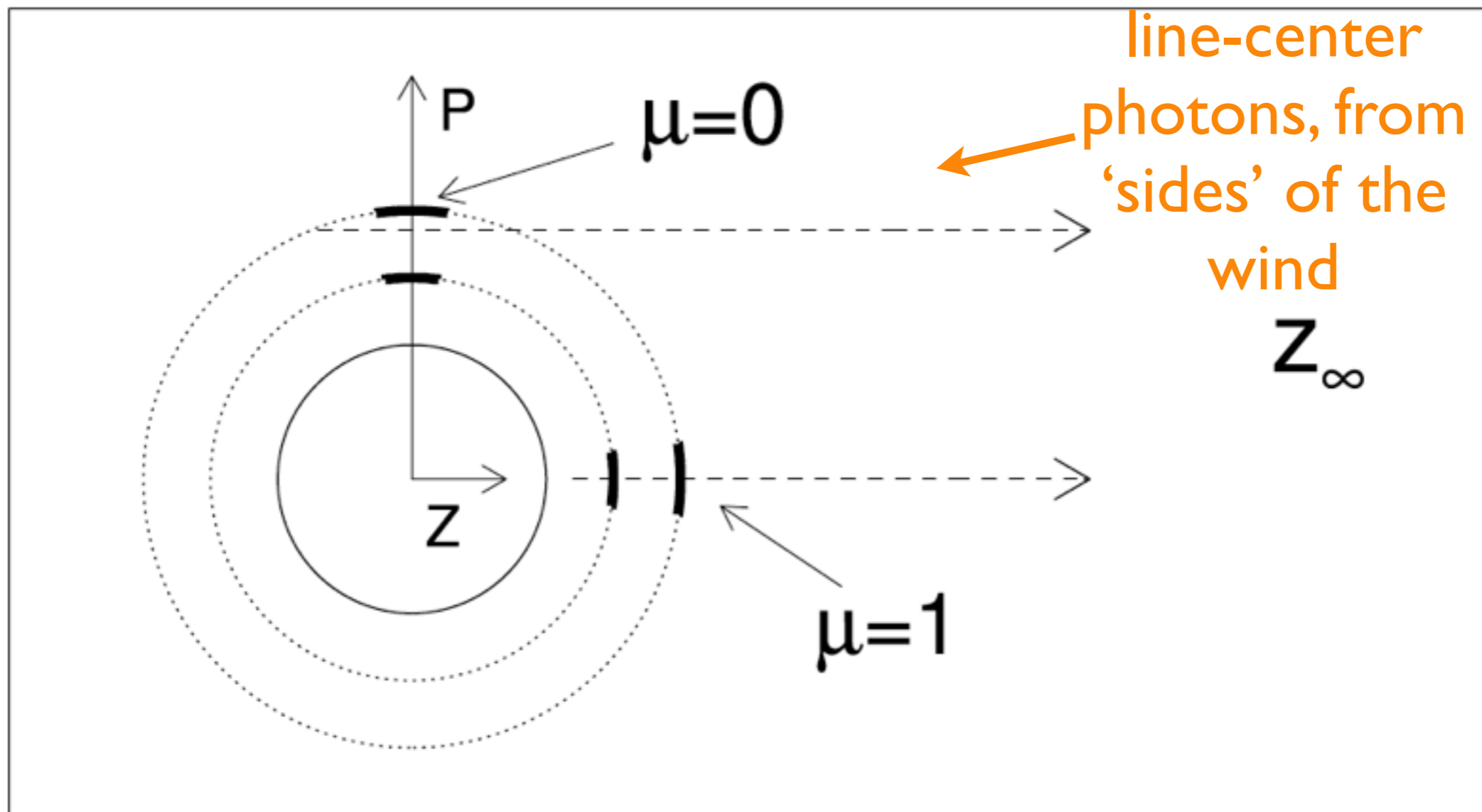line-center photons, from 'sides' of the wind

Figure 4. Illustration of the 'venetian blind' effect seen in porosity models using an anisotropic effective opacity. The dashed arrowed lines represent two different p-rays and the observer is assumed to be located at z_∞.

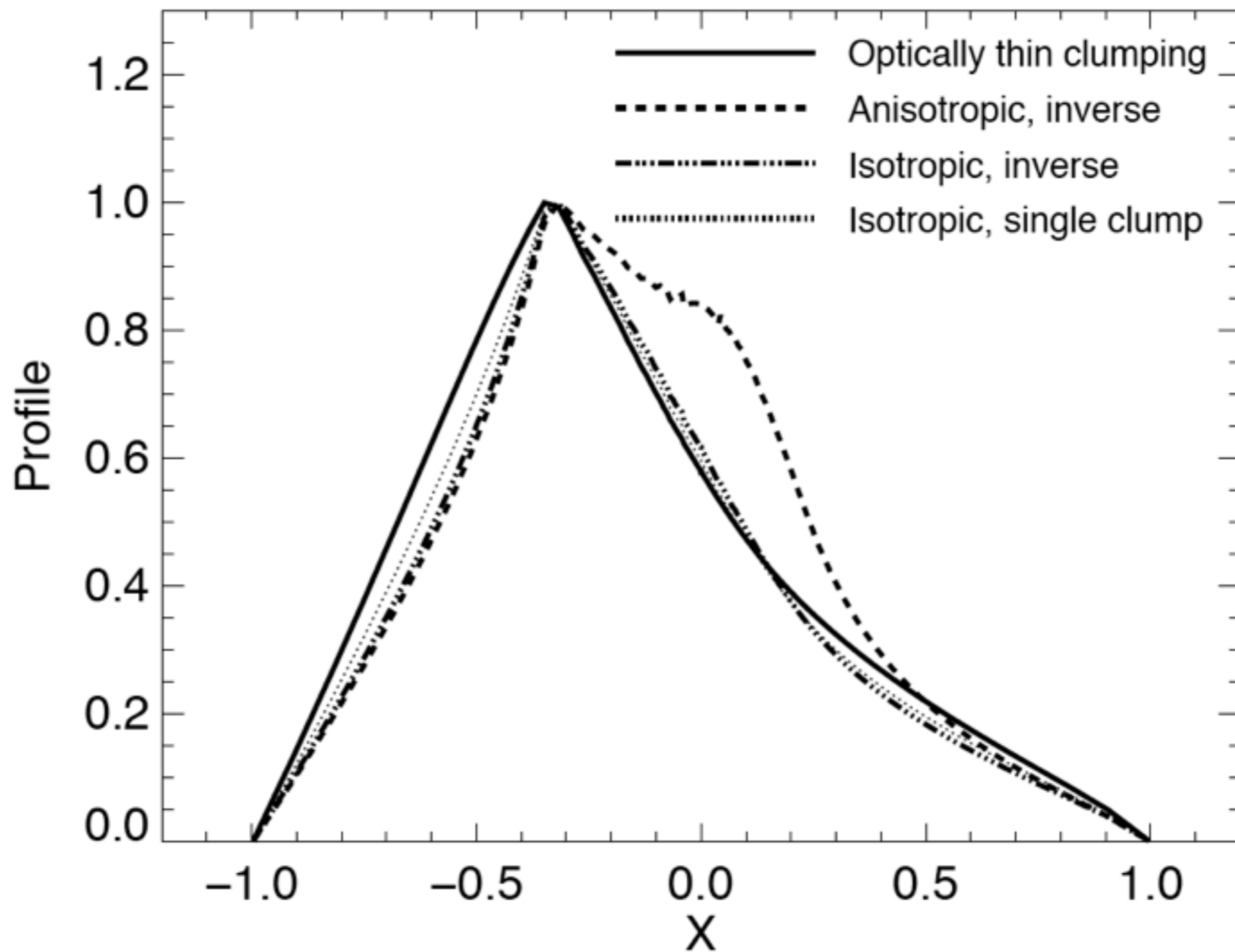# Venetian blind *bump*   lateral escape is enhanced

Figure 5. Line profiles for $h_\infty/R_\star = 1.0$ and $\tau_\star = 2.5$, using different effective opacity laws, as labelled.
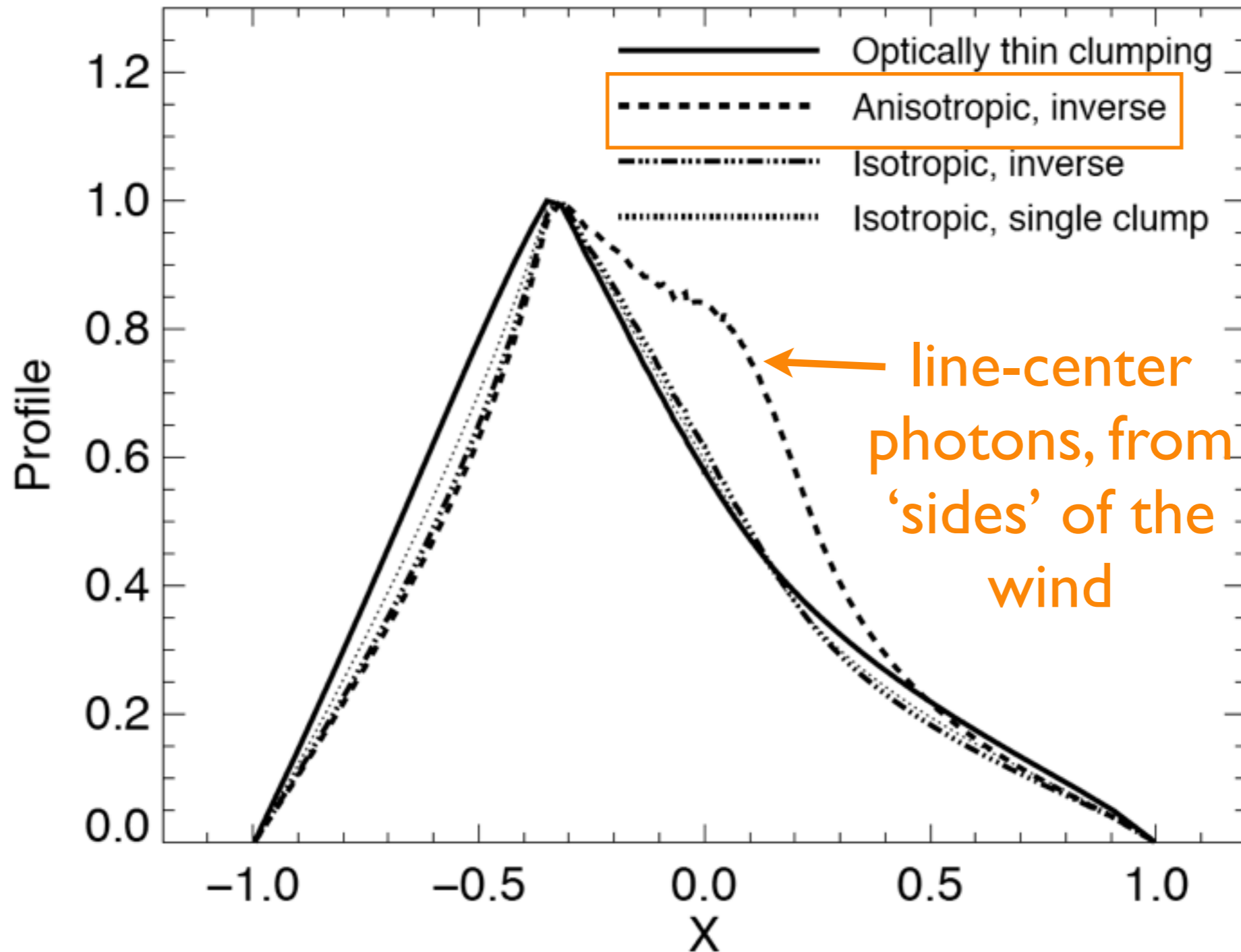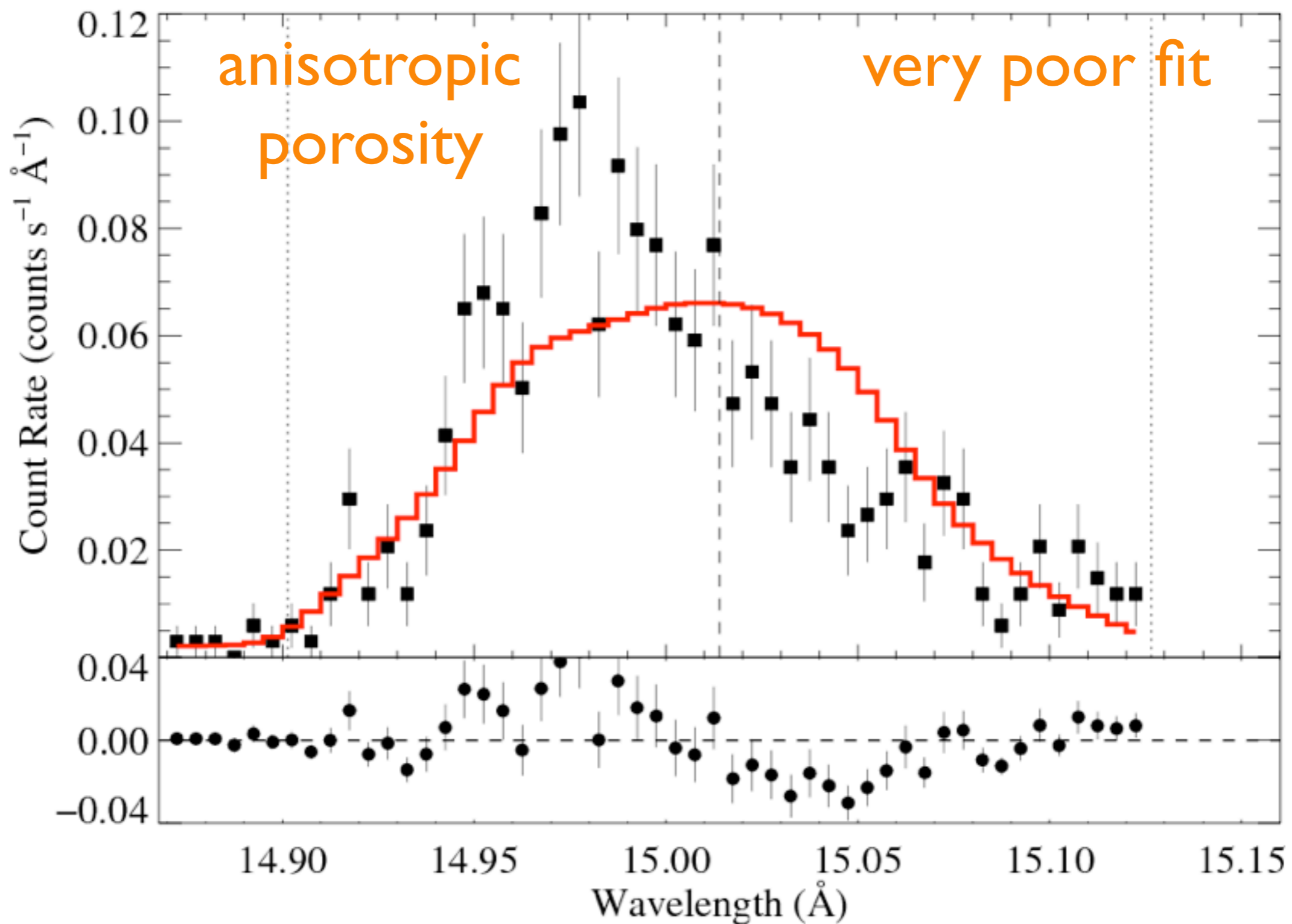
Venetian blind *bump*   lateral escape is enhanced
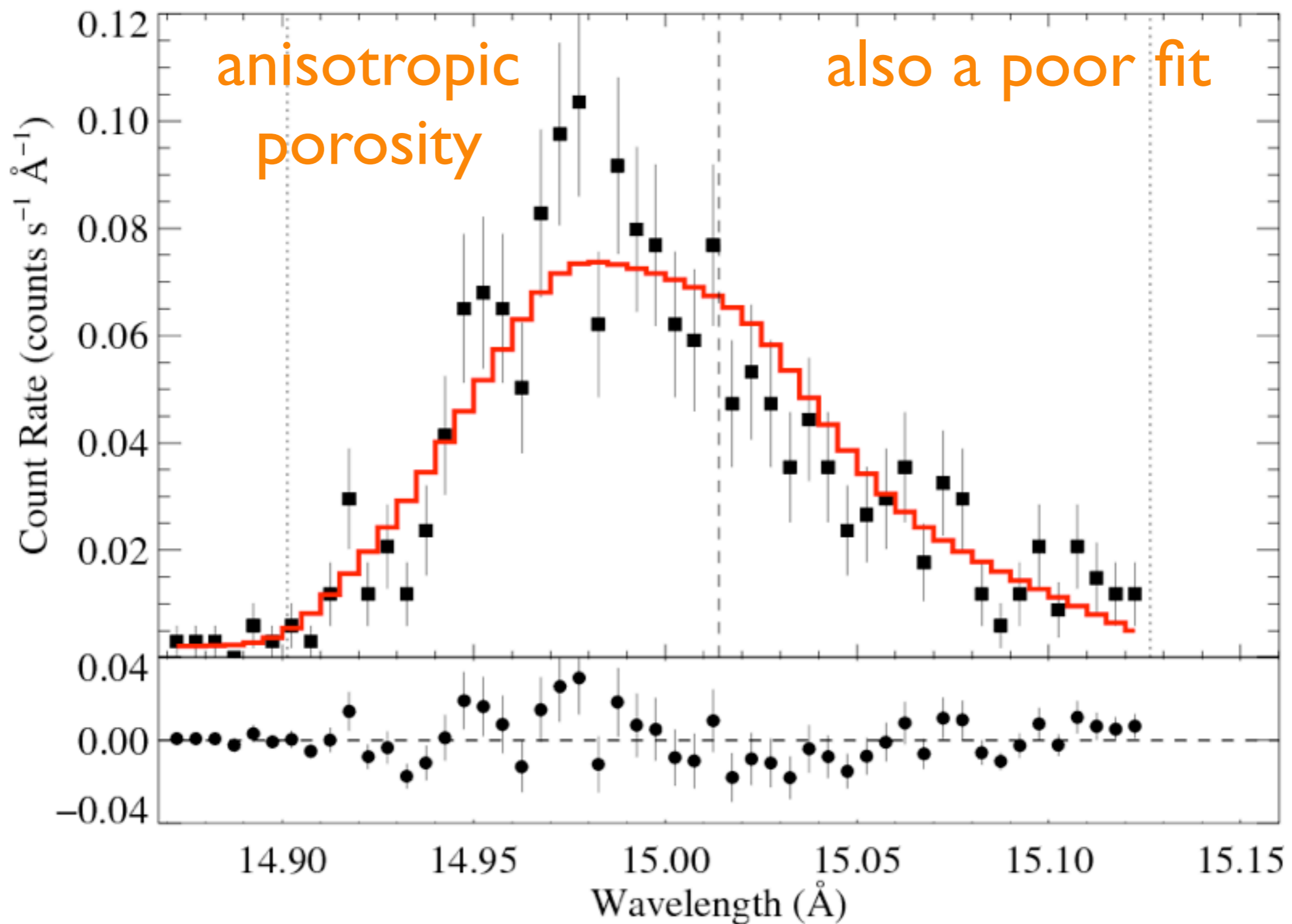
Optically thin clumping
Anisotropic, inverse
Isotropic, inverse
Isotropic, single clump

line-center photons, from 'sides' of the wind

Figure 5. Line profiles for $h_\infty/R_\star = 1.0$ and $\tau_\star = 2.5$, using different effective opacity laws, as labelled.

next: isotropic porosity

isotropic porosity (spherical clumps)
$h_\infty = 5\, R_\star$

$\tau_\star = 5.7$
$R_o = 1.7\, R_\star$

Confidence limits on h_∞ and $\tau_\star$

68%, 90%, 95%

Confidence limits on h_∞ and $\tau_\star$

68%, 90%, 95%

high porosity ruled out

modest porosity possible

taustar

h_inf
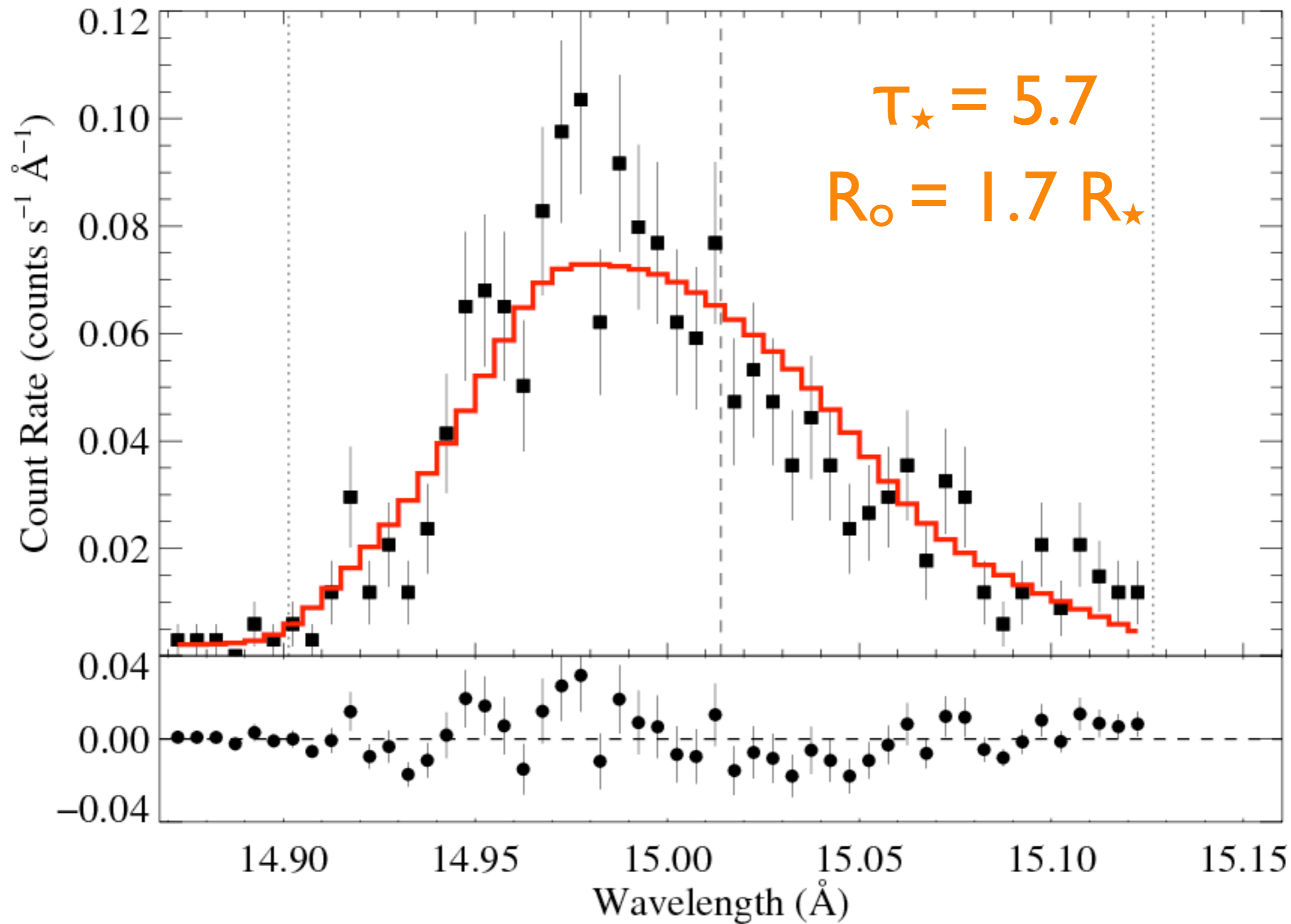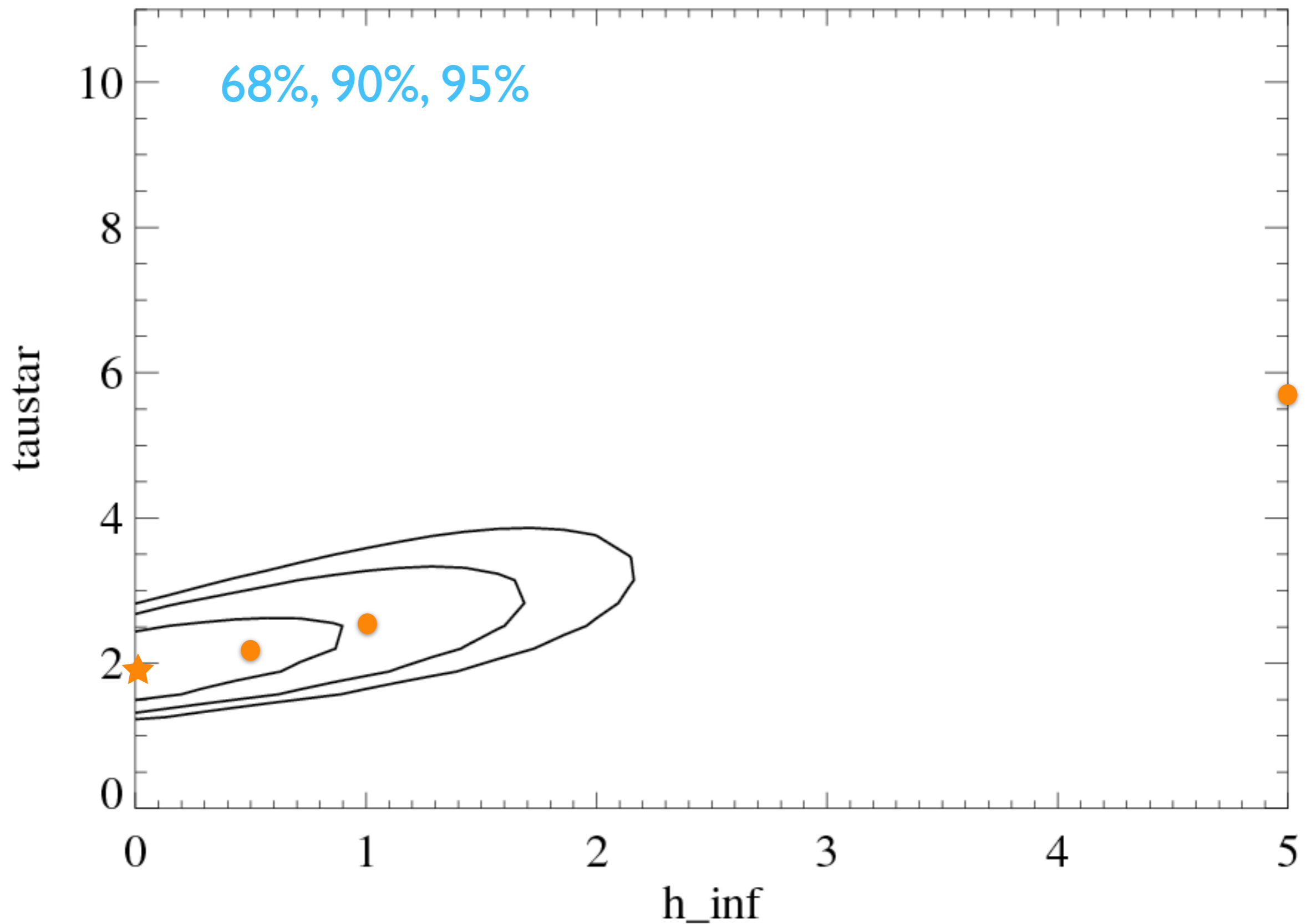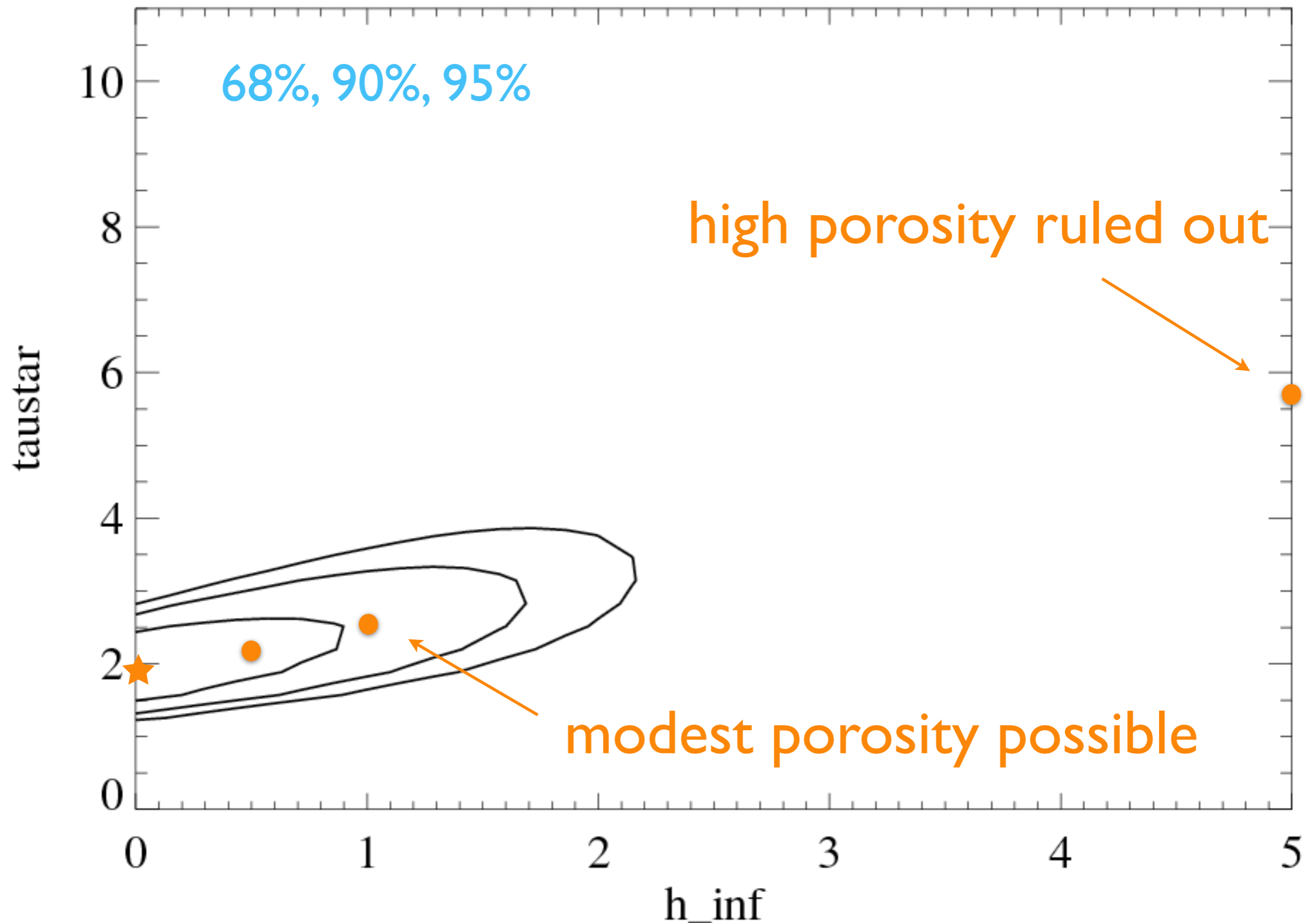
Conclusions for normal, single O supergiants

- Embedded wind shocks from LDI & clump-clump collisions
- X-ray plasma is small fraction of wind mass, distributed above r ~ 1.5 $R_\star$

- absorption signatures on X-ray line profiles show mass-loss rates factors of 3 to 5 lower than ρ^2 diagnostics that ignore clumping
- clumping factors of ~10 are thus implied
- clumping starts right at wind base (and X-rays only farther out)
- porosity is *not* important in these winds

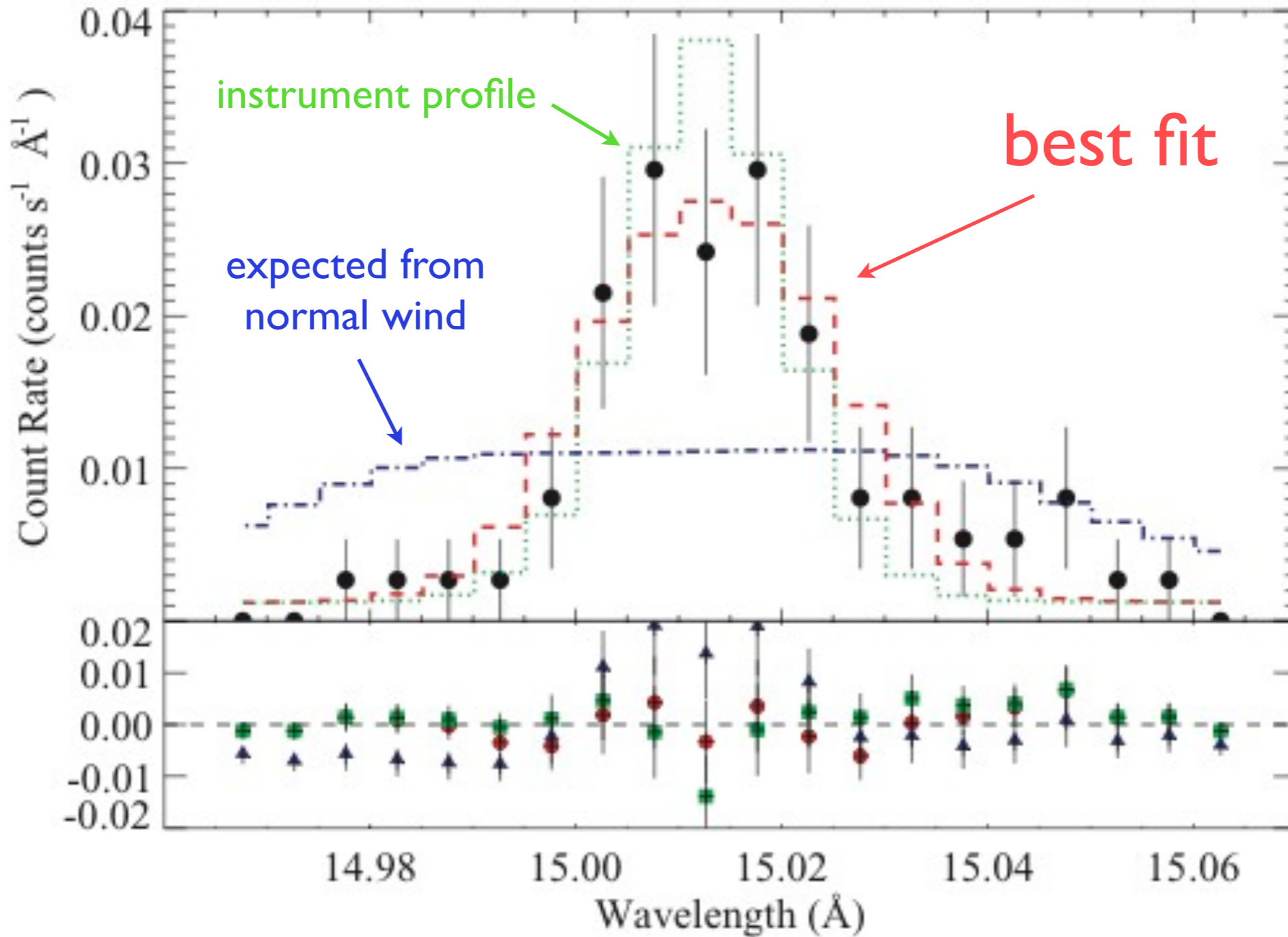# Two additional types of massive star X-ray emission

1. lower-density winds from later-type O and early-B stars

2. magnetic massive stars (MCWS: e.g. Asif ud-Doula's talk; also see Véronique Petit, on Friday)
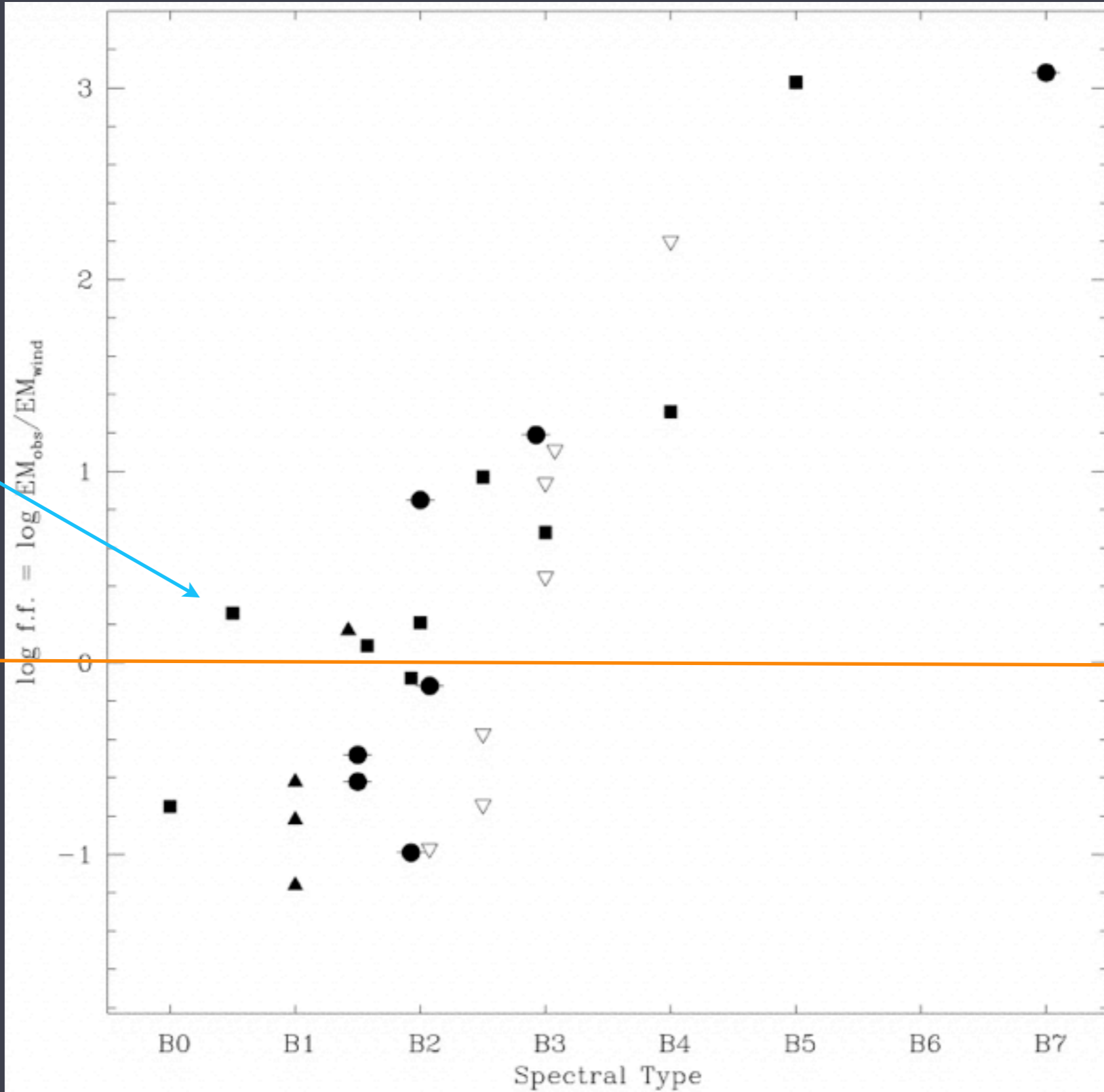
β Cru (B0.5 III)

Fe XVII line in the *Chandra* grating spectrum of β Cru (B0.5 III)

X-ray filling factors of B stars

β Cru

100%

log f.f. = log EM_{obs}/EM_{wind}

Spectral Type

B0 B1 B2 B3

Cohen et al. 1997

B star winds have low density, shocks are *adiabatic*

once the wind is shocked (at ~ 1.5 $R_\star$) it essentially *never* cools ⇒ outer wind is (nearly completely) filled with hot (few 10^6 K) plasma that is no longer radiatively driven
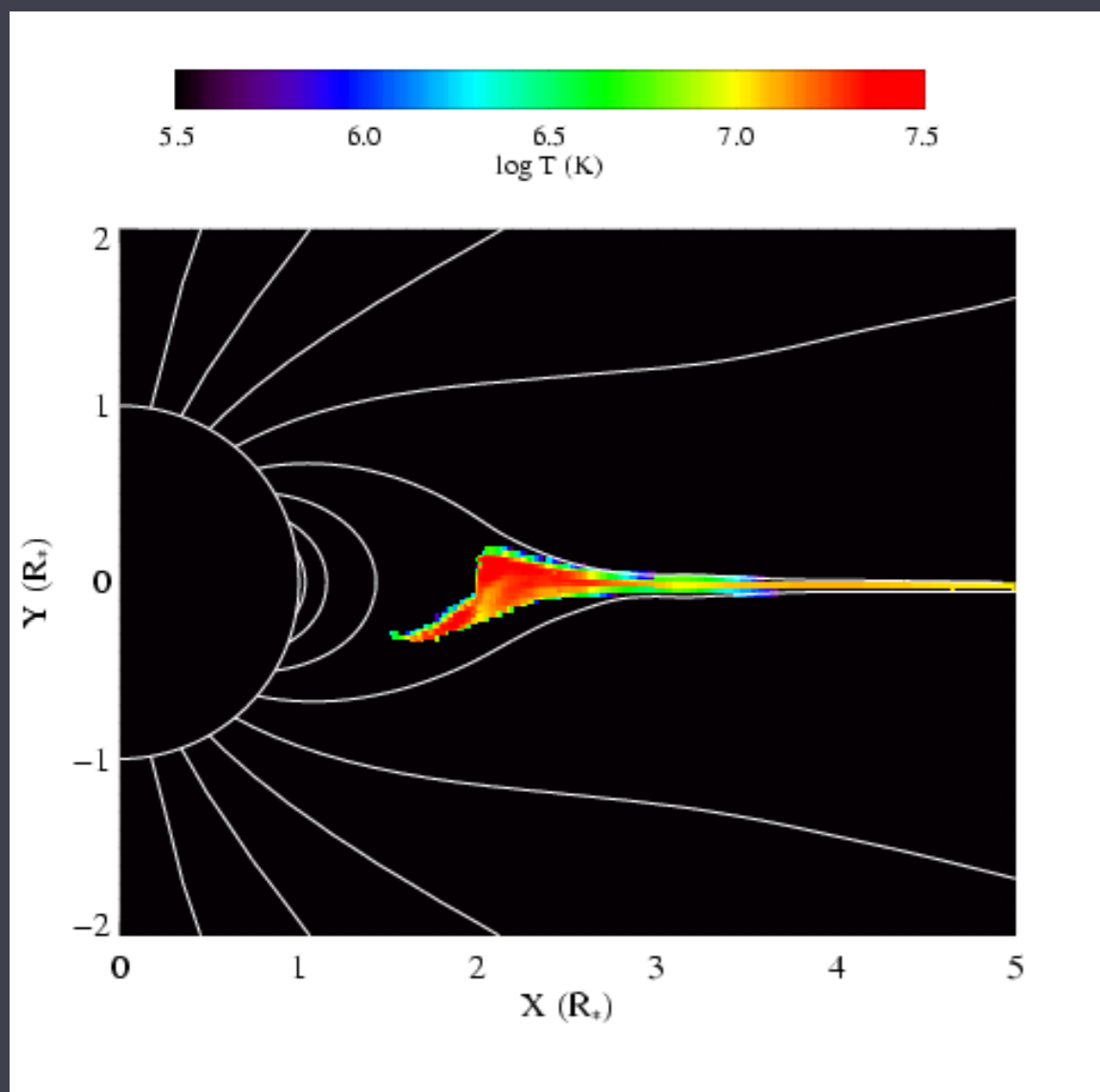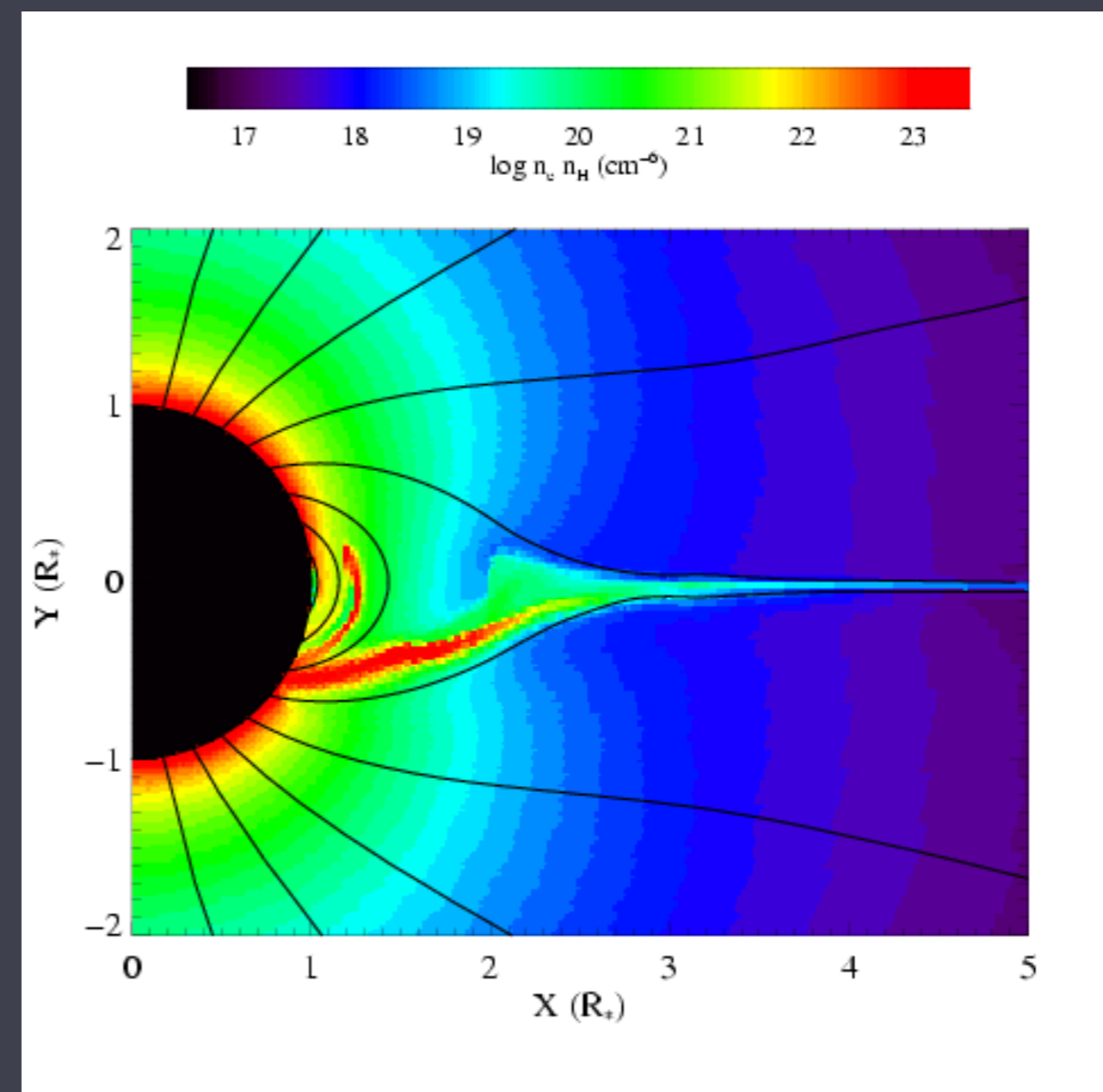
hence, narrow-ish X-ray lines

θ¹ Ori C: prototype magnetic O star
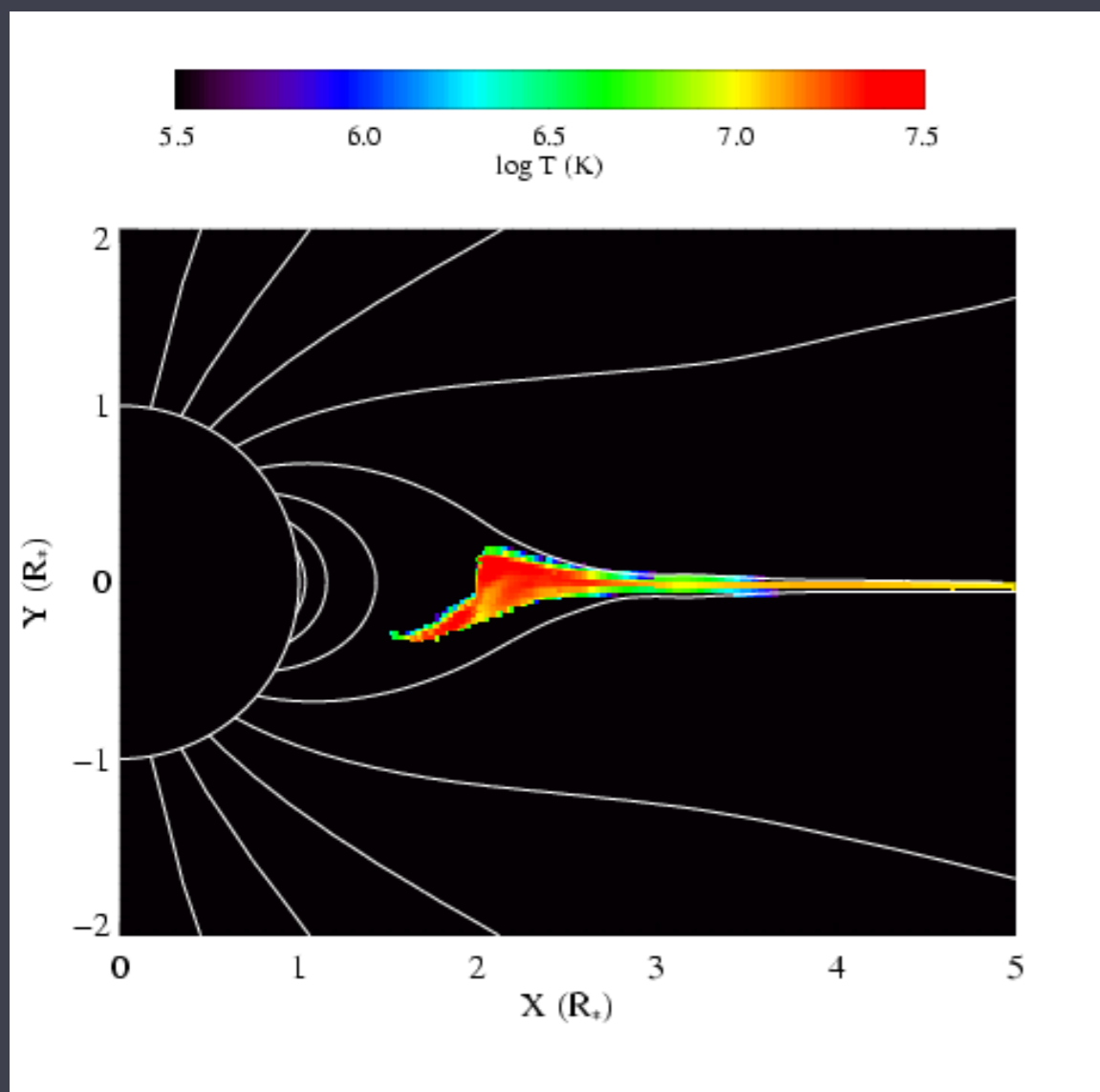
temperature

emission measure

simulations by A. ud-Doula; Gagné et al. (2005)
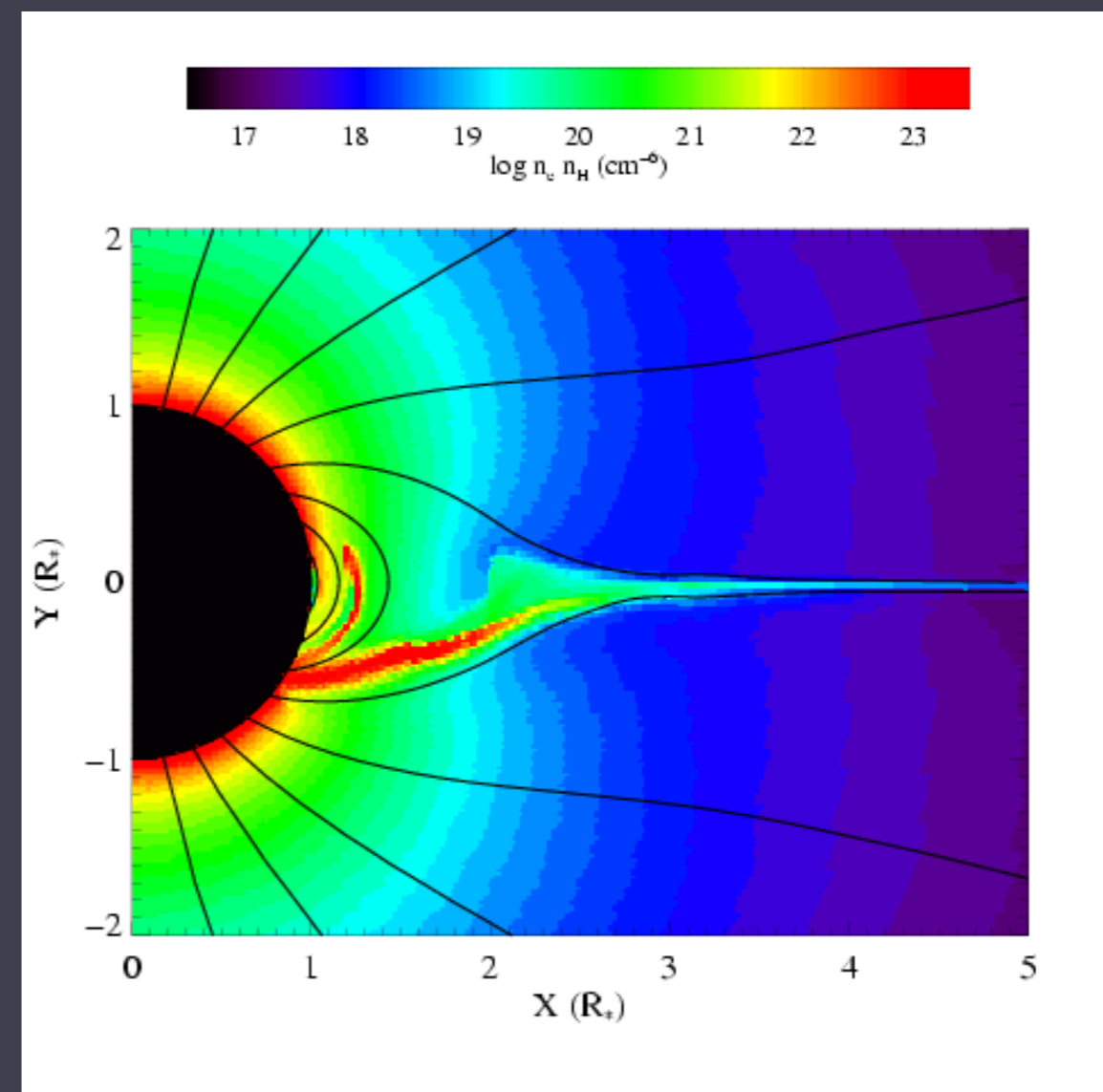
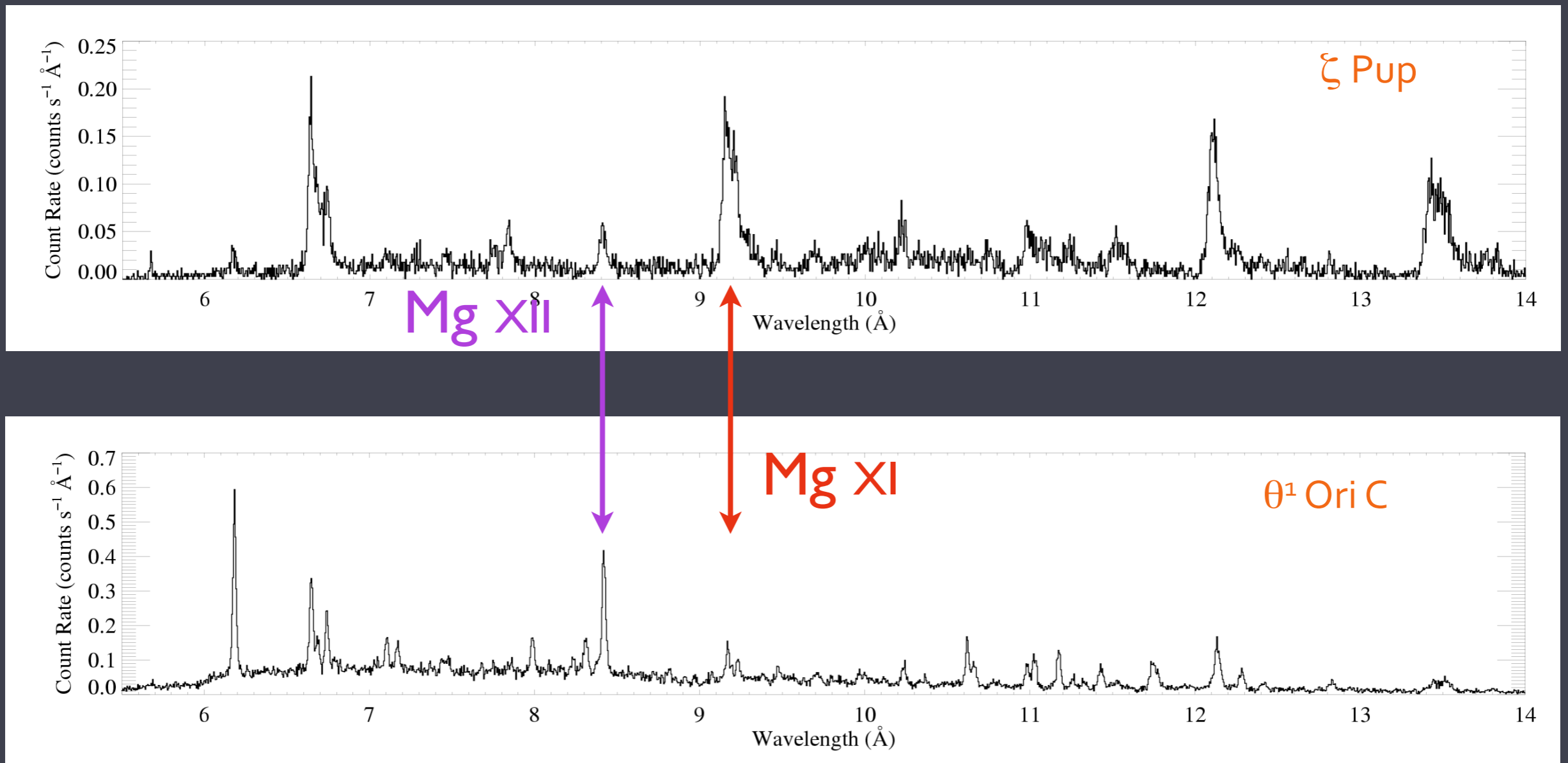# θ^1 Ori C: prototype magnetic O star

temperature

emission measure

simulations by A. ud-Doula; Gagné et al. (2005)
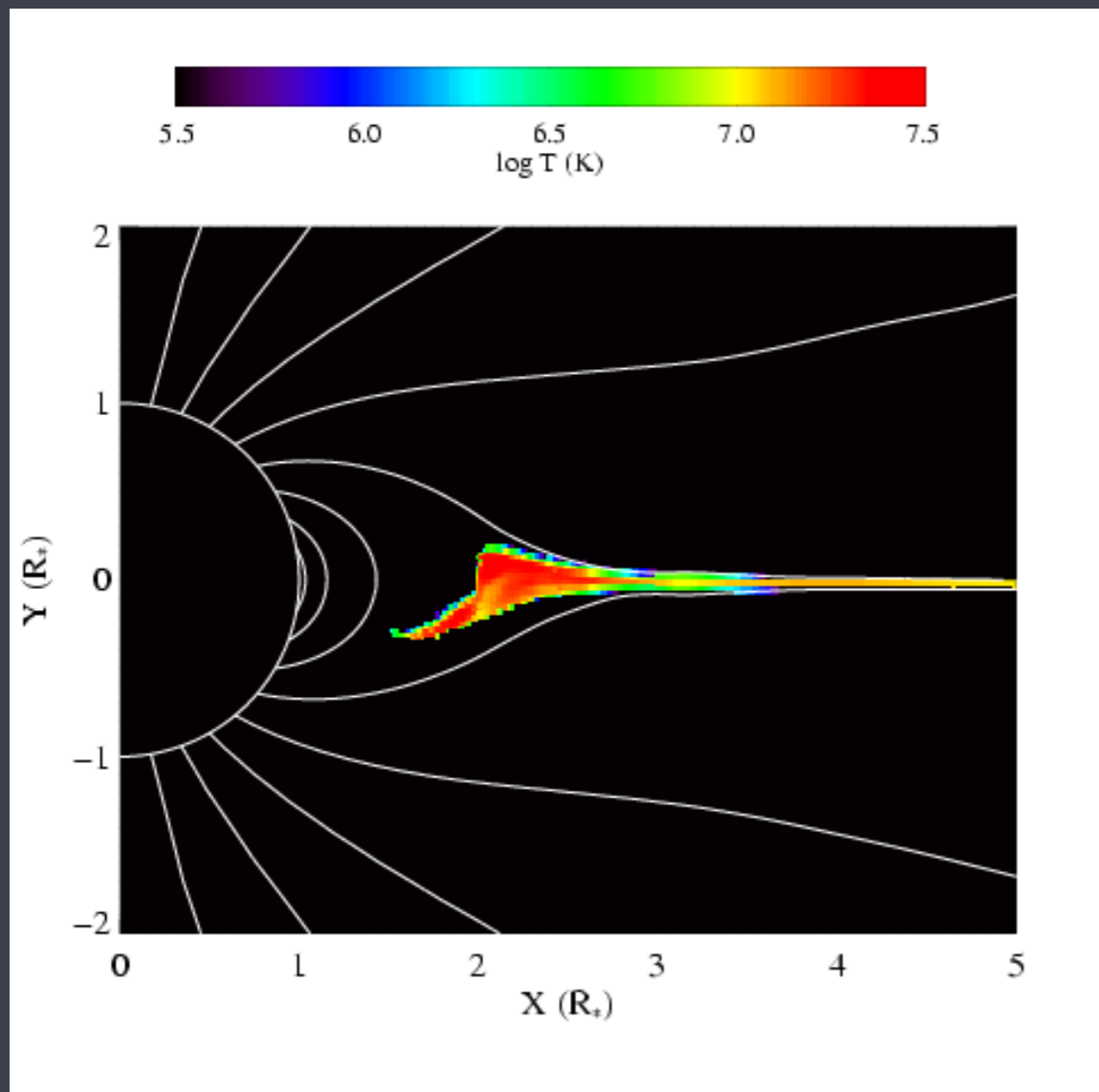
θ¹ Ori C: hotter plasma, narrower lines

Mg XII / Mg XI is proportional to temperature

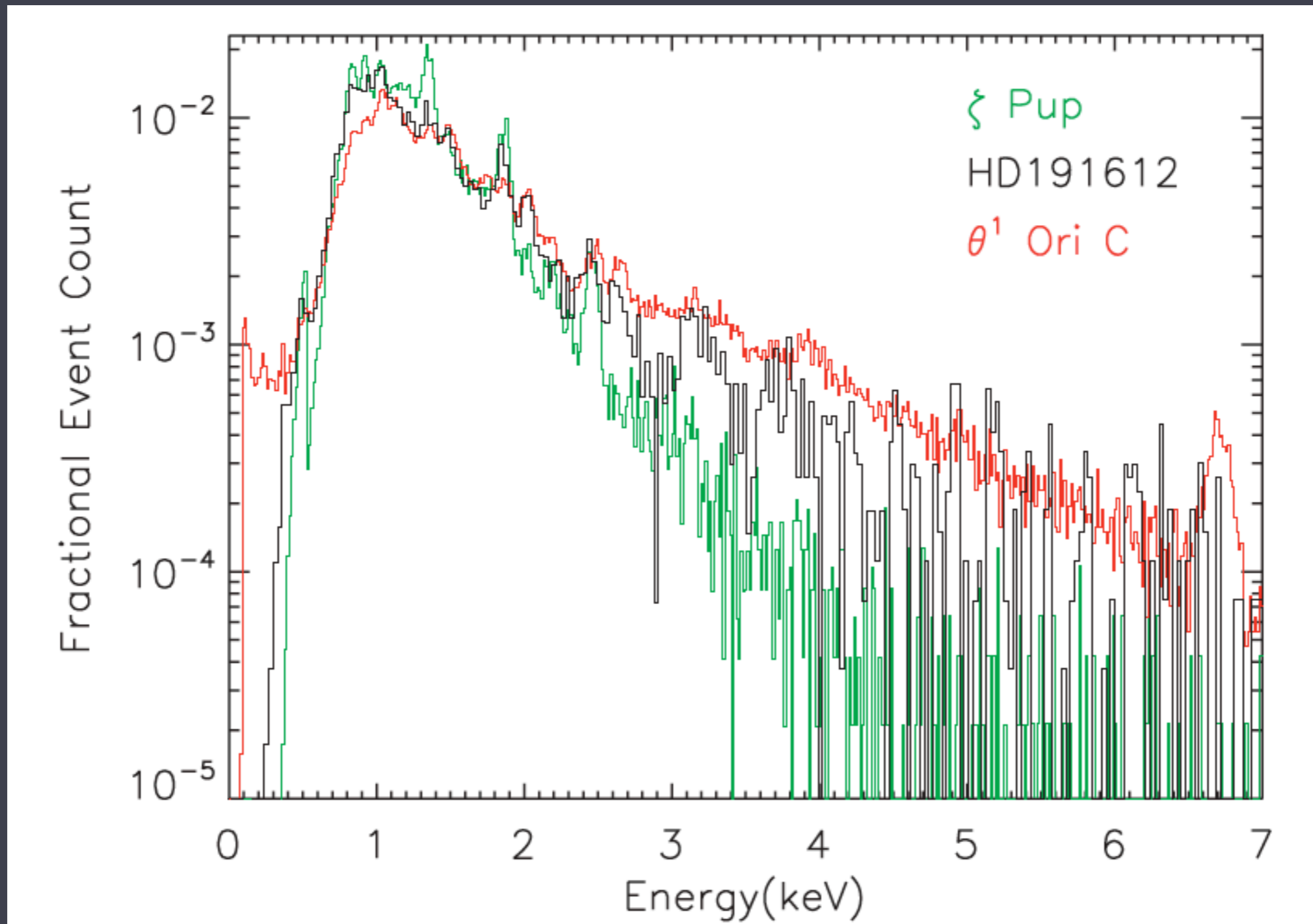# θ¹ Ori C: prototype magnetic O star

temperature

magnetic channeling : strong shocks = hotter plasma

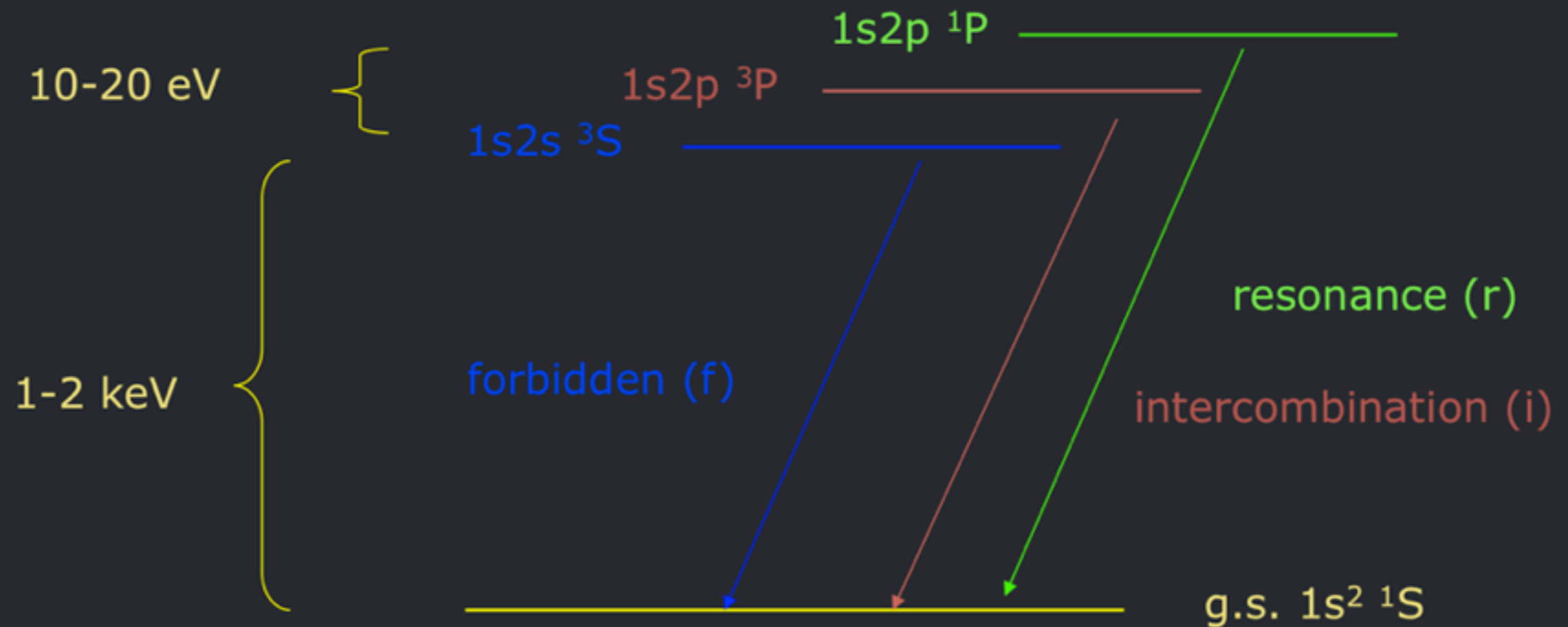magnetic confinement : low post-shock velocity = narrower lines

simulations by A. ud-Doula; Gagné et al. (2005)

other magnetic O stars (Of?p stars) have softer spectra and broader lines, but also have elevated X-ray luminosities
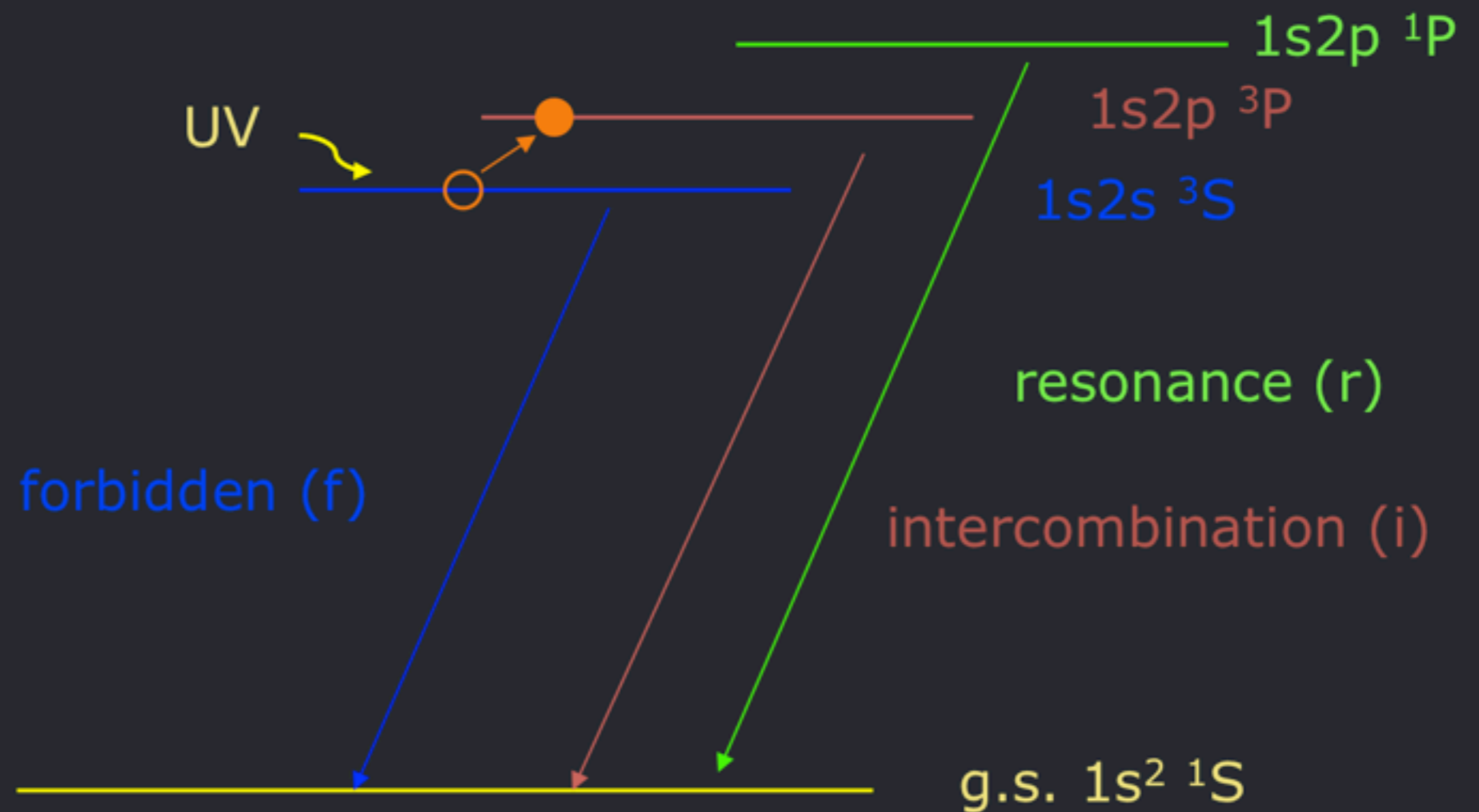
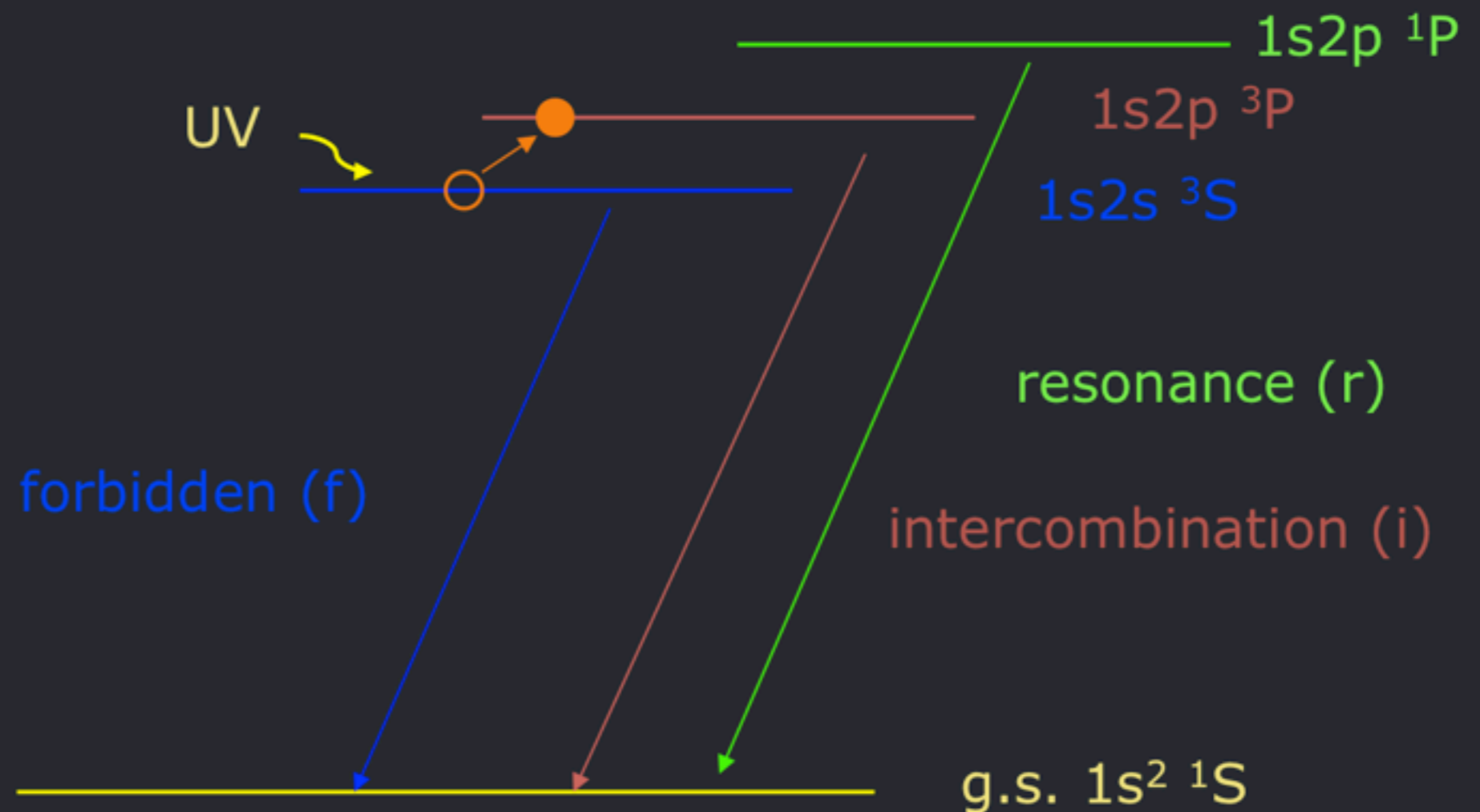*fli* ratios for diagnosing location of the hot plasma

Helium-like ions (e.g. O^{+6}, Ne^{+8}, Mg^{+10}, Si^{+12}, S^{+14}) – schematic energy level diagram

10-20 eV

1-2 keV

1s2p ^{1}P

1s2p ^{3}P

1s2s ^{3}S

forbidden (f)

resonance (r)

intercombination (i)

g.s. 1s^2 ^{1}S

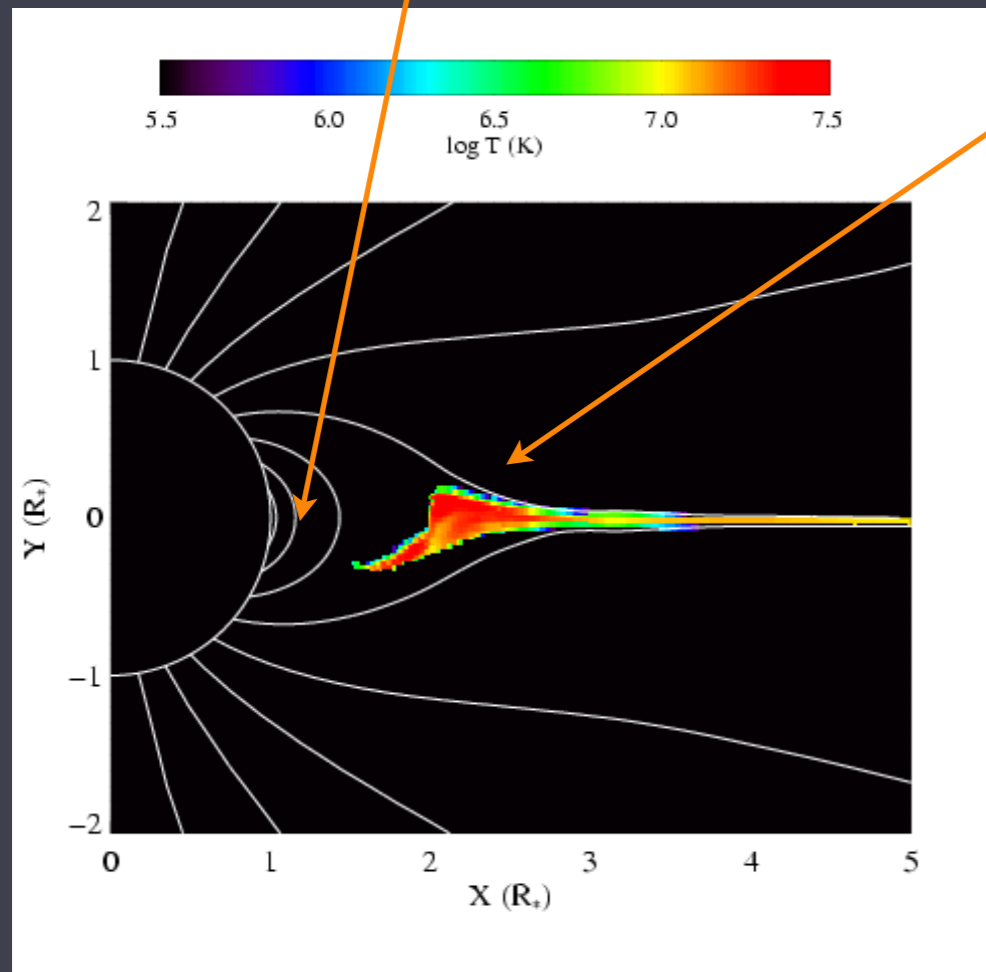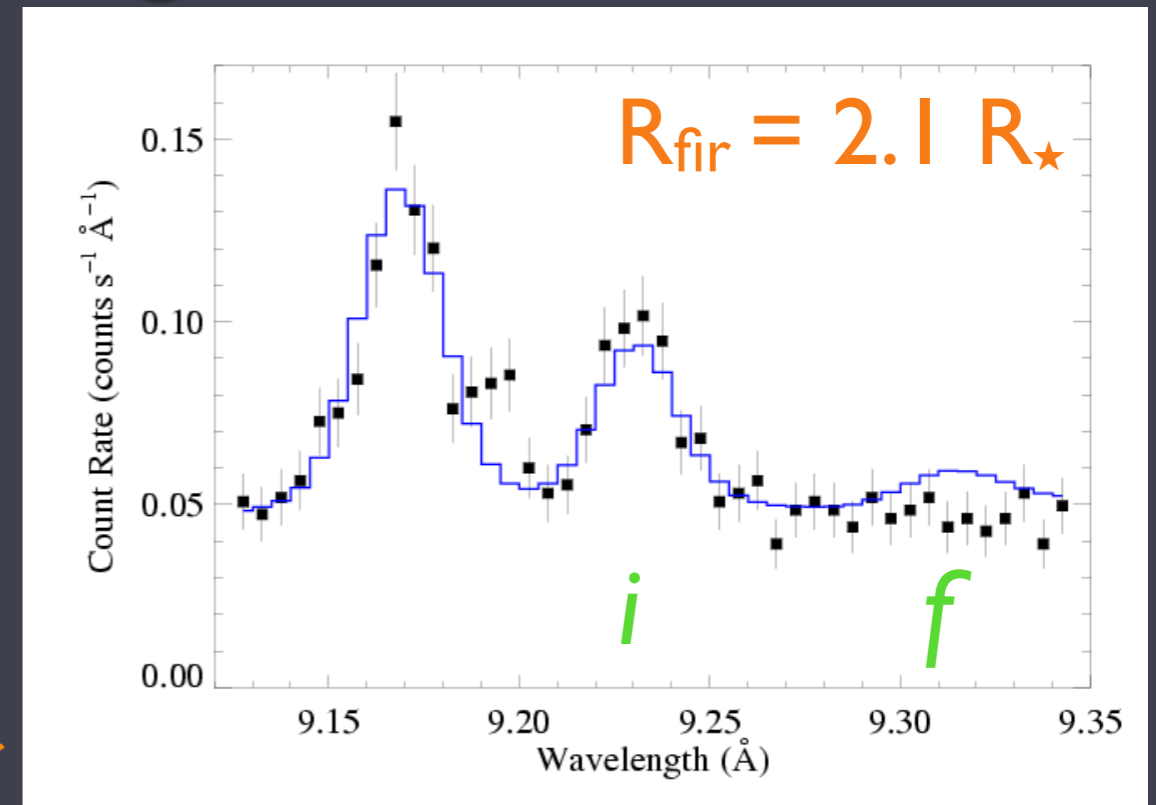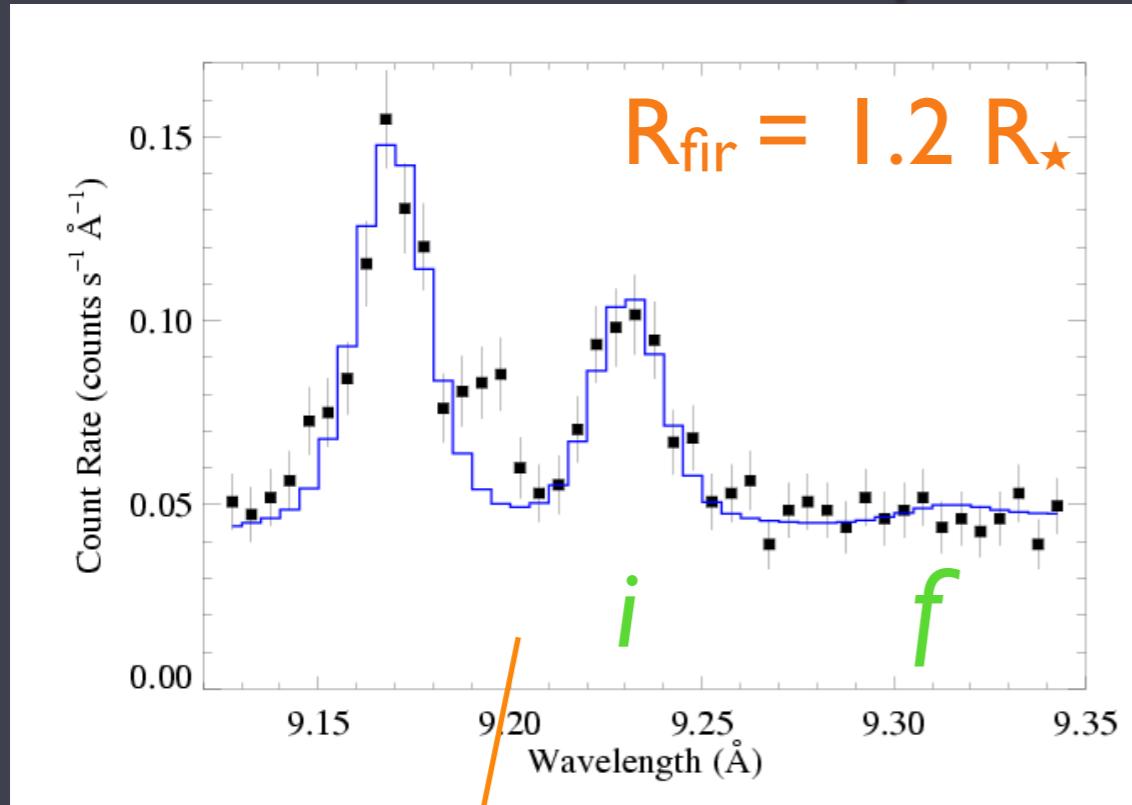The *f*/*i* ratio is thus a diagnostic of the strength of the local UV radiation field.

If you know the UV intensity emitted from the star's surface, it thus becomes a diagnostic of the distance that the x-ray emitting plasma is from the star's surface.

θ¹ Ori C: prototype magnetic O star

A. ud-Doula

θ¹ Ori C: prototype magnetic O star

R_{fir} = 1.2 $R_{\star}$

i f

R_{fir} = 2.1 $R_{\star}$

i f
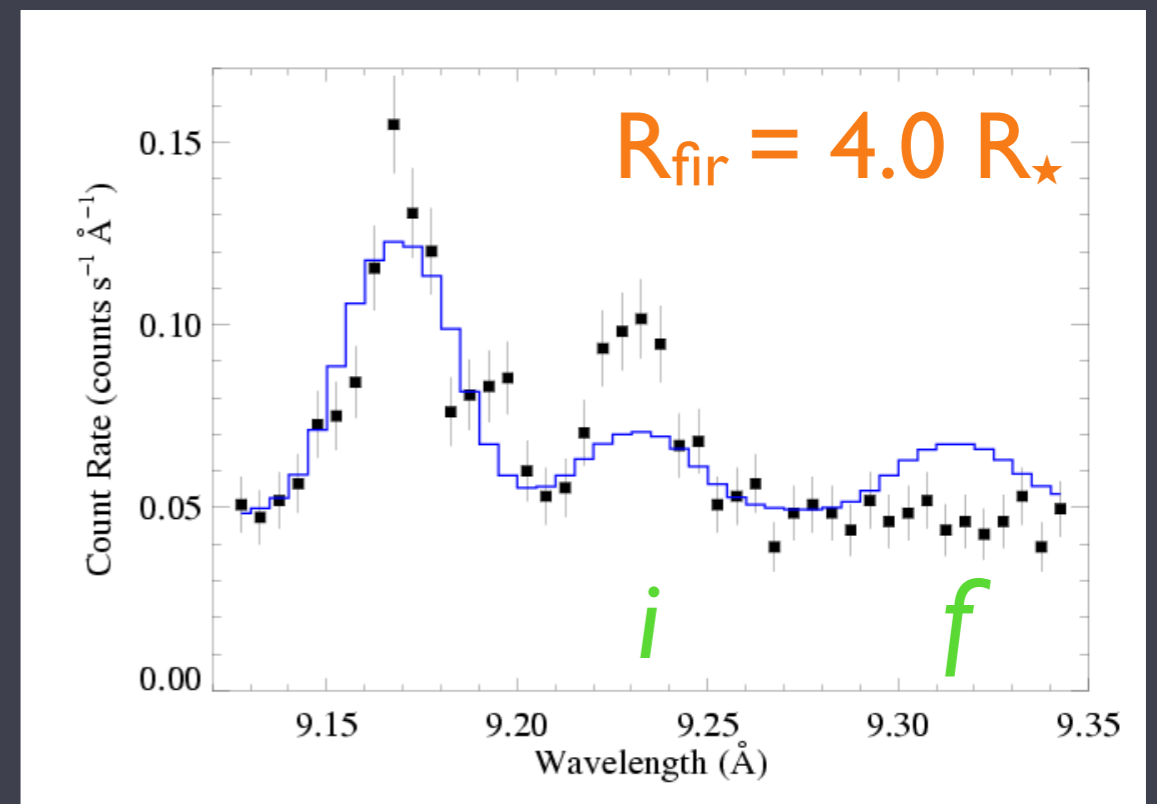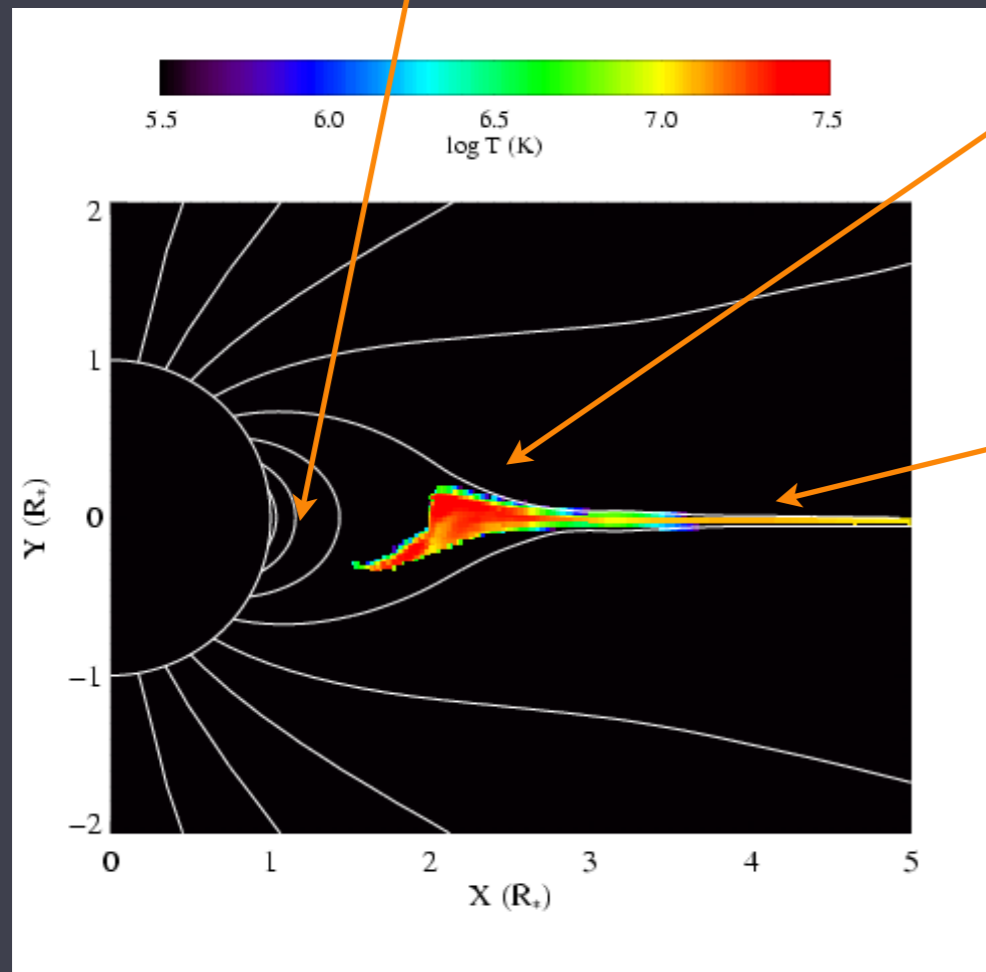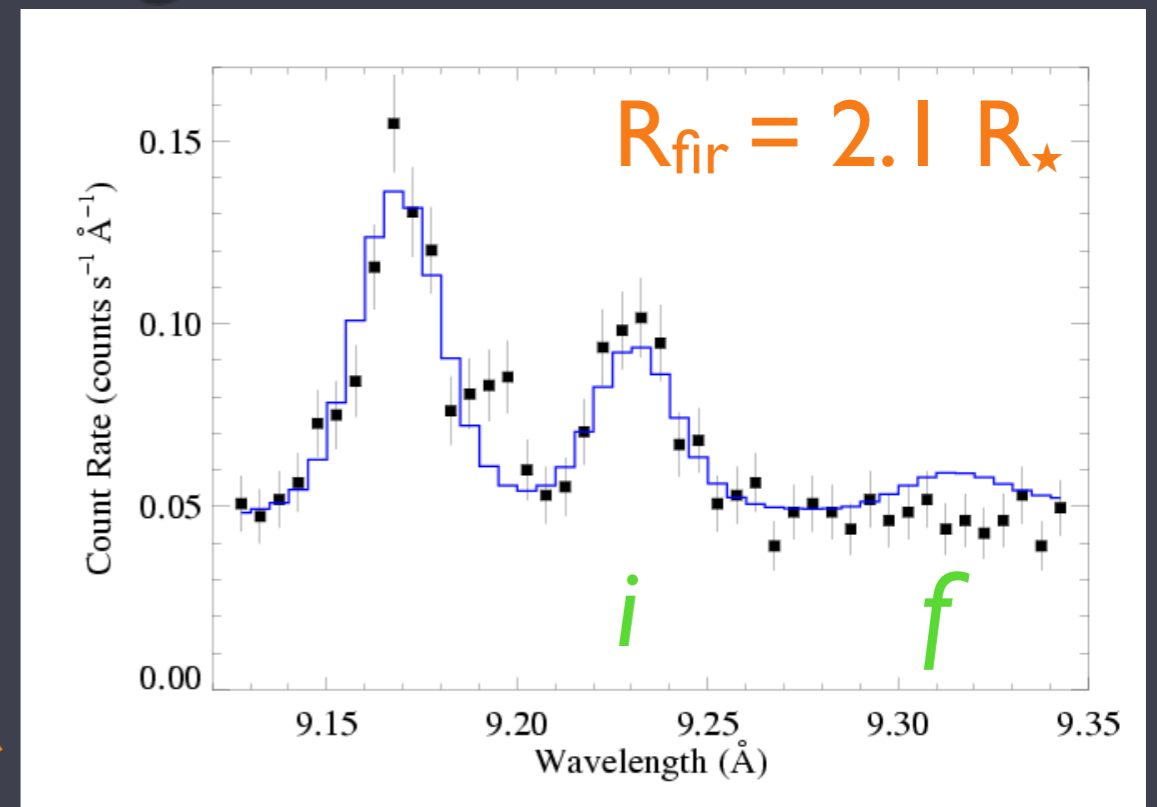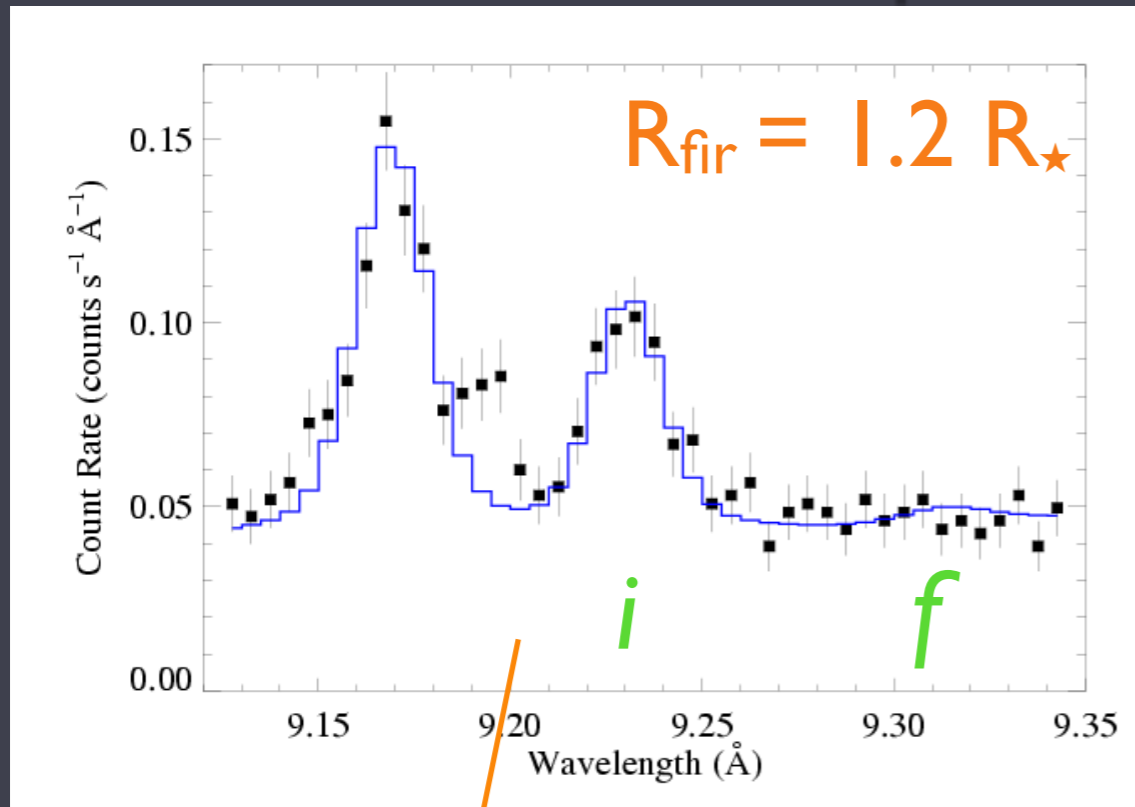
MDH simulations are only marginally consistent with *f/i* constraints

data say hot plasma is closer to the photosphere

A. ud-Doula

Conclusions, part 2

- early B stars may have very different wind-shock structure than O supergiants

- magnetic O stars (should) efficiently produce hard X-rays, showing evidence of confinement

- θ^1 Ori C agrees with this paradigm, though models predict shock heated plasma somewhat farther from the photosphere than observed

- But other magnetic O stars do not fit into the magnetically confined wind shock paradigm so well